A Novel Approach to Cardiac Health Assessment Using a Redesign of the Brachial Cuff Device

Thesis by
Alessio Tamborini

In Partial Fulfillment of the Requirements for the
Degree of
Doctor of Philosophy

CALIFORNIA INSTITUTE OF TECHNOLOGY
Pasadena, California

2023
Defended May 24, 2023

Alessio Tamborini
ORCID: 0000-0001-7651-3505

Ai miei genitori
e ai miei fratelli.

ACKNOWLEDGEMENTS

I would like to start of by expressing my deepest gratitude to my PhD advisor Prof. Mory Gharib. From my first day at Caltech Mory has been an incredible advisor, mentor, role model, and support. Mory has always believed in me and my potential, pushing the boundaries of what I thought I was capable of. Throughout my time in Mory's lab he has taught me the art of scientific investigation, how successes can be rewarding but how to find even more in failed attempts. The trust and independence Mory gave me during my PhD have helped me develop both professionally and personally. It has been an honor working in Mory's group for the past five years.

I would also like to thank all the people that have shaped my PhD journey. Firstly, I am incredibly grateful to the team at Avicena LLC for the opportunity to participate in such a big and challenging task, and for the constructive collaborations that have emerged. Thanks to their data sharing, we have applied all this work to real human data which has always been one of my goals. In particular, a special thank you to Sean Brady for the trust he placed in me and in my work, and Derek Rinderknecht for the mentorship that he provided throughout. The Caltech community was also a crucial part of my scientific experience and deserves much appreciation. A distinguished acknowledgement goes to Prof. John Sader whom has made me rediscover the beauty of mathematics on a white board. David Jeon has been my person of reference for any research related issue and his knowledge and support have been fundamental. I would finally like to acknowledge my office mate, Cong Wang, for sharing his guidance and experience with me, and all my lab members for the support and great memories that we have shared along the way.

My most heartfelt appreciation goes to my family for the endless support and unconditional love that they have given for the last 27 years of my life. Moving across the ocean to chase a dream was a tough decision for me but I am sure it was harder for them to let me go. They have always put me first and the sacrifices they have made have allowed me to get to where I am today, and for this I will be eternally grateful. From the very beginning they have taught me that in life you must enjoy the process and time will deliver results, and now, looking back, I must admit they have been right all along. Un grazie di cuore a tutti voi; Mamma, Papá, Teo e Imo, ve ne sarò infinitamente grato!

In my Caltech adventure I have also built a family of friends that have surrounded me with love and support. Over time I have developed a bond with every single one of you which made me feel more at home. The experiences we have shared and the memories I have created are a wonderful chapter in my life. To many more together: Olmo, Leo, Steve, Edo, Shane, Utku!

ABSTRACT

Current diagnostic methodologies in cardiology face large tradeoffs between procedure invasiveness and diagnostic reliability, ultimately requiring individuals to undergo cardiac catheterization for accurate diagnosis. Given the current societal burden of cardiovascular disease, there is a need for translational medical devices that bridge the accuracy gap between invasive and non-invasive measurements in the assessment of heart health. This thesis focuses on the development and validation of a high-resolution cuff-based system for assessment of central cardiovascular health.

Traditional pressure cuffs suffer low signal resolution when applied to non-invasive pulse waveform acquisition. In the first section of this thesis, we develop a cuff-based device with a pneumatic filter for high fidelity pulse waveform acquisition. This work discusses the design and functionality of the cuff-device, and investigates the repeatability of the cuff-based measurement. Furthermore, the derived mathematical model of the pneumatic filter is shown to have an equivalent behavior to an electrical low-pass filter inclusive of a time constant and a frequency response curve.

The accuracy and reliability of the pulse waveform features from the cuff-device are evaluated with human study data. Firstly, an IRB study is performed at Caltech on a young and healthy population showing that the cuff-device data lies within a narrow distribution indicative of the healthy nature of the population. Secondly, data from a clinical trial collecting simultaneous invasive catheter, cuff, and ECG is analyzed. The first analysis compared waveform parameters from the cuff in sSBP hold pressure with simultaneous aortic catheter, showing strong correlations between the two measurement modalities for both magnitude and fluctuations thereof.

Lastly, this work investigated the relationship between cuff-based parameters and left ventricular functions. We introduced a cuff-based method for extraction of the pressure-sound waveform, a pressure based surrogate of heart sounds. The results from this analysis showed that the pressure-sound features correlate with the strength of the left ventricular isovolumetric contraction and relaxation. Other important results from this work demonstrated the correlations between the heart-lung interactions in the left ventricle and cuff parameters: breathing fluctuations proportionally affect LV pressures and cuff sSBP waveform parameters. Overall these results support the accuracy and reliability of a cuff-based device for central cardiovascular health assessments.

PUBLISHED CONTENT AND CONTRIBUTIONS

[1] Alessio Tamborini and Morteza Gharib. "A Brachial Cuff Device Method for Cardiovascular Auscultation of the Left Side of the Heart." In Preparation. N.D.
A.T. developed the conceptual idea, performed the validation tests, and the data analysis.

[2] Alessio Tamborini and Morteza Gharib. "A pneumatic low-pass filter for high-fidelity cuff-based pulse waveform acquisition." Under Review. N.D.
A.T. developed the pneumatic filter, the cuff-based device, participated in the data collection, and performed the data analysis.

[3] Alessio Tamborini and Morteza Gharib. "A Supra-Systolic Cuff-Based Method for Accurate Measurement of Central Cardiovascular Pulse Waveform Features." In Preparation. N.D.
A.T. performed the entire data analysis.

TABLE OF CONTENTS

Chapter 1

INTRODUCTION

"La sapienza è figliola della sperienzia."
Wisdom is the daughter of experience.
— Leonardo Da Vinci, *Codice Foster III*

1.1 Motivation

The CDC estimates that every 34 seconds one person in the United States dies from Cardiovascular Disease (CVD). Currently, CVD is the leading cause of death in the United States for both males and females, accounting for one of every five deaths. In 2019 it was estimated that CVD were responsible for a total of 874 613 deaths. The annual direct and indirect costs associated with CVD in the US have been steadily growing and were estimated to be $378.0 billion in 2018 which account for 12% of the total US health expenditures [1]. Unrecognized and untreated CVD still represents a burden leading to severe cardiovascular complications such as myocardial infarction [2]. There is a strong medical need to develop devices and methods that improve diagnosis and facilitate monitoring of CVD in the population. This thesis developed and tested a novel technology for high-resolution pulse waveform acquisition with a cuff-based device at the brachial artery. This work aims to demonstrate the accuracy of the non-invasive cuff-based device in monitoring central cardiovascular health both at the ascending aorta and left ventricle. These results are intended to motivate and incentivize the wide-spread application of non-invasive pulse waveform analysis as a valuable diagnostic tool for CVD using cuff-based systems.

1.2 Basic Cardiovascular Physiology

Heart

The heart is a four chamber muscular organ responsible for providing oxygenated blood to the body. Blood flow in the heart is regulated by a complex pattern of contraction, elongation, and one-way valves. The four chambers of the heart collect and pump blood; the right side of the heart collects and pumps oxygen-poor blood while the left side of the heart collects and pumps oxygen-rich blood. In particular, the right atrium receives de-oxygenated blood from the veins and its contraction pushes blood into the right ventricle. The right ventricle pumps blood to the lungs via the pulmonary artery. Oxygenated blood from the lungs goes to the left atria via the pulmonary veins and is pushed into the left ventricle upon contraction. Lastly, the left ventricle is responsible to pump oxygenated blood into the cardiovascular system.

Heart valves are one-way passive valves that allow correct blood flow direction between the heart chambers. These valves are activated by pressure gradients, which cause the opening and closing mechanism. A positive pressure gradient open the valve pushing flow through it while a negative pressure gradient closes the valve separating the two communicating heart chambers. The tricuspid valve is between the right atrium and right ventricle, the pulmonary semilunar valve is between the right ventricle and pulmonary artery, the mitral valve is between the left atrium and left ventricle and the aortic semilunar valve is between the left ventricle and aorta. Interestingly, the tricuspid valve, pulmonary semilunar valve and aortic semilunar valve all have three cusps while the mitral valve only has two cusps. No scientific explanation has yet been provided for physiological difference in the valve structures.

Heart contractions are controlled by the heart's electrical activity. The sinoatrial node, located in the right atria, is the source of the electrical stimulus which initiates every heart beat. This electrical stimulus travels from the sinoatrial node to the atrioventricular node activating the atrial contractions. From here it progresses to the Bundle of His and separates into the Left Bundle Branch and Right Bundle Branch, which cause the contraction of the left and right ventricles, respectively. The sequential contraction of atria and ventricle causes filling and emptying of heart chambers, pumping blood through the system and into the body.

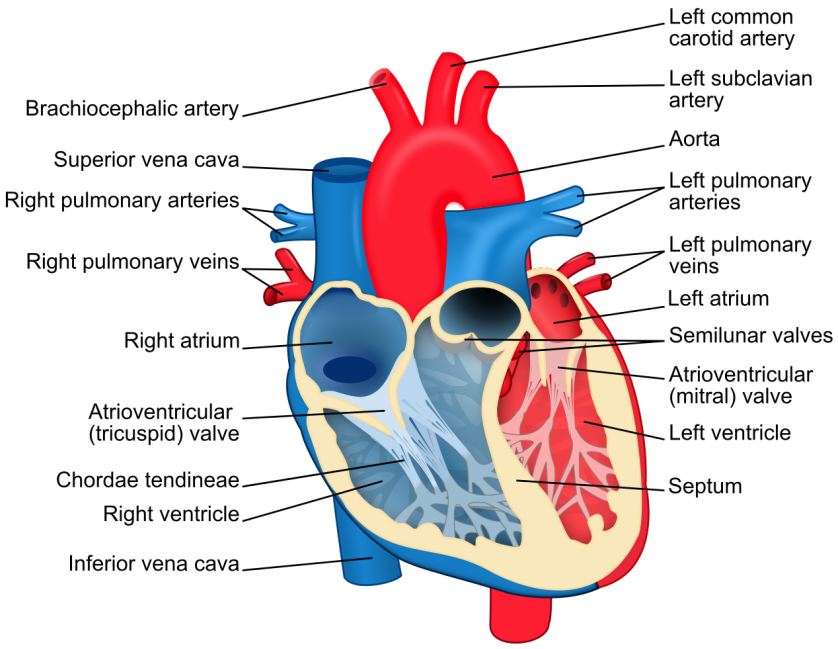

Figure 1.1: Heart diagram structure. [Digital Image] (2021, January 13). In Wikipedia. Retrieved May 5, 2023, from https://en.wikipedia.org/wiki/Heart_valve/media/File:Heart_diagram-en.svg

The Cardiac Cycle

The cardiac cycle is broken down in two phases: systole and diastole. Systole is the period of forceful contraction that pumps blood in the forward direction. Upon electrical stimulation, the chamber contracts rapidly increasing pressure. A positive pressure gradient is developed and the corresponding heart valve will open allowing blood to flow forward. Diastole is the period of cardiac expansion that fills the chamber with blood. Contrary to what previously believed, it has been shown that the heart experiences a contraction wave that shortens and expands the muscle. Thus, diastole is not a relaxation period but rather an expansion of the heart volume from the contraction wave [3, 4]. The volumetric expansion decreases pressure developing a negative pressure gradient that drives flow into the chamber. At rest, diastole is typically longer than systole as the filling process is slower and at lower pressures. Both atrias and ventricles experience these cardiac cycles, yet a phase delay is observed as the emptying of atrium fills the ventricle. Typically one pulse cycle starts at the onset of systole and terminates with the end of diastole.

The cardiac cycle for the left ventricle can be further broken down into four segments: (1) isovolumetric contraction, (2) ejection, (3) isovolumetric relaxation,

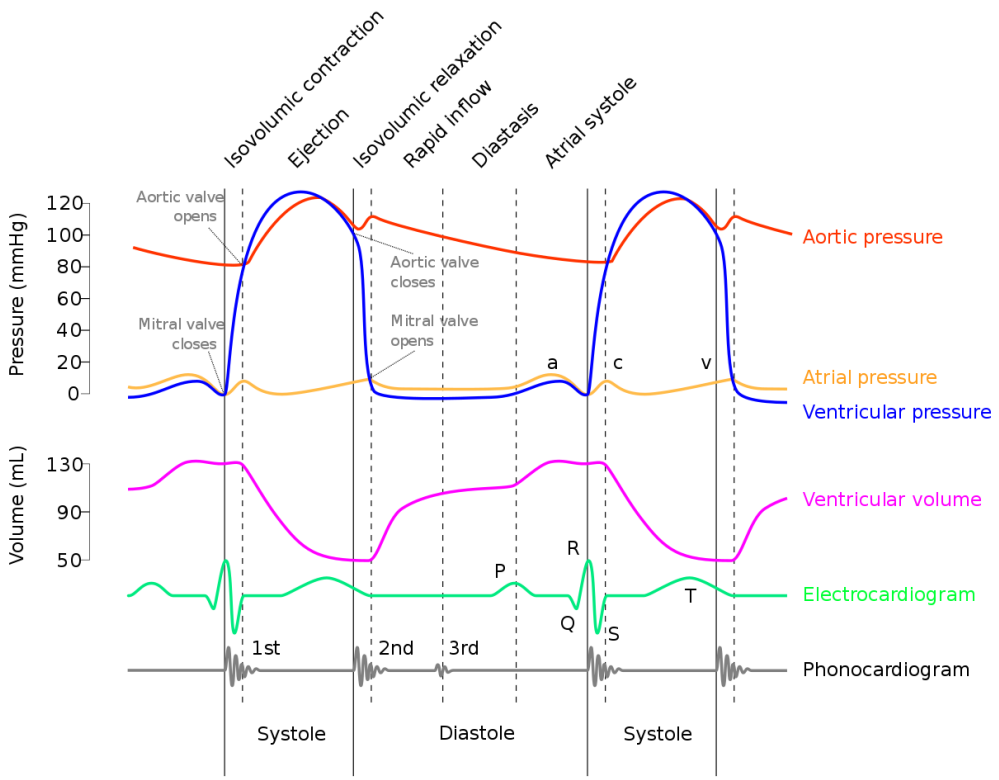

Figure 1.2: A Wiggers Diagram illustrating the Cardiac Cycles for the Left Side of the Heart. [Digital Image] (2021, June 17). In Wikipedia. Retrieved May 5, 2023, from https://en.wikipedia.org/wiki/Wiggers_diagram/media/File:Wiggers_Diagram_2.svg

and (4) filling. In this breakdown the systole is composed of phase (1) and (2), and the diastole is composed of phase (3) and (4). In isovolumetric contraction the left ventricle starts a forceful contraction that rapidly raises pressure, in this phase both mitral valve and aortic valve are closed. Upon ventricular pressure surpassing aortic pressure the aortic valve will open and start the ejection phase. The ejection will continue until 60 to 70% of the ventricular blood volume has been ejected. At this moment, the ventricular pressure will have dropped below the aortic pressure causing aortic valve closure. This closure of the aortic valve initiates the isovolumetric relaxation which rapidly decreases pressure in the left ventricle, both mitral and aortic valve are closed. The ventricular pressure will fall below the atrial pressure, the mitral valve will open and blood will be pushed in the ventricle, this is the filling phase. These contractions and relaxations are fundamental for the correct functionality of the heart's pumping motion.

Pulse Pressure Waveforms

During the left ventricular ejection phase, a pulse of blood is pumped into the arterial system. The ejected blood generates a propagating pressure and flow wave that travels along the viscoelastic arterial structure to bring flow towards the periphery. At locations of impedance mismatch the forward traveling wave is in part reflected back to the source. At any location within the arterial system the pressure time signal is composed from the superposition of forward and reflected waves, this is commonly called the pulse pressure waveform.

The pulse pressure waveform is divided in two main phases of systole and diastole, corresponding to the ejection phase when the aortic valve is open and the time period with the closed aortic valve, respectively. The start of systole occurs with the pressure rise corresponding to the ejection of blood and the arrival of the pressure wave. This wave increases local pressure, reaching a maximum pressure of SBP after which the pressure starts to fall. The transition between systole and diastole is clearly marked by a pressure incisura caused by the closing of the aortic valve, this is known as the dicrotic notch. During diastole we observe the pumping mechanism of the Windkessel effect, the aorta behaves like an elastic chamber and pumps blood accumulated during systole [5]. In this phase, pressure slowly decays as the windkessel effect diminishes and flow reduces. The pulse waveform shape is modified by subject specific characteristics and features pertinent to the heart and vascular arterial system. The study and analysis of the pulse waveform has been of great interest given the large quantity of information that is contained within this signal.

As the pressure wave propagates from the ascending aorta toward the peripheral arteries the waveform progressively changes shape and magnitude. This phenomenon is attributed to the effect of wave superposition which is the predominant factor in pulse pressure amplification, the increase in pulse waveform magnitude. Current literature strongly supports that the most physiologically significant cardiovascular information is obtained with the central pulse waveform as this gives the closest representation to the pressures at the heart [6].

1.3 Measuring the Heart's Vital Signs

Blood Pressure

The use of the pulse pressure waveform as a diagnostic tool dates back many centuries. Pulse sensing has played a critical role in Traditional Chinese Medicine

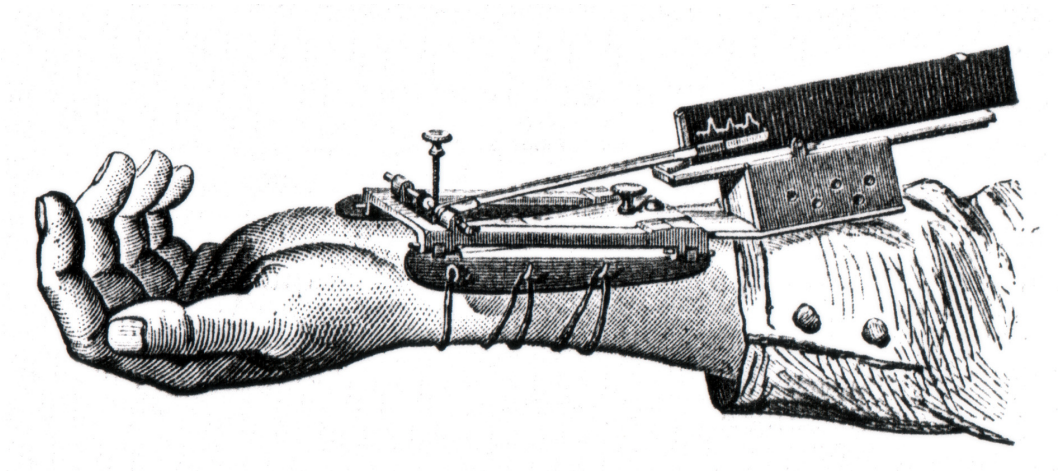

Figure 1.3: An illustration of the Sphygmograph designed by Marey. [Digital Image] (1860). In Wikimedia Commons. Retrieved May 5, 2023, from https://commons.wikimedia.org/wiki/File:Marey_Sphygmograph.jpg

and is still used today. In this practice, multiple fingers are applied at the skin along the artery allowing the trained physician to diagnose disease [7, 8]. The study of the pulse waveform also intrigued the famous Persian physician Ibn Sina, also known as Avicenna. During his cardiovascular studies in the 11th century he authored a book in Persian language on pulsology called Resaley-e-Ragshenasi. This treatise discussed the use of the pulse waveform for diagnosis, different parameters of the wave, and variability amongst individuals [9, 10].

A quantitative measurement of the pulse pressure waveform was first introduced in the 19th century. In 1821, Jean Leonard Marie Poiseuille first invented the mercury manometer to measure blood pressure which was used for this purpose in horses and dogs [11, 12]. This was an invasive method that requires puncturing and cannulation of the artery. In 1847, Carl Ludwig was the first to obtain a graphical view of the pulse waveform by redesigning Poiseuille's invention; he attached a pen to the mercury manometer and utilized a rotating cylinder to capture the waveform. The idea for a non-invasive technique to measure the pulse waveform was later proposed by Vierordt in 1854 which suggested to measure the necessary pressure to block pulsation in the artery. This effectively laid the basis for modern day applanation tonometry. Vierordt is attributed the invention of the sphygmograph, although, it was not till the 1860 when Etienne Jules Marey redesigned the functionality and shape factor of the sphygmograph that it gained worldwide attention (Figure 1.3) [13]. The design was further simplified by Samuel Siegfried Karl Ritter von Basch

Figure 1.4: Riva-Rocci's sphygmomanometer in use. [Digital Image] (1896). Wellcome Collection. Retrieved May 5, 2023, from https://wellcomecollection.org/works/fv6ckb78

that used an inflatable rubber bag as the sensing mechanism on the artery. Even with the elegant design, this device still proved to be too complicated to use in routine clinical settings. The big transition occurred when the Italian pathologist, Scipione Riva-Rocci, first introduced the cuff-based system for measuring blood pressure. In his 1896 publication in the Gazetta Medica di Torino, he discussed the new sphygmomanometer designed as a cuff-based system that wrapped around the arm. This system also provided a method to measure systolic blood pressure by pulse sensing at the radial artery (Figure 1.4). The full blood pressure measurement consisting of SBP and DBP using the cuff based system was only possible after Nikolai Korotkov (also known as Korotkoff) introduced the auscultatory technique. The surgeon in his 1905 communication reported that using a stethoscope on the brachial artery distal to the cuff would register ticking sound as cuff pressure was decreased from a fully occluded arterial state; the appearance and disappearance of these sounds marked the SBP and DBP pressures [13].

Modern day blood pressure cuffs have not changed much from their original invention. The auscultatory method, still often used in clinical practice, uses the same principles developed by Korotkoff in the 1900s. Current day systems also feature the

automatic oscillometric BP measurement method. This algorithmic approach looks at the variation of the cuff pulse amplitude throughout the cardiovascular pressure range. The cuff pulse amplitude creates an envelope over the pressure range in the system with a clear peak at MAP. SBP and DBP values are calculated from the MAP values based on proprietary algorithms which look at amplitude decay as the pressure is shifted from the maximum [14].

Much attention has also been given to the non-invasive measurement of the pulse pressure waveform. The current gold standard method is the tonometer, a handheld force sensor that is placed directly on the artery. Other methods rapidly gaining attention are centered around cuff-occlusive methods, that measure pressure changes in a cuff from radial arterial displacements. These systems measure a pressure time signal equivalent to that in the artery, giving more complete cardiovascular picture than just SBP and DBP.

Non-invasive systems only give a snapshot of the BP for an individual as measured at a peripheral artery. There are medical circumstances that require a continuous monitoring such as in an intensive care unit or that require localized pressure measurements such as in the diagnosis of heart failure. Direct BP monitoring via an invasive method is the most accurate and reliable method. Invasive BP methods consist of inserting a cannula or catheter directly in the arterial system for a direct measurement with a pressure transducer. A cannula is used for a localized continuous BP measurement at the brachial or radial artery. In contrast, pressure catheters are inserted via a peripheral artery and are guided via imaging to the measurement site which usually are the ascending aorta and the left ventricle. This procedure claims very high accuracy and precision given the direct and localized nature of the pressure measurement and is the current gold standard for diagnosis of heart failure and heart valve disease. This procedure is performed in a surgical room referred to as catheterization lab [15, 16].

Heart Sounds

The stethoscope is attributed to René Laennec, a physician at Necker-Enfantes Malades Hospital in Paris, who in 1816 invented a method to listen to the lungs without placing his ear on the chest. Indeed, the word stethoscope derives from greek, where 'stethos' means chest and 'skopein' means to observe. The first device was a tube wooden structure that would be placed on the patient's chest. He soon

realized that the tube with a membrane at its distal end amplified the sound providing a better auscultation [17].

In cardiology the stethoscope has gained much attention for its ability to auscultate the heart valvular movements during the cardiac cycle. Heart valves open and close generating very well defined sound signatures. Trained cardiologists using a stethoscope can identify conditions that are affecting valve operations and flow such as stenosis and regurgitation. In routine clinical practice different stethoscope placement positions are used to facilitate auscultation of the different valves.

Heart sounds are high-frequency pressure vibrations that are generated by the closing motion of heart valves. Closure of heart valves generates a two component sound ofter referred to 'lub-dub, lub-dub'. The first sound is generated by the closure of the mitral and tricuspid valve and the second sound is generated by the closure of the aortic and pulmonary valve. Heart valve disease alters these sounds by modifying closure mechanics and causing flow turbulence [18].

Electrical Activity

The first recordings of electrical activity with heart contractions was discovered by Dr. Carlo Matteucci in 1842, a professor of physics at The University of Pisa in Italy. But it was not till Dr. Willem Einthoven, a Dutch physiologist, that the Electrocardiogram (ECG) was born. Dr. Einthoven was able to capture the ECG wave with the PQRST deflections; the name electrocardiogram was first used in 1893 at the Dutch Medical Meeting. The turning point for the ECG system was with the invention of the new string galvanometer by Dr. Einthoven that allowed for higher sensitivity measurements and a practical system. The device at the time was big and bulky, utilizing buckets with electrolyte solution as electrodes (Figure 1.5) [19].

The ECG is a diagnostic test to non-invasively measure the electrical activity of the heart. The system consists of electrodes placed on the chest around the heart. This system can inform a trained cardiologist about the electrical signal propagation in the heart structure. An ECG system is typically used to detect conditions such as arrhythmia's, heart attacks, and heart conduction problems. The main components of the ECG signal are the P wave, the QRS complex and the T wave. The P wave marks the atrial depolarization and is the start of the cardiac cycle. The QRS complex indicated ventricular depolarization. Lastly, the T wave marks the re-polarization of the ventricle.

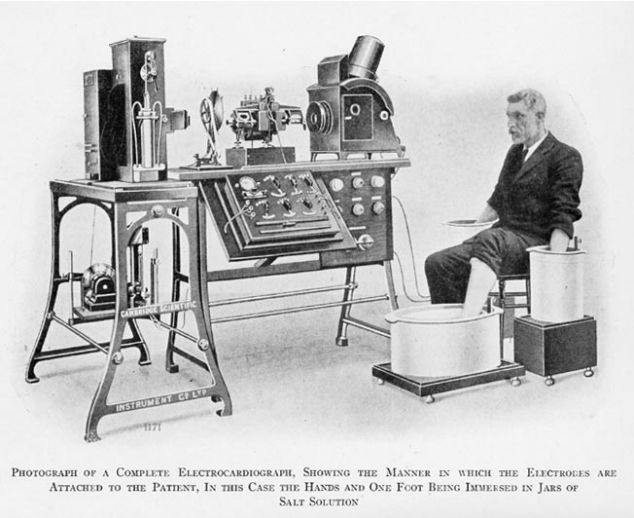

Figure 1.5: An early ECG system built by Cambridge Scientific Instrument Company dating back to 1911. This device was built following Dr. Einthoven's guidelines. [Digital Image] (1913). In Wikimedia Commons. Retrieved May 5, 2023, from https://commons.wikimedia.org/wiki/File:Willem_Einthoven_ECG.jpg

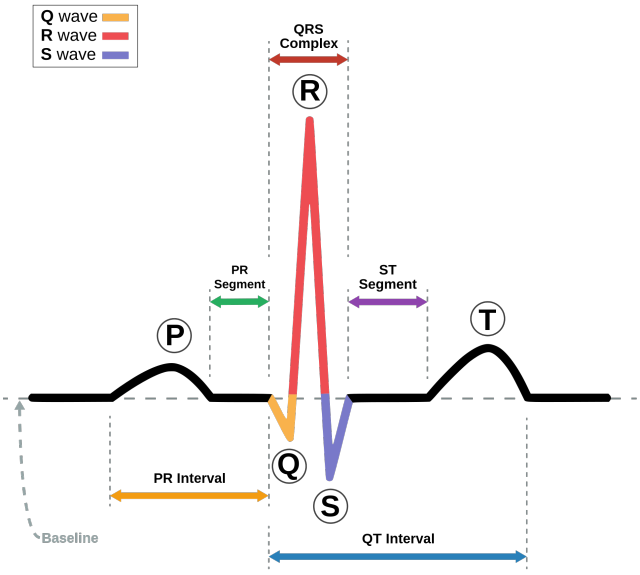

Figure 1.6: Labeled diagram of an ECG signal. [Digital Image] (2006). In Wikimedia Commons. Retrieved May 5, 2023, from https://commons.wikimedia.org/wiki/File:SinusRhythmLabels.svg

1.4 Non-Invasive Pulse Waveform Acquisition Systems

Tonometer

The tonometer is a handheld force sensor used for non-invasive pulse waveform measurement in arteries close to the skin surface. The tonometer high-fidelity pressure measurement is based on the law of Laplace which implies that at upon applanation of a radial surface, the external pressure is equal to the internal pressure

$$T = \frac{P_t r}{h} \quad \rightarrow \quad P_t = P_i - P_e = \frac{hT}{r} \quad \rightarrow \quad \lim_{r \to \infty} P_i = P_e$$

where T is the wall tension, P_t is the transmural pressure, r is the internal radius, h is the wall thickness, P_i is the internal pressure, and P_e is the external pressure. While the principle of this approach is valid, practical implementation is very complex. Successful applanation requires a solid base behind the artery to apply the necessary pressure and the artery must be fixed in place with the tonometer centered. These conditions are met only at the radial artery; at the brachial and carotid artery the soft surrounding tissue and breathing movements reduce measurement accuracy and repeatability. Yet for reasons previously specified, measurement at the radial artery is not ideal. From a fluid-dynamic perspective, the level of applanation will reduce the arterial lumen, inevitably changing the local pressure-flow relationships and therefore the measured waveform morphology. Furthermore, the tonometer requires cuff-based BP values as calibration since the sensor can only measure signal amplitude and does not have a reference point. Utilizing a tonometer requires specific training and suffers from high result variability between operators. For these reasons the tonometer has not reached wide-spread application in clinical practice and consequently limited the potential benefits of non-invasive PWA [20, 21].

Brachial Cuff

Occlusive cuff based systems are an alternative to the tonometer for non-invasive pulse waveform acquisition. These systems utilize the traditional brachial cuff with an inflate and hold approach: the cuff is inflated to a given pressure and is maintained for a period of time. The arterial radial expansions from the pressure wave cause proportional pressure pulsations in the cuff. These systems have the advantage of regulating the forcing condition at the artery, using the BP values from the oscillometric measurement allows to select subject-specific measurement conditions. The biggest limitation of these systems is the low signal resolution derived from the inherent limitations of pressure sensors. Given a form factor for a pressure sensor, there is an intrinsic opportunity cost between the signal resolution

and the operating range; signal resolution is typically a percentage of the full scale span of the sensor. In this measurement the sensors must operate in a 300 mmHg range yet the signals are about 1 mmHg in amplitude with important features being fractions thereof. Considering the automated and repeatable nature of the brachial cuff measurement, improvements to the system's signal resolution would highly stimulate the use in clinical practice.

Wearable Array Sensors

Much interest has been given to the continuous measurement of the non-invasive pulse pressure waveform as a diagnostic tool. The Tonometer and Occlusive Brachial Cuff cannot provide continuous measurement due to their modality of measurement. To this end, wearable pressure sensors that adhere to the skin at the measurement location have been developed. These systems use arrays of sensors for pulse wave monitoring that do not occlude the artery, therefore allowing continuous monitoring. In this domain multiple types of sensors have been developed, some of the most common include piezoresistive, capacitive, and piezoelectric. In general, all these sensors relies on an external perpendicular force to modify the spacing between plates in the sensor, yet the measurement is dependent on different principles [22].

Piezoresistive sensors measure the pulse waveform as the change in resistance across the device. These resistance across these sensors is governed by the following equation

$$R = \frac{\rho L}{A}$$

where R is the resistance, ρ is the material's resistivity, L is the length, and A is the contact area. Generally, as pressure is applied to the device from the radially pulsating artery, the deformations in the sensor cause changes in resistivity of the material. Alternatively, some sensor configuration also work upon geometrical configurations that modifying the length, L, or contact area, A, based on the applied pressure. Ultimately, these sensors result in a ΔR that is proportional to ΔP. Resistive sensors require battery power to operate[22].

Capacitive sensors measure the pulse waveform shape as the change in capacitance across the device. The sensor is composed of two electrode plates, an insulator and a substrate. Change in the separation distance between the two electrode plates

will result in a proportional change in capacitance, as dictated by

$$C = \frac{\varepsilon_0 \varepsilon_r A}{d}$$

where C is the capacitance, ε_0 is the space permittivity, ε_r is the dielectric material permittivity, A is the sensor area, and d is the electrode plate separation. These sensors are usually designed as parallel plates, in which a ΔC is proportional to a ΔP. Capacitive sensors require battery power to operate. [22]

Piezoelectric sensors work upon the principle that certain materials generate an electric potential in response to an applied external force. The sensor is constructed with two parallel electrode layers separated by a piezoelectric material layer. An externally applied force will modify the spacing between the layers and cause a charge accumulation in the electrode. These sensors are self powered as the change of state generates a current signal without an external source. Although, piezoelectric sensors only respond to dynamic changes as in the fixed state there is no current generated as no displacement occurs. The major limitation lies in the hardness of the materials required to fabricate these sensors which prevents flexilibity and good adherence to the skin [22, 23, 24, 25, 26].

Acoustic Based Sensors

Given the capacity of sound waves to propagate deep inside tissues, acoustic-based approaches have gained interest for imaging of the pulse pressure waveform. The viscoelastic nature of the arterial system allows to measure radial pulsations as a proportional surrogate of the pressure pulsations, where the proportionality is given by the material and structural properties of the artery. Ultrasound based systems have been designed to utilize time-of-flight and shear wave elastography techniques to measure the arterial radius as a function of time. As in the conventional ultrasound scanner, these systems send a focused acoustic beam and capture the reflected echoes. Acoustic beam reflections occur at the interfaces of two different materials, for example the interface between the arterial wall and the surrounding tissues. Therefore, this imaging modality will capture both the proximal and distal tube radius giving a measurement of the full tube diameter and wall thickness. These ultrasonic devices have been miniaturized and embedded in stretchable and wearable device to allow for continuous pulse waveform monitoring at the carotid, brachial, radial, and other accessible arteries [27]. These systems aim to overcome the limitations of tonometers and wearable array sensors which can only target superficial peripheral

arteries [23, 27, 28, 29]. Still these devices require waveform calibration with the conventional BP oscillometric cuff method to scale to physiological BP units.

Other Innovative Devices

The concepts presented above have also been integrated in other designs creating unique devices for the purpose of pulse waveform acquisition. In the studies cited below, these device have shown feasibility in capturing the pulse pressure waveform in a small population with optimal testing conditions. Further studies are required to validate their applicability in general population testing.

A piezoelectric sensor and a miniaturized cuff have been designed for application at the radial artery in the form of a pressure sensing watch. The cuff acts as the external force providing good contact between the skin and the piezoelectric sensor. The sensor measure the pulse waveform through the piezoelectric sensor and has a reference pressure from the miniaturized cuff [30].

A wearable microelectromechanical sensor is designed with a capacitive sensor and a gel bubble to be applied on the radial artery. The gel bubble helps project the force from the pulsating artery directly to the mechanical sensor. The sensor works on the capacitive principle described above. Multiple sensors, gel bubble and capacitive sensor, can be placed in a configuration along a wristband for continuous pulse waveform monitoring. The wristband serves to ensure good contact between the sensor and the skin [31].

The cuff-based principle of measuring the pulse pressure waveform as the pressure variation in a compliant air chamber from the radial pulsations is applied to a tonometer device shape factor. A handheld force force has an air chamber dome with a pressure sensor. The device's air chamber is then applied to a superficial artery such as the radial pulsations modify the pressure inside the device. This device reduces the tonometer results' dependence on the position of the force sensor probe on the artery. The additional benefit can also be seen from the air chamber conformation on the skin surface [32].

System Feature Comparison

The non-invasive pulse waveform acquisition systems listed above all address different aspects of the measurement that are currently limiting wide-spread application. In Table 1.1 is a summary of the different features that each design addresses. For this study, the cuff device addresses the majority of the limitations that the

authors believe have hindered the widespread application of the current systems. As such, the cuff device appears as the logical platform to improve.

Features	**Cuff Device**	**Tonometer**	**Wearable Sensors**	**Acoustic**
No Operator Training	X		X	
Known Applied Force	X			
Automated Measurement	X		X	
Calibration	X			
Measurement Repeatability	X		X	X
Continuous Modality			X	X

Table 1.1: Table compares the features between the major modalities of non-invasive pulse waveform acquisition measurement.

1.5 Thesis Outline

A cuff-based device for high-resolution pulse waveform acquisition at the brachial artery is presented in Chapter 2. This chapter gives an overview of the design process involved with the development of the device. The components and functionality are discussed in detail to facilitate the understanding of the results later in this thesis. Some preliminary tests are performed to show the repeatability and consistency of pulse waveform acquisition with cuff-based systems.

In Chapter 3 a mathematical characterization of the pLPF system is performed. This analysis derived a general model relating input to output pressure containing the system's time constant. Numerical analysis generated a frequency response curve that indicates the output signal gain given the input pressure frequency. Utilizing these models, the filter is designed specifically for pulse waveform acquisition at the brachial artery with a cuff-based system.

Chapter 4 discusses the results from the first human study performed at Caltech using the cuff-device. This study evaluated the device's accuracy and measurement repeatability in a young and healthy population. The high-resolution signal acquisition system captured pulse waveforms that clearly showed forward and reflected waves with all the typical features described in the literature.

Chapter 5 introduces the clinical study data that used the cuff-device in a catheter lab with human subject undergoing left-heart catheterization. This invasive data allowed to compare ascending aortic and cuff-based simultaneous pulse waveform signals. It is shown in this chapter that a cuff based device with sSBP hold pressure mode can accurately and reliably measure central cardiovascular health as measured with an invasive aortic catheter.

The clinical data analysis is taken one step further to evaluate the association between cuff based parameters and the left ventricular signal. In Chapter 6, we introduce a novel method for extraction of pressure-sound waveforms from the cuff measurement. The features in this waveform are shown to originate from aortic valve opening and closing pressure vibrations. A physiological link between these pressure vibrations and the LV contractile function is discussed and the data shows cuff-based pressure-sound waveforms parameters correlate with systolic and diastolic LV contractility.

In Chapter 7, the dynamic pressure fluctuations from the pulse waveform signal in the LV and cuff are compared. These pressure fluctuations originate from the heart-lung interaction during the breathing cycle. We observe the fluctuation magnitude of parameters in the LV catheter signal and in the cuff sSBP hold signal are linearly correlated.

References

[1] Connie W. Tsao et al. "Heart Disease and Stroke Statistics 2022 Update: A Report From the American Heart Association." In: *Circulation* 145.8 (Feb. 2022). DOI: 10.1161/cir.0000000000001052. URL: https://doi.org/10.1161/cir.0000000000001052.

[2] Anda Bularga et al. "Coronary Artery and Cardiac Disease in Patients With Type 2 Myocardial Infarction: A Prospective Cohort Study." In: *Circulation* 145.16 (Apr. 2022), pp. 1188–1200. DOI: 10.1161/circulationaha.121.058542. URL: https://doi.org/10.1161/circulationaha.121.058542.

[3] Anna Grosberg and Morteza Gharib. "Computational Models of Heart Pumping Efficiencies Based on Contraction Waves in Spiral Elastic Bands." In: *Journal of Theoretical Biology* 257.3 (Apr. 2009), pp. 359–370. DOI: 10.1016/j.jtbi.2008.11.022. URL: https://doi.org/10.1016/j.jtbi.2008.11.022.

[4] Anna Grosberg and Morteza Gharib. "A Dynamic Double Helical Band as a Model for Cardiac Pumping." In: *Bioinspiration &amp Biomimetics* 4.2 (May 2009), p. 026003. DOI: 10.1088/1748-3182/4/2/026003. URL: https://doi.org/10.1088/1748-3182/4/2/026003.

[5] Gustav G. Belz. "Elastic Properties and Windkessel Function of the Human Aorta." In: *Cardiovascular Drugs and Therapy* 9.1 (Feb. 1995), pp. 73–83. DOI: 10.1007/bf00877747. URL: https://doi.org/10.1007/bf00877747.

[6] Carmel M. McEniery et al. "Central Blood Pressure: Current Evidence and Clinical Importance." In: *European Heart Journal* 35.26 (Jan. 2014), pp. 1719–1725. DOI: 10.1093/eurheartj/eht565. URL: https://doi.org/10.1093/eurheartj/eht565.

[7] Kun-Chan Lan, Gerhard Litscher, and Te-Hsuan Hung. "Traditional Chinese Medicine Pulse Diagnosis on a Smartphone Using Skin Impedance at Acupoints: A Feasibility Study." In: *Sensors* 20.16 (Aug. 2020), p. 4618. DOI: 10.3390/s20164618. URL: https://doi.org/10.3390/s20164618.

[8] Yuh-Ying Lin Wang et al. "Past, Present, and Future of the Pulse Examination." In: *Journal of Traditional and Complementary Medicine* 2.3 (July 2012), pp. 164–177. DOI: 10.1016/s2225-4110(16)30096-7. URL: https://doi.org/10.1016/s2225-4110(16)30096-7.

[9] Mohammad M. Zareshenas et al. "Ibn Sina's Treaties on Pulsology." In: *International Journal of Cardiology* 146.2 (Jan. 2011), pp. 243–244. DOI: 10.1016/j.ijcard.2010.10.057. URL: https://doi.org/10.1016/j.ijcard.2010.10.057.

[10] Mohammad M. Zarshenas and Arman Zargaran. "A Review on the Avicenna's Contribution to the Field of Cardiology." In: *International Journal of Cardiology* 182 (Mar. 2015), pp. 237–241. DOI: 10.1016/j.ijcard.2014.12.145. URL: https://doi.org/10.1016/j.ijcard.2014.12.145.

[11] S P Sutera and R Skalak. "The History of Poiseuille's Law." In: *Annual Review of Fluid Mechanics* 25.1 (Jan. 1993), pp. 1–20. DOI: 10.1146/annurev.fl.25.010193.000245. URL: https://doi.org/10.1146/annurev.fl.25.010193.000245.

[12] Mary Gavaghan. "Vascular Hemodynamics." In: *AORN Journal* 68.2 (Aug. 1998), pp. 211–226. DOI: 10.1016/s0001-2092(06)62515-5. URL: https://doi.org/10.1016/s0001-2092(06)62515-5.

[13] J Booth. "A Short History of Blood Pressure Measurement." en. In: *Proc. R. Soc. Med.* 70.11 (Nov. 1977), pp. 793–799.

[14] Charles F Babbs. "Oscillometric Measurement of Systolic and Diastolic Blood Pressures Validated in a Physiologic Mathematical Model." In: *BioMedical Engineering OnLine* 11.1 (2012), p. 56. DOI: 10.1186/1475-925x-11-56. URL: https://doi.org/10.1186/1475-925x-11-56.

[15] Xavier Bobbia et al. "Ultrasound Guidance for Radial Arterial Puncture: A Randomized Controlled Trial." In: *The American Journal of Emergency Medicine* 31.5 (May 2013), pp. 810–815. DOI: 10.1016/j.ajem.2013.01.029. URL: https://doi.org/10.1016/j.ajem.2013.01.029.

[16] Michelle G. Glowny and Frederic S. Resnic. "What to Expect During Cardiac Catheterization." In: *Circulation* 125.7 (Feb. 2012). DOI: 10.1161/circulationaha.111.025916. URL: https://doi.org/10.1161/circulationaha.111.025916.

[17] R T H 'laennec. *A Treatise on the Diseases of the Chest and on Mediate Auscultation (1835).* New York; Philadelphia: Desilver, Thomas & Co.

[18] Morton E. Tavel. "Cardiac Auscultation." In: *Circulation* 113.9 (Mar. 2006), pp. 1255–1259. DOI: 10.1161/circulationaha.105.591149. URL: https://doi.org/10.1161/circulationaha.105.591149.

[19] Majd AlGhatrif and Joseph Lindsay. "A Brief Review: History to Understand Fundamentals of Electrocardiography." In: *Journal of Community Hospital Internal Medicine Perspectives* 2.1 (Jan. 2012), p. 14383. DOI: 10.3402/jchimp.v2i1.14383. URL: https://doi.org/10.3402/jchimp.v2i1.14383.

[20] Gary M. Drzewiecki, Julius Melbin, and Abraham Noordergraaf. "Arterial Tonometry: Review and Analysis." In: *Journal of Biomechanics* 16.2 (Jan. 1983), pp. 141–152. DOI: 10.1016/0021-9290(83)90037-4. URL: https://doi.org/10.1016/0021-9290(83)90037-4.

[21] Hiroshi Miyashita. "Clinical Assessment of Central Blood Pressure." In: *Current Hypertension Reviews* 8.2 (June 2012), pp. 80–90. DOI: 10.2174/157340212800840708. URL: https://doi.org/10.2174/157340212800840708.

[22] Keyu Meng et al. "Wearable Pressure Sensors for Pulse Wave Monitoring." In: *Advanced Materials* 34.21 (Mar. 2022), p. 2109357. DOI: 10.1002/adma.202109357. URL: https://doi.org/10.1002/adma.202109357.

[23] Zhiran Yi, Wenming Zhang, and Bin Yang. "Piezoelectric Approaches for Wearable Continuous Blood Pressure Monitoring: A Review." In: *Journal of Micromechanics and Microengineering* 32.10 (Aug. 2022), p. 103003. DOI: 10.1088/1361-6439/ac87ba. URL: https://doi.org/10.1088/1361-6439/ac87ba.

[24] Huimin Li et al. "Wearable Pulse Wave Sensor and Interface for Real-Time Dynamic Blood Pressure Monitoring." In: *2021 IEEE International Electron Devices Meeting (IEDM)*. Ieee, Dec. 2021. DOI: 10.1109/iedm19574.2021.9720662. URL: https://doi.org/10.1109/iedm19574.2021.9720662.

[25] Yan-Yun Liu, Yu-Xiang Lv, and Hai-Bin Xue. "Intelligent Wearable Wrist Pulse Detection System Based on Piezoelectric Sensor Array." In: *Sensors* 23.2 (Jan. 2023), p. 835. DOI: 10.3390/s23020835. URL: https://doi.org/10.3390/s23020835.

[26] Jie Wang et al. "Wearable Multichannel Pulse Condition Monitoring System Based on Flexible Pressure Sensor Arrays." In: *Microsystems &amp Nanoengineering* 8.1 (Feb. 2022). DOI: 10.1038/s41378-022-00349-3. URL: https://doi.org/10.1038/s41378-022-00349-3.

[27] Chonghe Wang et al. "Monitoring of the Central Blood Pressure Waveform Via a Conformal Ultrasonic Device." In: *Nature Biomedical Engineering* 2.9 (Sept. 2018), pp. 687–695. DOI: 10.1038/s41551-018-0287-x. URL: https://doi.org/10.1038/s41551-018-0287-x.

[28] Ronny X. Li, William Qaqish, and Elisa E. Konofagou. "Performance Assessment of Pulse Wave Imaging Using Conventional Ultrasound In Canine Aortas ex vivo and Normal Human Arteries in vivo." In: *Artery Research* 11.C (2015), p. 19. DOI: 10.1016/j.artres.2015.06.001. URL: https://doi.org/10.1016/j.artres.2015.06.001.

[29] Nicole Di Lascio et al. "Ultrasound-based Pulse Wave Velocity Evaluation in Mice." In: *Journal of Visualized Experiments* 120 (Feb. 2017). DOI: 10.3791/54362. URL: https://doi.org/10.3791/54362.

[30] Xiaoxiao Kang et al. "A Wearable and Real-Time Pulse Wave Monitoring System Based on a Flexible Compound Sensor." In: *Biosensors* 12.2 (Feb. 2022), p. 133. DOI: 10.3390/bios12020133. URL: https://doi.org/10.3390/bios12020133.

[31] Matti Kaisti et al. “Clinical Assessment of a Non-Invasive Wearable MEMS Pressure Sensor Array For Monitoring of Arterial Pulse Waveform, Heart Rate and Detection of Atrial Fibrillation.” In: *npj Digital Medicine* 2.1 (May 2019). DOI: 10.1038/s41746-019-0117-x. URL: https://doi.org/10.1038/s41746-019-0117-x.

[32] David Zambrana-Vinaroz et al. “Non-Invasive Device for Blood Pressure Wave Acquisition by Means of Mechanical Transducer.” In: *Sensors* 19.19 (Oct. 2019), p. 4311. DOI: 10.3390/s19194311. URL: https://doi.org/10.3390/s19194311.

Chapter 2

CUFF DEVICE FOR HIGH FIDELITY NON-INVASIVE PULSE WAVEFORM ACQUISITION AT BRACHIAL ARTERY

"Scientists study the world as it is,
engineers create the world that never has been."
— Theodore von Kármán

This chapter is partially based on the work in the following publication:

Alessio Tamborini and Morteza Gharib. "A pneumatic low-pass filter for high-fidelity cuff-based pulse waveform acquisition." Under Review. N.D..

2.1 Introduction

Non-invasive PWA is a valuable diagnostic tool for assessing cardiovascular health. Yet capturing a non-invasive accurate representation of the pulse pressure waveform has proven to be a challenge. In the past, methodologies for PWA helped characterize cardiovascular features such as pulse wave velocity and augmentation index to inform therapeutic decisions better [1, 2]. The current clinical gold standard for non-invasive pulse waveform measurement is the tonometer, a handheld force sensor to measure arterial radial pulsations. Operation of tonometers on the peripheral artery requires arterial applanation: flattening of the arterial wall such that only internal pressure variations are measured. Overall, this process is time-intensive and needs a trained clinician. From a fluid dynamic perspective, the force applied at the artery compressing the walls influences local pressure-flow relationships. Inconsistency in this process impacts the repeatability of the results. For direct measurement of central pressure, a tonometer also requires the usage of the

brachial cuff for BP calibration [3, 4]. These shortcomings severely limit the clinical application of PWA.

An alternative solution for capturing the pulse waveform is to utilize the brachial cuff with inflate and hold capabilities [5, 6, 7, 8, 9, 10, 11]. The waveform is autonomously measured by maintaining the cuff at a constant pressure around the arm; the brachial artery radial pulsations will generate pressure fluctuations in the cuff proportional to the actual pulse waveforms. Controlling the cuff pressure ensures that the forcing condition is known and consistent throughout the measurement. The main shortcoming of the above cuff-based pulse waveform acquisition is that the pressure sensor resolution is spread over the signal range, which consists of mean and pulsatile components. To address this issue, one iteration of the traditional cuff device utilizes a valve and multiple pressure sensors to capture a base pressure as a measurement reference [12]. In this respect, the valve closure upon reaching the target-pressure would effectively create a constant pressure reservoir. A high-resolution differential pressure sensor measures the difference between the signal and reservoir, effectively capturing the pulsatile component. While this methodology captures the small amplitude signals in an extended measurement range, it requires three pressure sensors to be utilized. Considering the system does not measure the mean pressure dynamically, any pressure decays that frequently occur in pneumatic systems must be corrected by active valve control. Such dynamic opening and closing of the valve result in data losses and discontinuity within the system [12].

In this chapter, we outline a cuff-based device for pulse waveform acquisition that tackles the issues of signal resolution mentioned above. We propose a fluid-dynamic method to dynamically monitor mean pressure to isolate the pulse waveform using a passive pneumatic low pass filter and a single high-resolution differential pressure sensor. The combination of the cuff-based acquisition system and the enhanced resolution from the method proposed herein generates a device that autonomously and non-invasively captures high-resolution pulse waveforms in a repeatable manner. This section of my thesis guides through the design of an autonomous device for pulse waveform acquisition at the brachial artery.

2.2 Device Components

The device described herein is a cuff-based system with oscillometric algorithms for BP measurement and inflate and hold capabilities for non-invasive pulse

waveform acquisition. The electrical and pneumatic components of the device are contained within a medical-grade enclosure.

The electrical components perform the measurement sequence, acquiring and transmitting the data. The main electrical components include the OEM NIBP module, an Arduino nano, a differential pressure sensor, a digital-to-analog converter, and a relay. The device is powered using a medical grade 12V power supply with a maximal current rating of 1.5 amps. The 12V powers the NIBP module, the voltage is stepped to 6V to power the Arduino, and the 5V output from the Arduino is used for the remaining components. Data out is in analog format from 0V to 5V at an update speed of 1kHz.

The NIBP OEM module is a programmable BP measuring unit with tourniquet capabilities from PAR Medizintechnik. This module is designed as a subsystem upon which a medical device is built. The BP measurement is performed using the oscillometric method in inflation (default) or deflation mode and outputs the results in the form of SBP, DBP, MAP, and HR. The tourniquet mode allows the user to define a target pressure and hold time for the inflate and hold method; the inflate and hold method consists of inflating the brachial cuff to a specified pressure and maintaining this pressure for a set time. Bidirectional connection with the board is performed via serial asynchronous communication with a baud rate of 4800 Baud. This subsystem is certified for basic electrical safety according to the standard EN 60601-1 and EN 60601-2 and for safety requirements of the BP measurement IEC 80601-2-30.

The device uses an Arduino Nano as the central micro-controller that runs the measurement sequence. The Arduino algorithm is responsible for communication with the NIBP module, error checking, and outputting the results to the analog DAQ. Communication of integer based values from the NIBP module and the arduino to the analog DAQ requires a consistent scaling method, herein referred to as pressure-voltage encoding. The pressure-voltage encoding equation is $V_{out} = \frac{x}{300} * 5V$ where x is the number to be encoded as a voltage. The 300 factor comes from the maximal number that can be reported, the maximal cuff BP value, and the 5V factor comes from the operating voltage. The NIBP module operation requires communication in both directions in the form of ASCII characters. The oscillometric BP measurement results from the NIBP module are read from the Arduino and outputted as analog voltages using the following pressure-voltage encoding.

The differential pressure sensor used for the high-resolution measurement is the Honeywell HSCDRRN002NDAA5 sensor. This is a differential pressure sensor with ±2 inH20 (3.73 mmHg) operating range and a 0.03% FSS resolution, which is a 0.002 mmHg resolution. The sensor supply voltage is of 5V and output is analog from zero to supply voltage. While the sensor is analog, the onboard electronics convert the signal from analog to digital to analog thus the sampling frequency is limited at 1000 Hz. At a zero-pressure differential the sensor output will be half the supply voltage. A positive pressure difference in the measurement port will generate a voltage above half supply and a negative pressure difference will generate a voltage below half supply.

The pneumatic components are responsible for the pulse-sensing mechanism of the device. The main components include the BP brachial cuff, the connective tubing, the RC filter, and the stainless-steel medical grade quick connector for the cuff. The device uses tubing with an elasticity of 24 MPa, 1.59 mm internal radius, and 1.59 mm wall thickness for external connections. For internal connections, the device uses tubing with an elasticity of 24 MPa, 0.79 mm internal radius, and 0.79 mm wall thickness. The brachial cuff used with this device is the AND Medical Wide Range Replacement Cuff that accommodates arm circumferences between 22 cm to 42 cm (Ref: UA420).

2.3 Device Electronics

The supply voltage for the device is a 18W 12V 1.5A Medical USA plug. The supply voltage directly powers the NIBP board. The 12V input voltage is then stepped down to 6V to serve as the input voltage for the Arduino Nano board. The other electrical components on the board are 5V rated are all powered from the 5V output pin on the Arduino Nano.

The device is fully operated from a wired remote control. The remote is connected to the device via a 4 pin Hirose connector. The remote control has two buttons: start (green) and abort (red). The start button is responsible for initiating the measurement sequence; it is wired as a pull-up resistor and the Arduino script is waiting to read a high value on input pin 4 as an input. The abort button is a kill switch for the device, temporarily cutting the connection between the device and power, effectively resetting the entire measurement process. Upon pressing the abort button, the entire system deflates, and initial conditions are reset. The design is such that the device is powered only when the remote is attached.

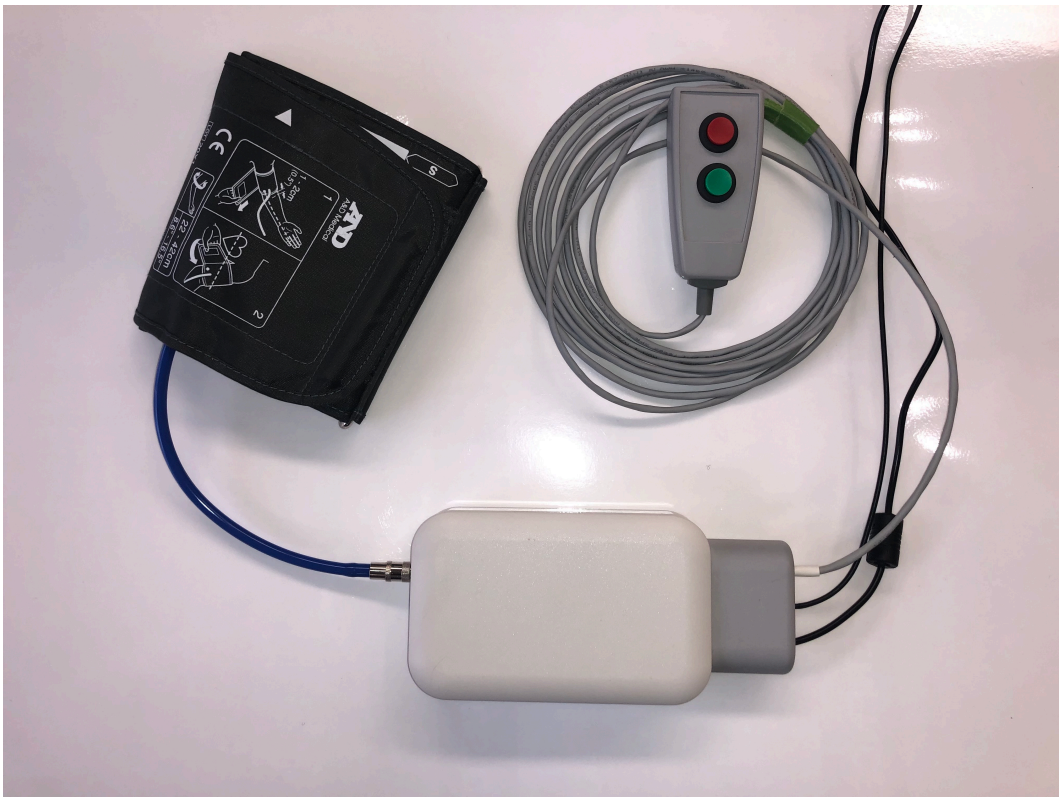

Figure 2.1: Picture of the Cuff-Based device illustrating the medical enclosure with the electronics, the wired remote and the cuff.

The output of the device is of analog format from 0V to 5V, which feeds directly into a the DAQ unit with a BNC cable. The system has two separate outputs that need to feed into a single DAQ channel: the first from the pressure sensor and the second from the NIBP module. A relay switch was used to switch between the two outputs. The Arduino controls the direction of the relay switch during the measurement. The output from the pressure sensor is directly sent to the relay. The output from the NIBP module BP measurement is first encoded using the equation above and then converted to a voltage using a DAC to send to the DAQ.

Data Acquisition System

The device data output is of the analog format in the 0-5V range with a max update speed of 1000Hz. The data output is via a wired BNC cable. In this thesis, the data acquisition from this device is performed on the AD Instrument PowerLab 26 Series system with the LabChart software. This is a high-speed sampling DAQ with 16-bit resolution on all gain ranges; the systems provide 2, 4, 8 simultaneous input channels based on the model. AD Instruments has medical grade instruments for

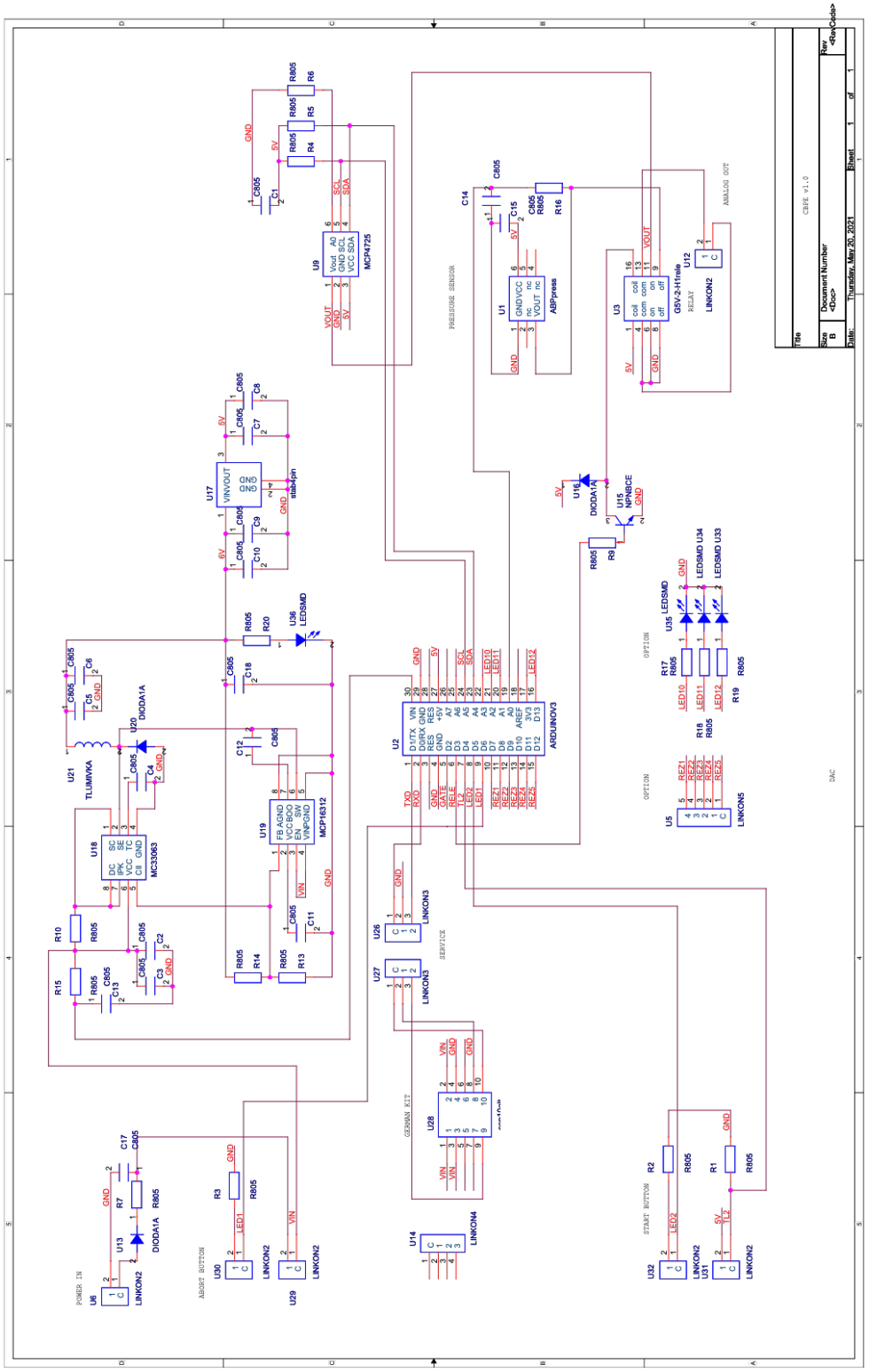

Figure 2.2: Electronic schematics of cuff device.

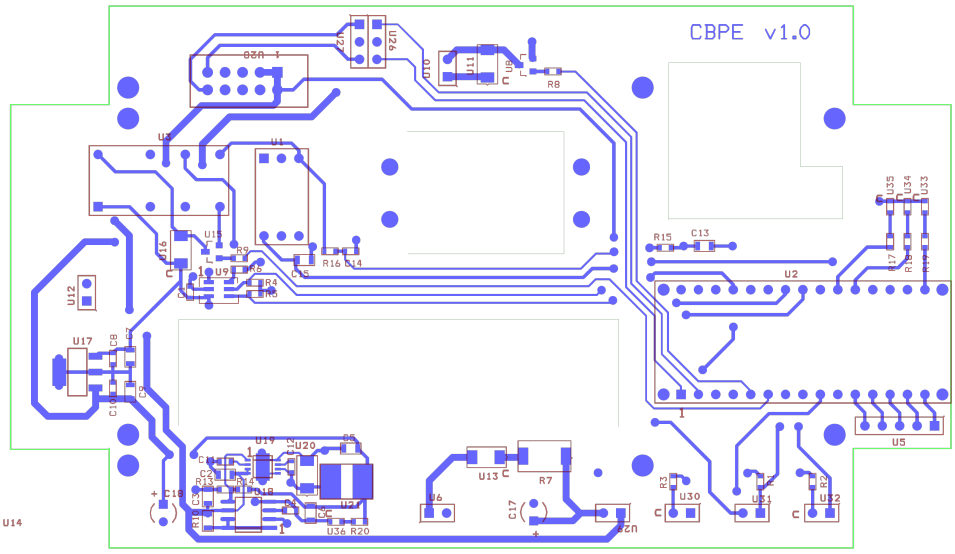

Figure 2.3: PCB layout of cuff device.

ECG and invasive BP measurement that make this an ideal platform for simultaneous measurement from multiple devices.

2.4 Device Pneumatics

The pneumatics of the system create connections between the NIBP module, the pressure sensor, the pneumatic filter, the cuff connector, and the cuff. Device design was optimized to reduce wave propagation time such that the measured signal is a closer representation of the instantaneous pressure in the arm; this was achieved by minimizing the distance between the cuff and the differential pressure sensor and using high durometer value tubing for pneumatic connections. The NIBP module contains several pneumatic elements fundamental for the operation of the device, these include the air pump, the release valves, and the absolute pressure sensors. Figure 2.4 shows a macroscopic overview of the pneumatic layout of the device.

The Young's modulus of the tubing was experimentally calculated for all three linearly elastic tubes used in the device. Tube 1 is used with 1/8 in barbed fitting connections, these are found between the cuff and the quick connector and between the NIBP module and the quick connector. Tube 2 is used for 1/16 in barbed fitting, these are found for connections internal to the device. Lastly, tube 3 is the compliant element in the pneumatic filter, more details on this tubing component

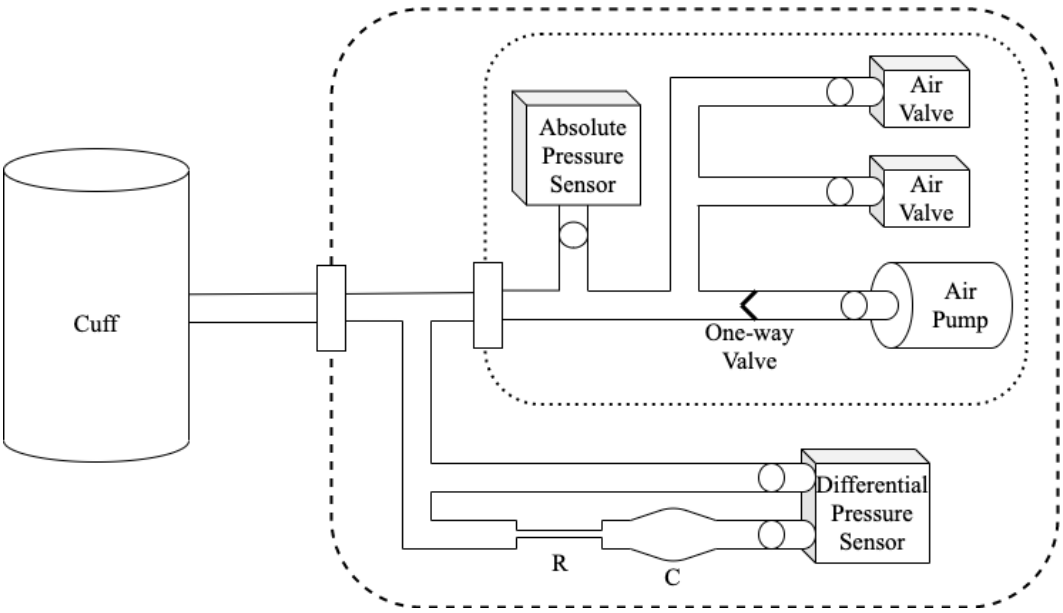

Figure 2.4: The pneumatic layout of the device. The elements enclosed in the dotted line represent the ParBerlin NIBP UP module. The elements enclosed in the dashed line are the pneumatic components within our device. The cuff connects on the outside of the device. Note that multiple tubing sizes are used, which have not been accounted for in this schematic.

will be discussed later. In the device all tubing is axially constrained, thus the strain in the tube will occur in the circumferential direction. It is well known that tube properties are distinct between the circumferential and axial directions. Thus, to quantify the circumferential Young's modulus of the tubing, the tubing is cut open on the circumference and stretch along this direction. Testing has been performed using the Instron machine Model 5943. The results for the linear strain-stress Instron test is shown in Figure 2.5. The calculated Young's Modulus, E, in MPa for the three tubes in the 1-7.5% strain range is: tube 1 22.0 MPa, tube 2 24.2 MPa, and tube 3 is 1.4 MPa. Typically, the non-linearities at high deformations are part of the plastic deformation of linearly elastic material. Although in this experiment these originate from the slippage of the tubing in the clamps as not enough grip could be provided, no plastic deformation was observed in the test elements.

To estimate the signal delay between the cuff and the recorded signal we calculate the total path length from the cuff to the sensor which is of 304 mm, of which 212 mm is in tubing 1 and 92 mm is in tubing 2. Wave propagation speed in the device is dependent on the speed of pressure waves in air, for the purposes of this application it can be estimated with the speed of sound in air of

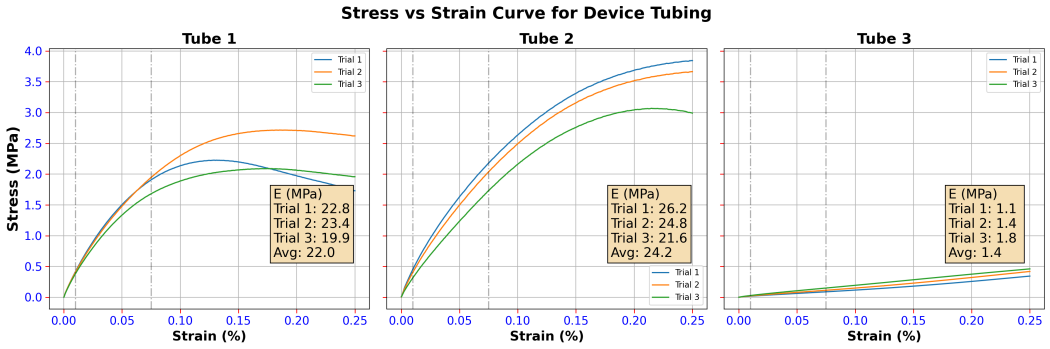

Figure 2.5: Stress strain curve up to 25% strain for three main pneumatic tubes used in the cuff-device.

343 $\mathrm{m\,s^{-1}}$. Therefore, the travel time for pressure wave propagation from cuff to measurement port is estimated to about 1 milliseconds. This number will only affect time intervals measured between waveform parameters in the cuff and another measurement modality. Most importantly, the time delay is constant for the device and therefore a systematic error should only be expected if applied in the device-to-device time delay comparisons with other devices. To all practical purposes, we do not expect this time delay to be a limitation of the device.

	Tube 1	**Tube 2**	**Tube 3**
ID (mm)	3.18	1.59	1.59
OD (mm)	6.35	3.18	3.18
h (mm)	1.59	0.79	0.79
Shore A	75A	80A	50A
E (MPa)	22.0	24.2	1.4

Table 2.1: Summary of the material properties of the tubes used along the path from cuff to pressure sensor measurement port. Note that diameters, thickness, and shore A readings are reported per the manufacturer specifications.

2.5 Sensor Principles

In pressure sensors, given a form factor, there exists a trade-off between resolution and operating range: as the operating range of a pressure sensor increases the resolution decreases. The measurement of the non-invasive pulse pressure waveform at the brachial artery using an arm cuff incurs the challenge of a small signal in a large operating range (Figure 2.6). The brachial arm cuff signal has a static component, the absolute cuff pressure, and a dynamic component, the brachial artery pulsations. Typical dynamic signal amplitudes are of 1 to 5 mmHg with funda-

mental waveform characteristics that are a fraction of the amplitude. On the other hand, the measurement range, static component, is up to 300 mmHg. Conventional commercial board-mount pressure sensors have a resolution of 0.03% FSS, which if spread over the entire operating range would result in a resolution of 0.09 mmHg which is insufficient for PWA. Our approach is to isolate the dynamic portion of the signal using fluid dynamic principles such that the range of the pressure sensor can be focused on the valuable signal components.

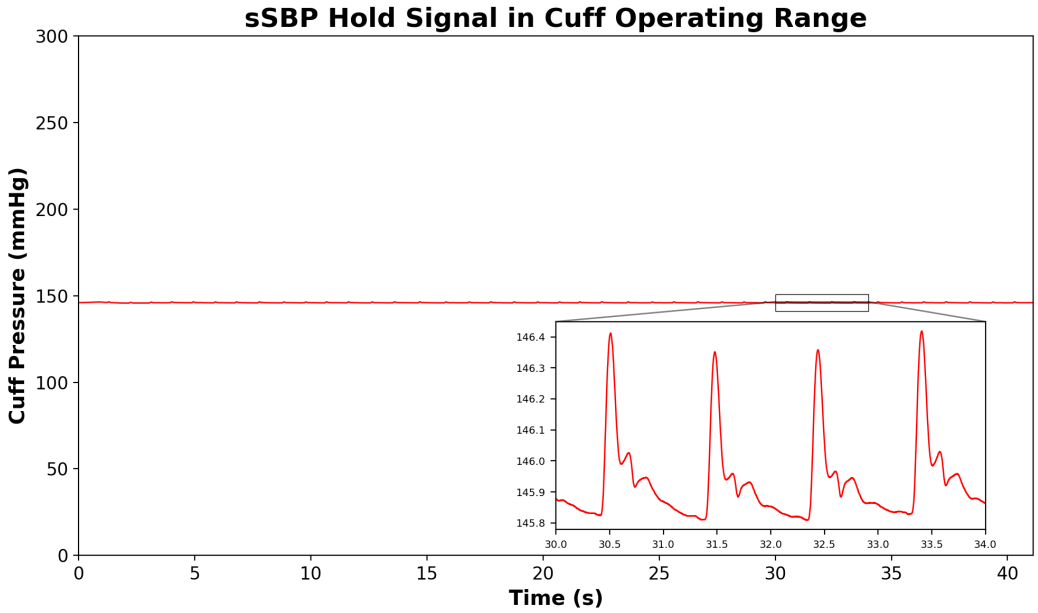

Figure 2.6: Small signal in large measurement range problem. Figure shows the relative amplitude of the signal versus the measurement range in the sSBP hold pressure. Inset is a zoomed in visualization of the signal shown.

Our high-fidelity pulse waveform acquisition device combines a passive pLPF with a high-resolution differential pressure sensor to capture the small signal in a large operating range. This system does not require active control as the filter behavior is fully determined by fluid dynamic principles. The filter characteristcs are application specific and are calculated using our modeling equations presented in Chapter 3.

A differential pressure sensor outputs the pressure difference between measurement and reference port. In our device, the differential pressure sensor measures the difference between the full signal (static and dynamic components) and the signal mean (static component). The resulting output signal from the sensor is only the dynamic component. The challenge is to obtain the static component from a time

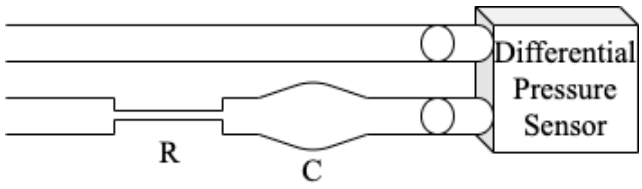

Figure 2.7: Pneumatic Layout of pLPF. Figure shows a schematic of the composition of the pLPF and the differential pressure sensor. In the pressure sensor, the top port is the measurement port and the bottom port is the reference port.

dependent oscillatory signal. This is accomplished using a proprietary system that acts as fluid dynamic low-pass filter, herein referred to as pLPF, which is directly connected to the reference port of the pressure sensor.

The pLPF is composed of a resistive element and a capacitive element connected in series (Figure 2.7). The resistive component acts as a resistance by limiting pressure-driven flow rate across its element, this element will be referred to as R. The capacitive element acts as a capacitance by storing the mass from element R in the form of pressure, this element will be referred to as C. Given the device is operating in air, the capacitive element sees contributions from both tube elasticity as well as fluid compressibility. Together the R and C elements are designed to reduce and store airflow such that the output pressure will only be affected by sustained pressures and not by transient oscillatory perturbations. The combination of these elements resembles an RC pneumatic filter. The R component is made from a rigid wall capillary tube. The C component is made up of a fixed volume and a compliant volume. The compliant volume is from an elastic tube and the fixed volume is from rigid tubing and connectors which have cylindrical internal volume. The compliant tube is restricted in axial motion. The pLPF component properties are summarized in Table 2.2 below.

2.6 Device Measurement

Measurement Structure

The measurement from the cuff-based devices has two main segments: the oscillometric BP measurement and the tourniquet mode for the inflate and hold modality. The tourniquet phase performs multiple inflate and hold measurements utilizing at patient specific pressure conditions. The sequential nature of the measurement structure allows to have subject-specific values for the tourniquet mode. The measurement has a total duration of approximately 120 seconds, the variability

Variable	Value
Element R	
$r_0(\mu m)$	31.5
L_0 (mm)	30
Element C	
Compliant	
r_0 (mm)	0.8
L_0 (mm)	40
h_0 (mm)	0.8
E (MPa)	1.4
Fixed	
r_0 (mm)	0.8
L_0 (mm)	36

Table 2.2: The geometrical and structural properties of the RC filter elements.

comes from the length of the BP measurement. The entire measurement duration is capped at 180 seconds to comply with regulatory safety standard. The device is designed to constantly gives the operator feedback, being familiar with the measurement structure will allow the operator to understand the measurement stage.

The first measurement segment performs a conventional oscillometric BP measurement. The NIBP module has onboard algorithms to perform the oscillometric measurement with inflation or deflation mode: inflation mode measures BP during cuff inflation and deflation mode measures BP during cuff deflation. The device is programmed to perform the measurement in inflation mode, upon failure of the inflation mode it automatically resorts to deflation mode. Inflation mode on average has a significant time advantage, this factor could be critical depending on the application. The manufacturer claims the results are equivalent between the two modes, in-house testing has also been performed to validate these results. During the first segment the device initiates the oscillometric BP measurement, the pump will activate and inflates the cuff. An encoded voltage representing the nominal cuff pressure is outputted to the DAQ at refresh rate of 5Hz during cuff inflation to inform the user of the current state. The same argument is valid if the device deviates to deflation mode. Upon BP measurement completion, the SBP, DBP, MAP, and HR are output in encoded voltage format. The first measurement segment terminates once the output voltage returns to zero after communication of the BP results. The first measurement segment has an expected duration between 20 second to 40 seconds, depending on the measurement mode and the subject's BP value.

The second measurement segment consists of the tourniquet mode for pulse waveform acquisition. In tourniquet mode the NIBP module inflates the cuff to a specified pressure and holds constant for a set amount of time. The current measurement is structured to have three sequential holds at incremental pressure values of DBP, MAP, and sSBP for a duration of 30, 20, and 40 second, respectively. The proposed measurement structure will test different forcing conditions on the arterial wall altering the local pressure-flow relationship for different waveform morphology. Each hold pressure will output three different signals: the target inflation pressure, the raw high-resolution waveform, and the nominal cuff pressure. The target inflation pressure is a signal outputted at the beginning of the measurement to indicate the inflation pressure, this signal is pressure-voltage encoded. The high-resolution waveform is outputted directly from the differential pressure sensor to the DAQ in real time at 1000 Hz. Lastly, the nominal cuff pressure comes from the NIBP module at a rate of 5 Hz; during the measurement, the Arduino stores the nominal cuff pressure reported as integer values at 5Hz by the NIBP module and upon hold termination, these values are outputted using the pressure-voltage encoding at a time compression factor of 20x (see Figure 2.8 for reference).

Idle State

The powering of the device initiates the Arduino setup function that contains all the status checks for the device. During this period, a constant voltage of 2.5V is outputted to the DAQ. Upon completion of the setup, the Arduino enters an IDLE state in which it is waiting for the start measurement command. During this phase, a square wave oscillating between 2.0V and 2.5V at a rate of 0.5Hz is sent to the DAQ. This signal informs the operator that the device is ready for measurement.

Error Handling

Device operation might incur errors that require the operator's immediate attention. The NIBP has inbuilt a status communication that can be used to infer the nature of the error. Upon our software detecting a module error, the system will evaluate the nature of the error. If the detected error is software based, the system will attempt a module reset. Upon completion if the error is still present, the device will enter error mode and output the error signal. If the detected error is hardware based, the system will directly output the error signal. The error signal is a 0V to 5V triangle wave with a rate of 0.5 Hz.

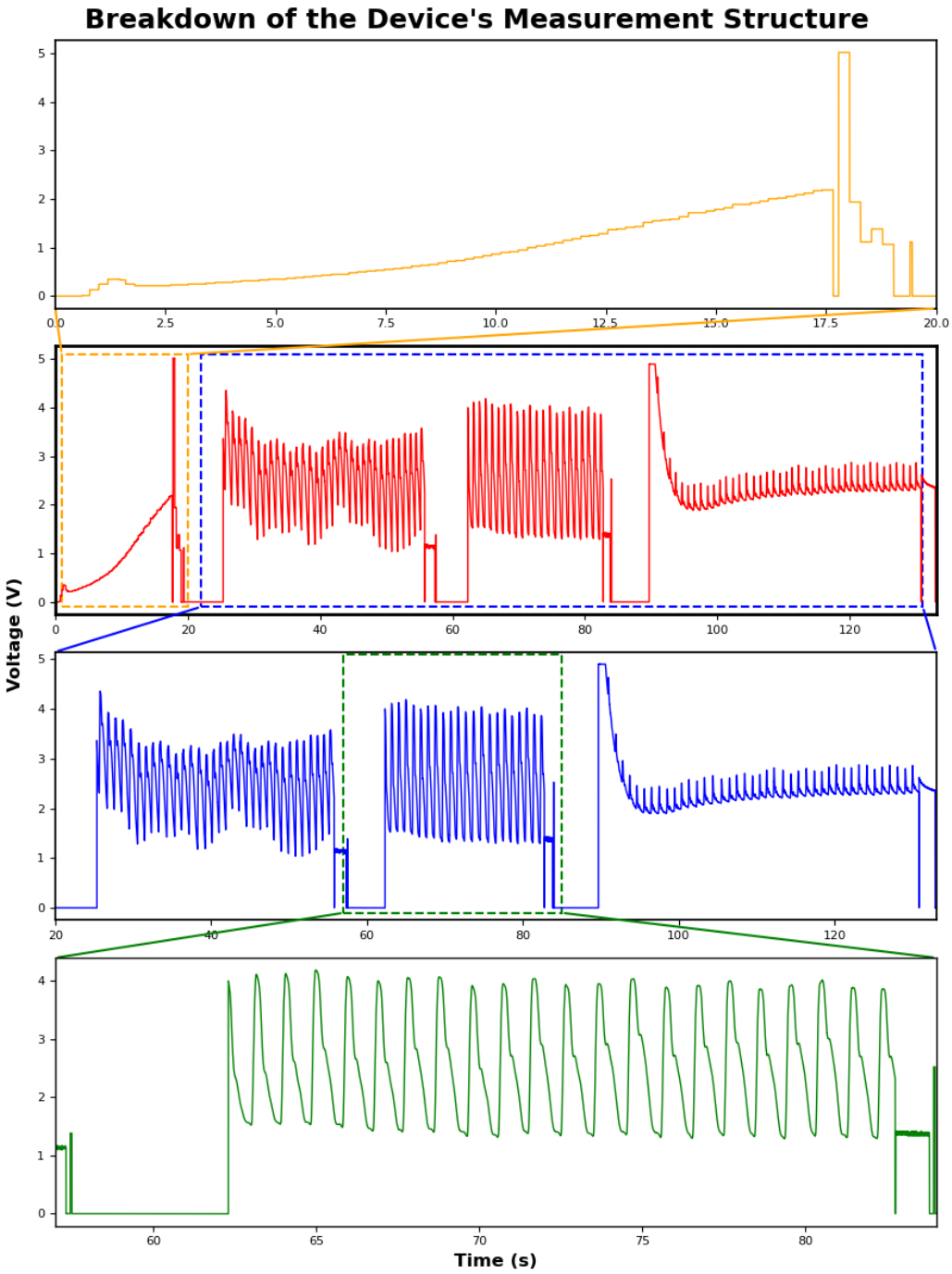

Figure 2.8: Device measurement structure. (Row 1) Oscillometric BP measurement showing pressure readout followed by pressure-voltage encoded results. (Row 2) Full measurement. (Row 3) Pressure hold segments of DBP, MAP, and sSBP. (Row 4) MAP pressure hold, highlighting target pressure, high-resolution signal and nominal cuff pressure.

Subject Preparation

BP measurement and pulse waveform acquisition are extremely sensitive to body positioning and state. A consistent subject preparation is necessary to ensure measurement quality and repeatability. Measurements will be performed in supine position with a five-minute rest period with no talk or external stimuli. Arms will be positioned along the body, hands will be maintained open, and legs will lie down without crossing. The measurement is performed on the left arm as the left subclavian artery directly branches from the ascending aorta. The cuff must be in direct contact with the skin. The cuff will be placed two centimeters from the elbow crease with the tube pointing towards the hand. The cuff should be rotated such that the tubing follows the upper inner side of the arm, the location closest to the brachial artery. Cuff must wrap firmly around the arm without blocking the circulation; the device operator should be able to slide two fingers between cuff and arm. The device will be connected to the cuff and can lie on the testing bed next to the subject or attached to the cuff. For the entire measurement duration, the subject will be asked to maintain regular breathing pattern and avoid any movement. If during measurements, the subject experiences discomfort the measurement will be aborted immediately.

2.7 Fluid Dynamics of the Hold Pressure Method

The hold pressure method is used for pulse waveform acquisition at the brachial artery using a cuff-based system. A pressurized cuff-based system applied at the arm will put a constant pressure across its entire circumference. An elastic artery undergoing pressure pulsations, as in the case of the brachial artery, will experience proportional radial pulsations. These arterial radial pulsations will change the force balance between the arm and the cuff proportional to the radial displacement of the artery. The changing force will change the pressure inside the cuff. This process will capture a pulse waveform that has the same morphology as the pressure pulsation in the artery but a different scaling that reflects the signal damping from the arm and cuff combination. One of the main advantages of this methodology is the ability to accurately control the boundary conditions on the arm by changing the hold pressure. Three subject specific physiological pressures were selected for the holds in our measurement: DBP, MAP, and sSBP (SBP+35 mmHg).

In elastic collapsible tubes, the force balance at the tube wall will determine the shape of the tube. The cuff hold pressure generates a constant symmetric force around the entire arm that influences the radius of the collapsible brachial artery.

At a hold pressure of DBP, the cuff pressure is always equal to or smaller than the arterial pressure. As such the arterial radius does not collapse and the physiological local flow conditions in the brachial artery are maintained. At the other extreme, we have the hold pressure of sSBP, that is a cuff pressure always significantly greater than the maximal arterial pressure. In this case, the radius collapses completely blocking flow through the artery. Lastly, any pressure between the DBP and SBP, will generate arterial wall collapse for the time segment during the pulsation in which the cuff pressure is greater than the arterial pressure. Effectively, by increasing the cuff hold pressure we are proportionally decreasing the flow through the brachial artery. The three selected hold pressures in our device represent cardinal points in the pressure flow regime: DBP corresponds to unaltered flow condition, MAP corresponds to maximal cuff signal amplitude from the pressure flow combination, and sSBP corresponds to a no flow condition.

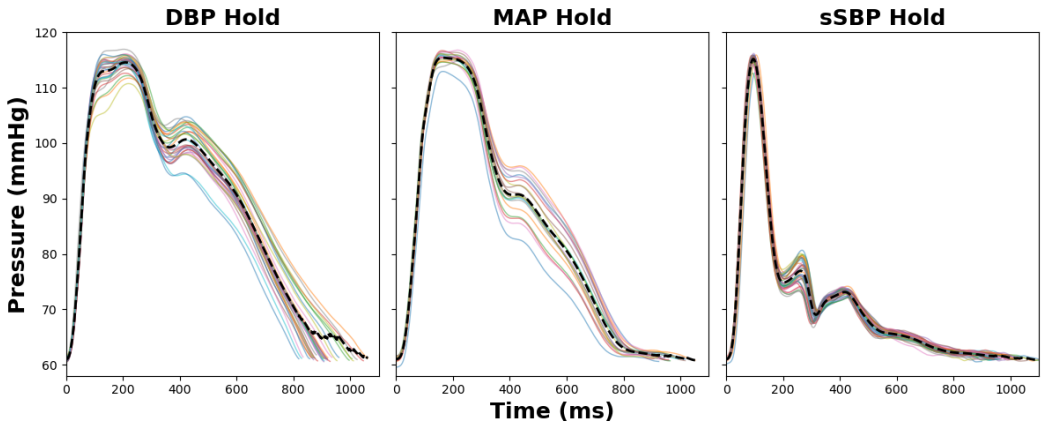

Figure 2.9: Calibrated cuff waveforms comparison. The figure shows the calibrated waveforms from the three different holds: DBP, MAP, and sSBP. Dashed line is the average of the individual pulse waveforms within a pressure hold.

For the analysis in this thesis, the sSBP hold pressure is of particular importance and requires further physiological justification. In the sSBP hold, the flow in the left subclavian artery is completely obstructed and only the pressure wave can propagate. In this model, the pressure wave travels along the artery unaffected in shape. At the basal end of the cuff, the radial occlusion causes an abrupt impedance mismatch reflecting the pressure wave. Since the pressure wave is fully reflected at the basal end of the cuff, no wave reflection from the impendance mismatch at the distal end of the cuff and radial artery are present to disturb the signal [13]. The left subclavian artery is a direct branch of the ascending aorta, therefore, the waveform

measured at the left arm with the sSBP hold is an undisturbed representation of the central pressure wave. In practical terms, the sSBP hold is equivalent to measuring the pressure at the origin of the left subclavian artery branch. As such, the sSBP waveform is considered the closest approximation to the aortic waveform when measured via the pressure hold method.

2.8 Signal Calibration

To give clinical significance to the pulse waveform acquired with the brachial cuff, it is important to scale the differential pressure signal to physiological pressure units. As previously shown, the measured cuff signal amplitude and mean during the pressure holds do not represent the actual BP values. The cuff signal amplitude is a damped representation of the actual signal due to the wave propagation from the artery, through the arm and to the cuff. Indeed, a typical BP waveform amplitude is around 40 mmHg while the measured arm cuff signal is only 1-2 mmHg. On the other hand, the cuff hold pressure does not represent any physiological BP value but is simply a forcing condition that alters the pressure-to-flow relationship. Therefore, the entire signal needs to be scaled and shifted using patient specific BP values to reflect a physiological cardiovascular waveform. Within this thesis, this process of scaling and shifting the pulse waveform will be referred to as signal calibration. The typical pulse waveform has a value of SBP at the peak and a value of DBP at the minima. Thus the objective of the signal calibration is to shift the pulse waveforms signals from the cuff device such that peaks occur at SBP and minimas occur at DBP. To scale the pulse waveforms, the BP values from the oscillometric measurement in the form of SBP, DBP, and MAP will be used; the PP value is calculated as the SBP minus the DBP.

Static Signal Calibration

In the literature, all the discussed signal calibration methods involve individually scaling the measured waveforms to the oscillometric BP values [14, 15]. Some methods use the SBP and DBP values as reference, while others use the MAP and PP values as reference. The calibrated waveforms from this method will differ slightly depending on the relative form factor of the waveform as the oscillometric algorithm values calculate SBP and DBP with a fixed equation from MAP. The typical scaling procedure involves the following steps:

1. Eliminating signal drift from the pressure-time signal.

2. Segment the waveforms using start and stop indexes.
3. Unit normalize each waveform to an amplitude of 1.
4. Scale waveform to an amplitude of PP (SBP-DBP).
5. Shift waveform to physiological BP value.

The steps listed above can be applied for both the Systolic blood pressure (SBP) and DBP method and the MAP and PP method; the only modification is in the shifting procedure. For the former, the shifting will move the minima of the waveform to DBP. For the latter, the shifting will first move the mean of the PP scaled waveform to zero, and then shift the minima by MAP. While this method gives a waveform that has physiological BP units, the scaling procedure eliminates the dynamic information present in the signal. As will be shown later in this thesis, the BP is not a static parameter but rather is dynamically changing with every beat. For a more accurate non-invasive representation of the cardiovascular pulse waveform, extracting this dynamic information is a challenge to address.

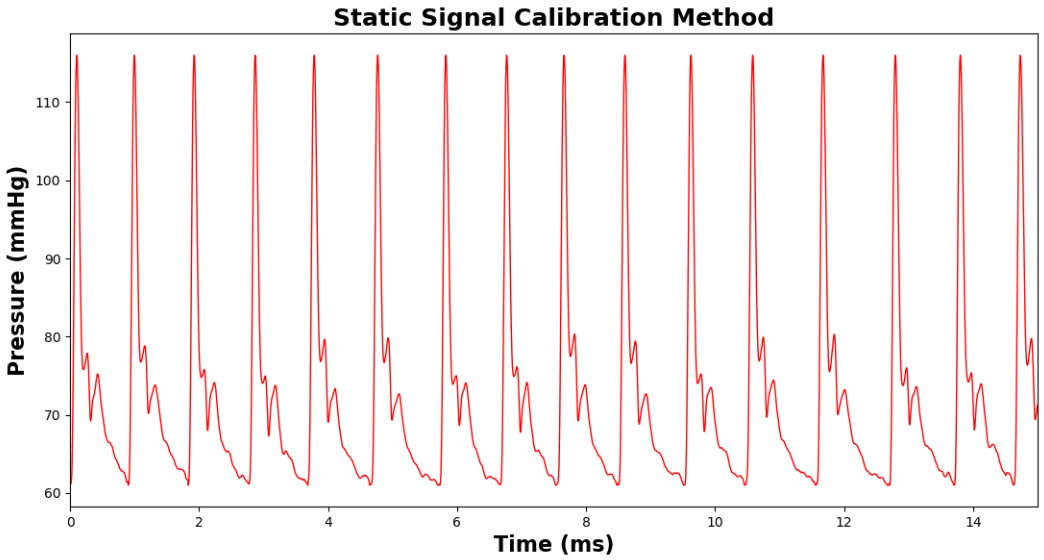

Figure 2.10: Static calibration method example. Figure shows an example segment of the pulse waveforms processed with the static signal calibration methodology scaled to SBP and DBP.

Dynamic Signal Calibration

This section proposes a signal calibration method that dynamically adjusts the BP values of the waveform to account for physiological breathing. The high-

resolution device presented in this thesis captures the dynamic BP fluctuations in response to breathing as shown in Figure 2.13 below. The method described herein proposes using the oscillometric envelope function to calculate the BP shift for each pulsation. The envelope function reflects the hemodynamics of the measured subject at the current BP level. The envelope function is calculated using the measurement data such that each scaling procedure is specific to the subject and current cardiovascular conditions.

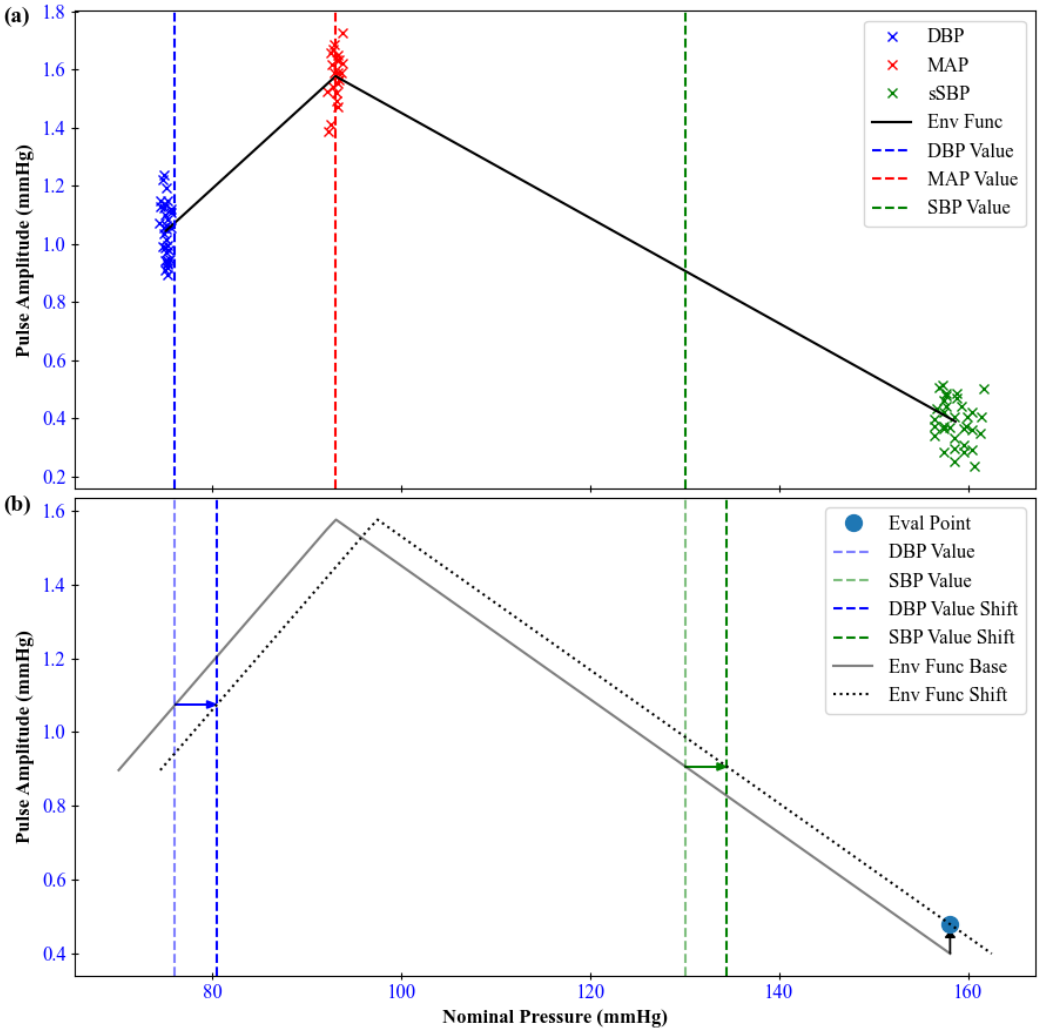

Figure 2.11: Dynamic signal calibration with envelope function. (Top) shows a reconstruction of an envelope function utilizing the DBP, MAP and sSBP pressure holds. The vertical dashed lines represent the BP measurement results. The solid lines connecting DBP to MAP and MAP to sSBP lay the outline of the envelope function. (Bottom) Illustrates the concept behind BP change estimation using the envelope function. The delta in pulse amplitude at sSBP (black arrow) shifts the DBP and SBP points as shown from the blue and red arrows, respectively.

Reconstruction of the envelope function is performed using the sparse pressure hold data. The envelope function is the relationship between the peak-to-peak pulse amplitude measured in the cuff to the nominal cuff pressure. For each pressure hold, the high-resolution differential signal and the high-range pressure signal are analyzed to extract peak-to-peak pulse amplitude and nominal cuff pressure data pairs for all identified pulsations. Plotting the data pairs from the three hold pressures and connecting the pressure hold data pair means constructs a triangle shape envelope function as shown in Figure 2.11. This envelope function reconstruction with sparse data requires the following assumptions: a linear interpolation between the hold pressures and that the SBP value lies along this linear interpolation. In this estimation, one expects the MAP pressure hold to have the largest amplitude and a decreasing amplitude as the pressure moves diverges from the MAP value.

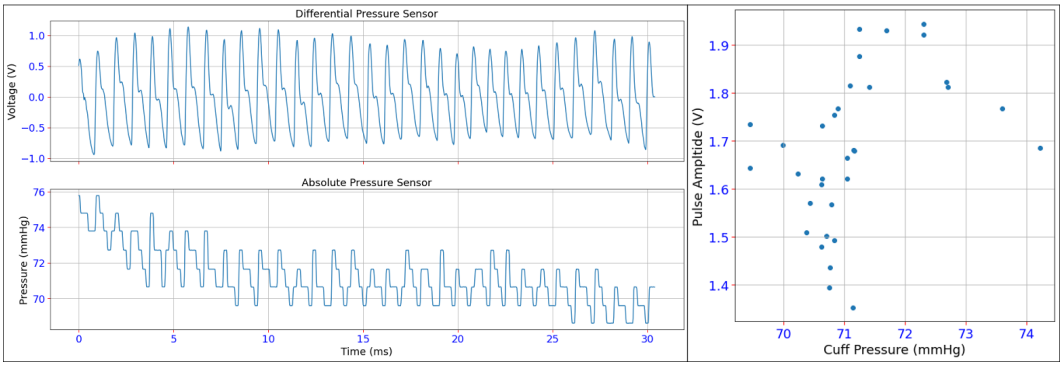

Figure 2.12: Pulse amplitude versus nominal pressure for cuff-based recording. (Left) shows an example of time synched high-resolution signal (Top) and the absolute pressure signal (Bottom) at the DBP hold. (Right) shows the relationship between the pulse amplitude and the cuff pressure for the DBP hold.

For discussion purposes, the procedure described below is applied to the sSBP pressure signals, yet with minor modifications this can be applied to the other pressure hold data. BP fluctuations are calculated for each individual pulsation using the deviation from the envelope function. As shown in the Figure 2.11, the pulse amplitude at a given hold pressure fluctuates around the mean. These variations represent the breathing induced BP fluctuations, decreasing during inhalation and increasing during exhalation. Assuming that BP fluctuations are small enough not to alter the envelope function shape and that BP values are algorithmically calculated around the mean, the change in BP can be estimated by shifting the envelope function. An illustration of this concept is shown in Figure 2.11. This theory can be represented mathematically with the equations presented below. The

equations allow to calculate the SBP and DBP shift on a beat-by-beat basis to reflect the breathing BP fluctuations.

$$SBP_{shift} = SBP + \frac{\Delta PA}{slope_{m-to-s}} \tag{2.1}$$

$$DBP_{shift} = DBP + \frac{\Delta PA}{slope_{d-to-m}} \tag{2.2}$$

where the ΔPA is the pulse amplitude difference from the mean at that hold, the $slope_{d-to-m}$ is the slope from the DBP hold to MAP hold, and the $slope_{m-to-ss}$ is the slope from the MAP hold to the sSBP hold.

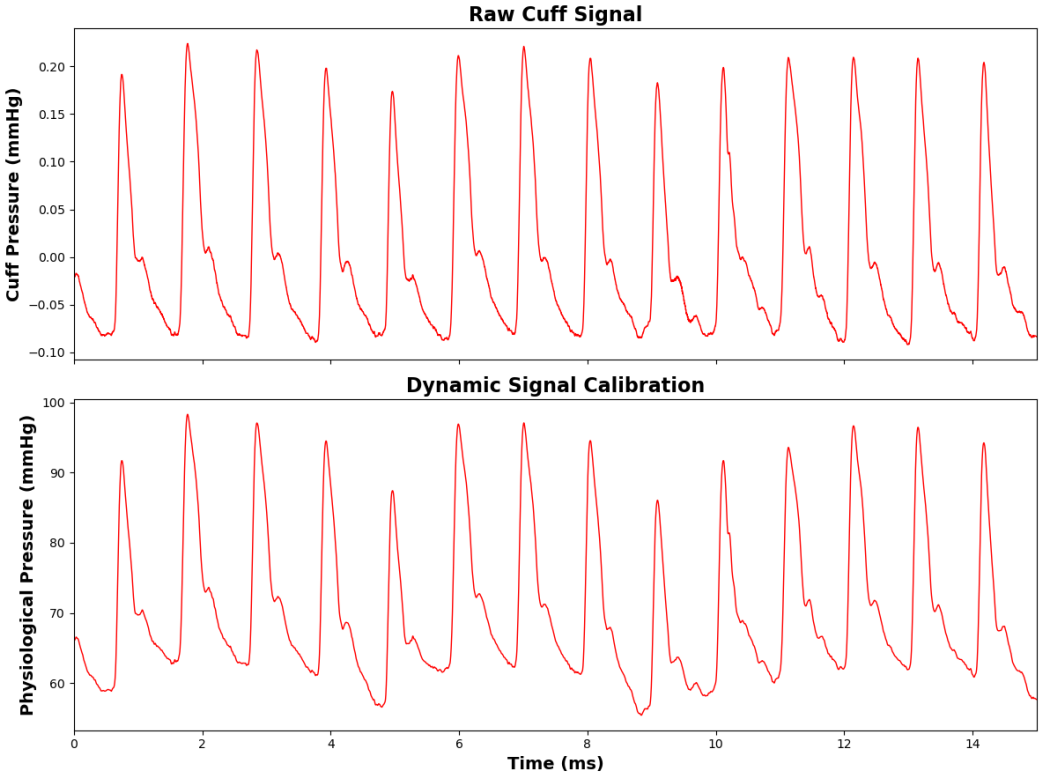

Figure 2.13: Dynamic signal calibration output example. Figure shows how the dynamic signal calibration maintains the physiological BP fluctuations from breathing. (Top) shows the raw cuff signal that displays pulse amplitude fluctuations. (Bottom) shows the dynamical signal calibration method results highlighting the SBP and DBP fluctuations.

2.9 System Evaluation

Inflation and Deflation Mode Equivalence

The common deflation based oscillometric BP measurement has an accepted measurement uncertainty of 3 mmHg as reported by the user manuals in the monitors [16]. This part of the study will evaluate the error associated with BP measurement in the deflation and inflation mode using the Fluke Biomedical ProSim 8 Vital Signs Simulator (hereafter the ProSim8) to ensure that the additional components influence the measurement. The ProSim 8 is a vital signs simulator to measure the performance of cardiovascular monitors. This study will utilize the pneumatic NIBP capabilities of the simulator to model the oscillometric BP measurement. The ProSim8 and the cuff-device are connected utilizing a T joint between the device and the cuff. The cuff is tightened around a mandrel to give a resistance upon inflation, this is done to emulate the arm.

The ProSim8 NIBP simulator allows to modify the SBP, DBP, HR and envelope function shift for model evaluation. The BP measurement error was assess under two test conditions: (1) envelope function shift and (2) nominal BP values. An envelope function shift is a skew movement of the entire envelope function in the positive or negative direction. The envelope function shift evaluated four different skew factors at a nominal BP of 120/80 mmHg at 60 BPM, the tested skew factors are 0%, +2%, −2% and −4%. The ProSim8 has prebuilt BP modalities to reflect different physiological BP conditions. Three different conditions were investigated to mimic healthy (normal), hypertensive (high), and hypotensive (low) subjects: normal BP was 120/80 mmHg at 60 bpm, high BP was 160/120 mmHg at 80 bpm, and low BP was 100/60 mmHg at 50 bpm. For the second test, an envelope function skew of −4% was used. Three repeats (n=3) for every test condition were performed.

The error between actual and measured values for the SBP, DBP, and HR in the two tests are summarized in Figure 2.14. The first test evaluating the envelope function shows that the negative shift reduced the residual for both SBP and DBP. SBP and DBP are consistently overestimated from the device and the overestimation appears to be larger for the deflation mode. The average SBP and DBP error with inflation mode was of −3.9 and −3.5 mmHg, respectively. The average SBP and DBP error with deflation mode was of −5.3 and −3.4 mmHg, respectively. The HR did not have any measurement error. The second test evaluating three different physiological BP conditions showed a propensity to underestimate SBP values at high BP and overestimate DBP values at low BP. Both measurement modes gave

similar average BP errors: in inflation mode the average SBP and DBP error was 1.6 and −0.4 mmHg, respectively, and in deflation mode the average SBP and DBP error was −0.2 and −1.2 mmHg.

Overall, the measured error is around the expected uncertainty of cuff-device oscillometric BP measurement of 3 mmHg. The first test showed a moderate dependence of the measurement error with the envelope function skew, a negative skew appears to reduce the measured residual. The second test showed SBP underestimation for high BP and DBP underestimation for low BP. There does not appear to be a significant difference between inflation and deflation mode results, at best the inflation mode reported slightly smaller error throughout the tests. These results suggests that the two modes can be used interchangeably during clinical testing.

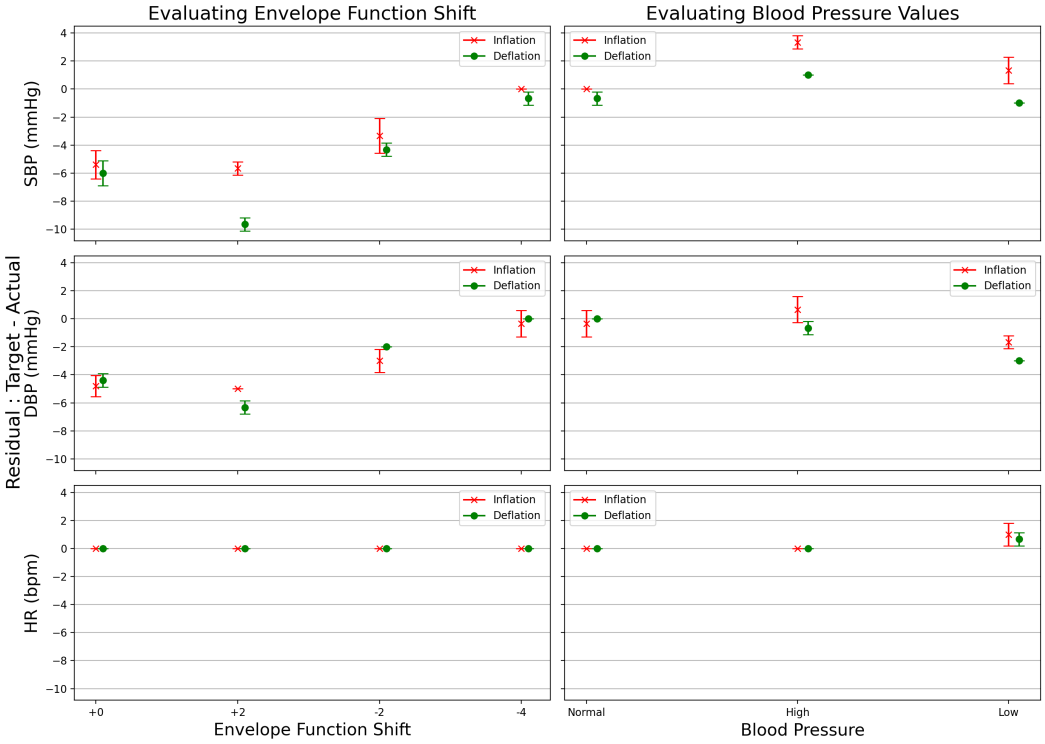

Figure 2.14: BP measurement evaluation test results. Figure shows the residual, as the difference between target and actual, for SBP, DBP, and HR oscillometric parameters (left) for the envelope function shift test and (right) for the physiological BP value test.

Effect of Cuff Placement on Signal Quality

One of the main motivations behind pursuing a cuff-based systems to improve measurement repeatability lies in the universality of the brachial cuff. Current

cuff designs are approaching the one-size-fits-all, or most, models. This design advantage incentivizes the development of cuff-based system for general population pulse waveform acquisition. Yet, it must be recognized that simplifying a system does not make a system immune to human operational errors. For our cuff-based device, the main source of error lies in the incorrect cuff placement, which is hard to quantify and in certain settings cannot be controlled. In this section we aim to study the effect of human error in cuff placement on the device measurement results.

The brachial arm cuff features an asymmetric cylinder to best accommodate the physiological shape of the arm. In the arm, maximal circumference occurs at the center of the humerus and decreases as one moves towards the elbow. This decreasing circumference is a characteristic of the arm cuff which allows to create optimal contact between the cuff and the arm. Brachial cuffs also have a closure hinge and a connective tubing which are exactly opposite each other, the correct placement for maximal signal is with the tubing along the brachial artery. This cuff asymmetry enforces a directionality to cuff placement on the arm for optimal measurement. The cuff used on this device is the AND Medical Wide Range Replacement Cuff that accommodates arm circumferences between 22 cm to 42 cm. The tests performed in this system evaluation will independently modify each aspect of the correct cuff placement to measure the variation. For each test, multiple conditions are sequentially tested on the same day to maintain a semi-constant cardiovascular state for a given repeat. In each test, three repeats across different days will be performed to reduce arm stress from repeated consecutive measurements. Considering the physiological BP variability during the circadian cycle, each testing day was started at 10:00am. The tests were performed on a single individual in the supine position on the left arm (n=1); a 5-minute rest period between consecutive tests was required. The following tests will be performed:

1. Cuff tubing direction.
2. Angular alignment of connection tube.
3. Cuff tightness.
4. Cuff distance from elbow crease.

The conical asymmetry of the brachial cuff forces the cuff to be placed with the connective tubing pointing towards the hands for optimal cuff adherence. Reversing

the directionality would result in a progressively looser cuff as you move further from the points of maximal circumference. This first test will evaluate the effect of incorrect cuff placement from tubing directionality. Two testing conditions will be performed: (1) cuff tubing points towards the hand and (2) cuff tubing pointed towards the shoulder (see Figure 2.15 for reference). During testing, the cuff-device performed all the oscillometric BP measurements with the inflation method. The measured BP values show a minimal decrease in test condition number 2 when compared with test condition 1. A possible reason for this could be the larger volume of air in the cuff causing a dampening of the signal. This drop could also originate from a more relaxed vascular state in the left brachial artery following the BP measurement resulting in lower BP. Nevertheless, the observed drop is always within 1-5 mmHg which is the expected measurement variability. The pulse waveform in the sSBP hold does appear to be affect by the cuff tubing directionality. In the repeats from day 1 and day 3, the tube pointing to the arm (T1) and the tube pointing to the shoulder (T2) have fully overlapping average waveforms. In day 2, the T2 average waveform featured a moderately more prominent forward wave with a weaker reflected wave but the diastolic portion closely matches between the two tests. The observed variation is well within the physiological variability from day to day and can be attributed to a multitude of factors. Overall, these results show that tubing direction does not affect the measured BP values with the oscillometric method and the waveform morphology captured during the pressure hold.

The second test evaluated the effect of the tube's angular alignment with the brachial artery on the device measurement results. The recommended cuff placement requires the tube to be aligned with the brachial artery; this favors maximal signal amplitude and quality as the sensor is closest to the source. In this test, the alignment with the brachial artery is taken to be with the tube on the inner side of the arm, and is referenced as the 0°. In a clinical setting, the tubing is often placed anywhere between our 0° mark and the 90° mark on the bicep. Four test conditions are evaluated: (1) 0°, (2) 90°, (3) 180°, and (4) 270°. The oscillometric BP measurement results from the second test do not show any correlation between the BP value magnitude and the test conditions. The measured fluctuations are most likely a byproduct of physiological variability of the BP values with time and the uncertainty associated with the measurement modality. We can therefore conclude that the angular rotation of the cuff does not affect the oscillometric BP reading. The average sSBP waveforms within each repeat showed very consistent morphol-

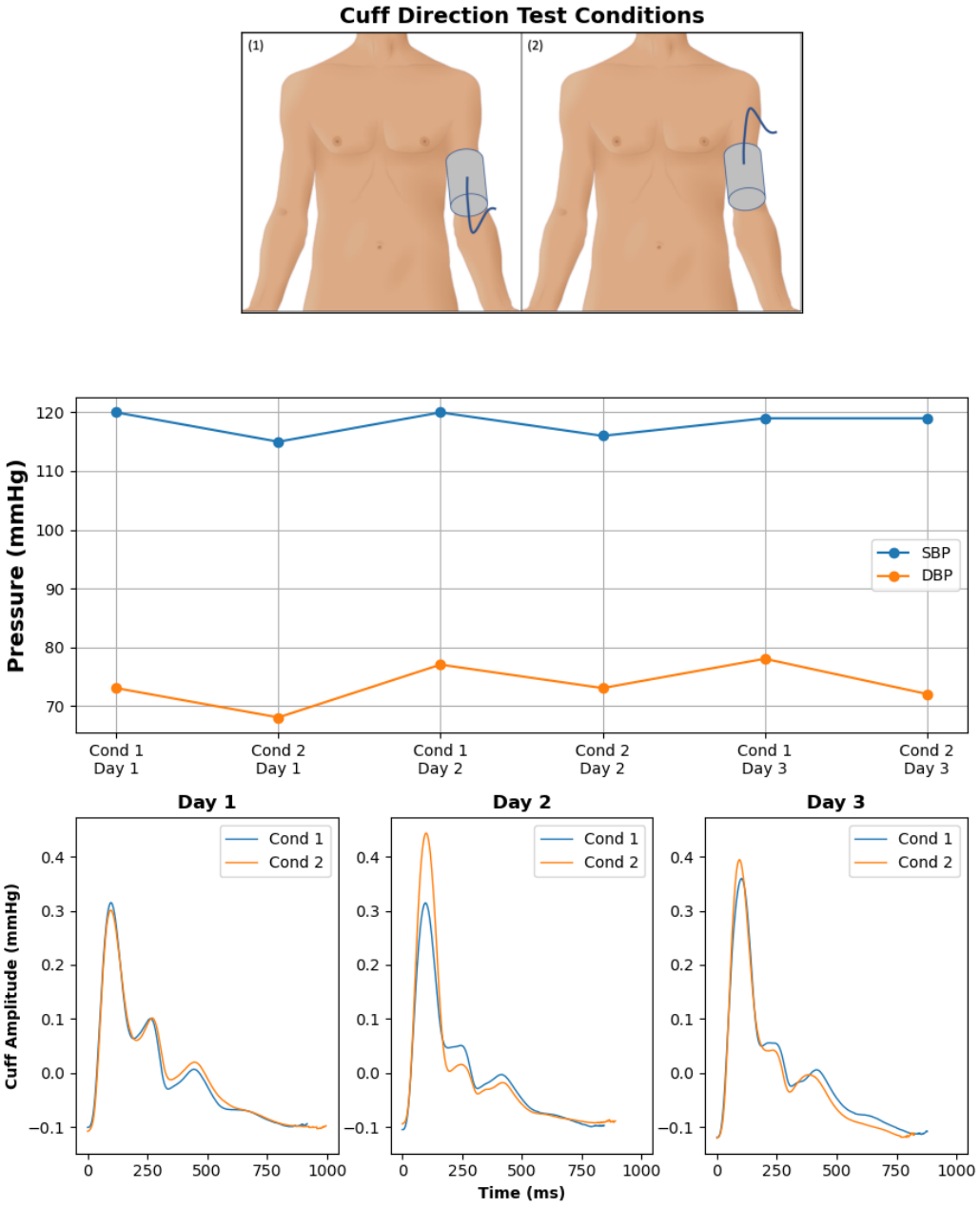

Figure 2.15: Cuff device results from cuff direction test. (Top) shows the tested orientations of the cuff. (Middle) shows the SBP and DBP throughout the test. (Bottom) shows the averaged sSBP pulse waveform shape for the different testing days. [Digital image; modified]. (n.d.). Created by Goran tek-en. Retrieved May 2, 2023, from Wikimedia Commons website: https://commons.wikimedia.org/wiki/File:Male_front-back_3d-shaded_human_illustration.svg

ogy. The systolic portion had similar forward and reflected waves. The diastolic component showed a very similar notch, decay profile and duration within each repeat. Minor variability in the raw amplitude of the signal is observed between the repeats; no clear raw amplitude pattern is present in the data. The air volume injected in the cuff affects signal amplitude. The slight variability in cuff fit between the repeats explains the raw amplitude differences observed. Summing up all the points, the rotation of the cuff does not affect the device measurement for pulse waveform features.

The third test looked at the effect of cuff tightness on the device measurement results. The cuff tightness directly influences the amount of air required to pressurize the cuff. Considering the volume of the cuff acts as a capacitor, a larger cuff volume will result in larger damping of the signal. Typical BP guidelines suggest a cuff tightness such that a one finger can be comfortably placed between cuff and arm. Quantitatively, this recommendation corresponds to fitting the cuff to the arm's circumference plus once centimeter. This test will evaluate three conditions: (1) arm circumference plus one centimeter, (2) arm circumference plus three centimeters, and (3) arm circumference plus five centimeters. The cuff BP measurement results did not show any correlation with the cuff circumference. Oscillometric algorithms to measure BP utilize amplitude ratios to calculate SBP and DBP from the MAP value; the absolute amplitude is not expected to have any effect on this calculation. The waveform morphology shows decreasing amplitude with increase cuff circumference corroborating the capacitor analogy presented previously. As shown in figure 2.17, the raw sSBP waveform amplitude is largest at condition (1) and smallest at condition (3). The same waveform characteristics are present in all three test conditions and are constant throughout the repeats. Overall, the cuff tightness proportionally increases the cuff signal amplitude yet no morphological changes are observed.

The fourth and last test evaluated the effect of cuff distance from elbow crease on the device measurement results. Cardiology guidelines indicate that the cuff should be placed at 2 centimeters from the elbow crease for optimal signal quality. Three test conditions were examined: (1) at elbow crease, (2) 2 centimeters from elbow crease, and (3) 4 centimeters from elbow crease. The BP measurement results show no correlation to the placement of the cuff on the arm. The cuff distance from elbow crease affects the amplitude of the raw sSBP signal. The signal amplitude increases as the cuff distance to the elbow crease increases, effectively having the

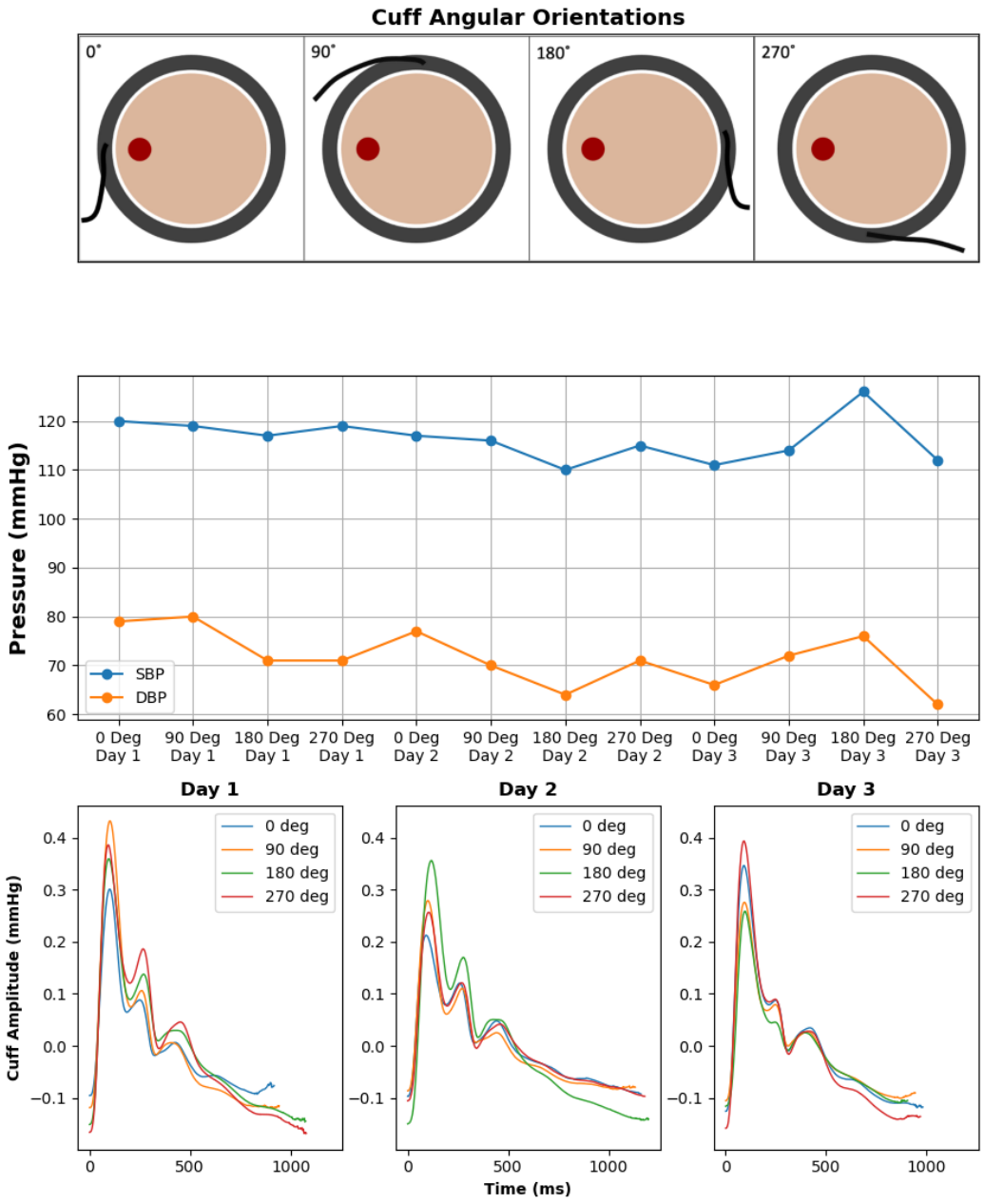

Figure 2.16: Cuff device results from cuff angular orientation test. (Top) shows the tested angular orientations of the cuff. (Middle) shows the SBP and DBP throughout the test. (Bottom) shows the averaged sSBP pulse waveform shape for the different testing days.

cuff higher up the arm. One potential explanation for this observation is the relative overlap of the cuff with brachial artery as well as the improved cuff fit to the arm shape. Cuff pulse waveform features are consistent between the successive repeats

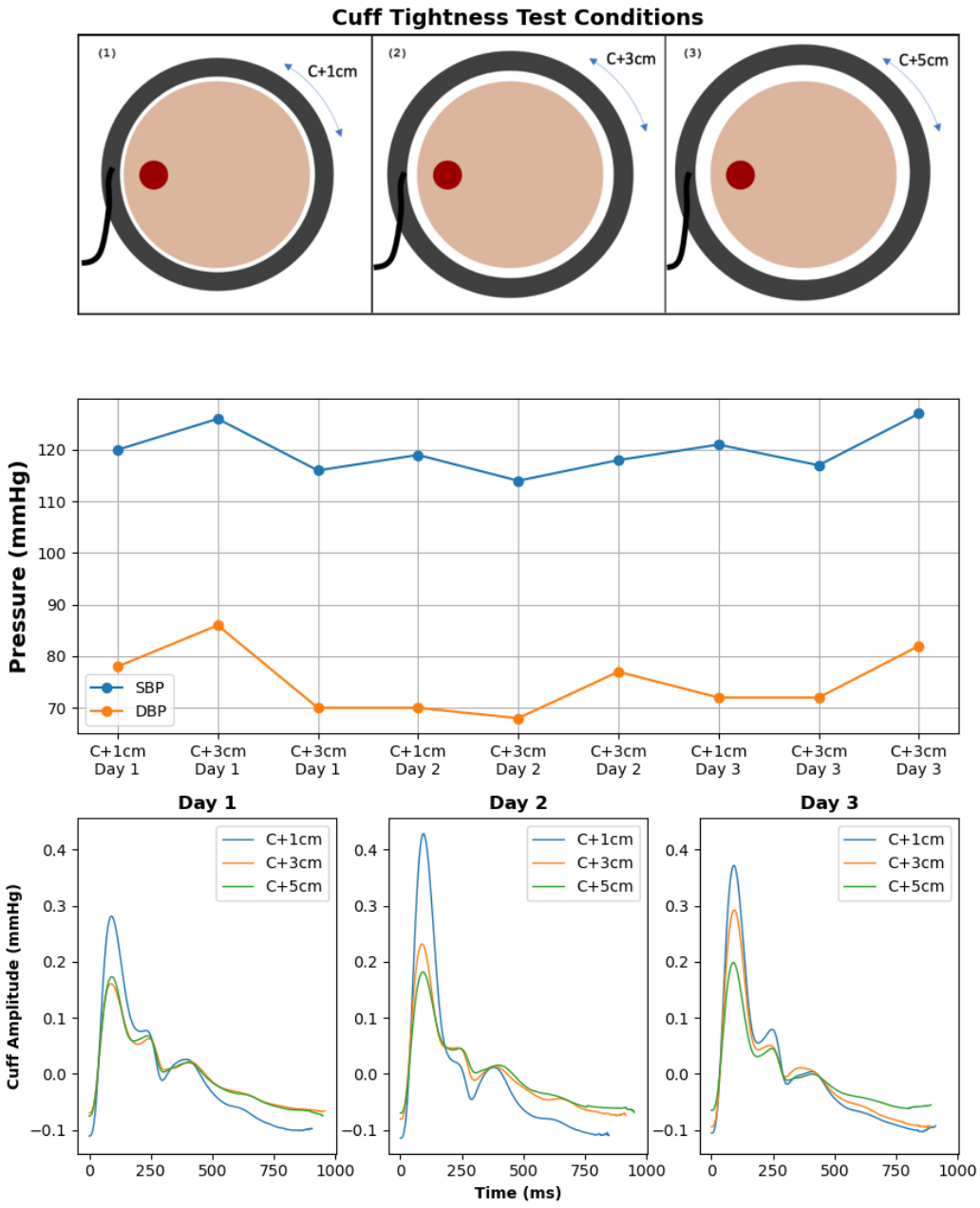

Figure 2.17: Cuff device results from cuff tightness tests. (Top) shows the tested cuff tightness conditions. (Middle) shows the SBP and DBP throughout the test. (Bottom) shows the averaged sSBP pulse waveform shape for the different testing days

and conditions. Placement of the cuff above the elbow crease will give optimal signal quality and amplitude.

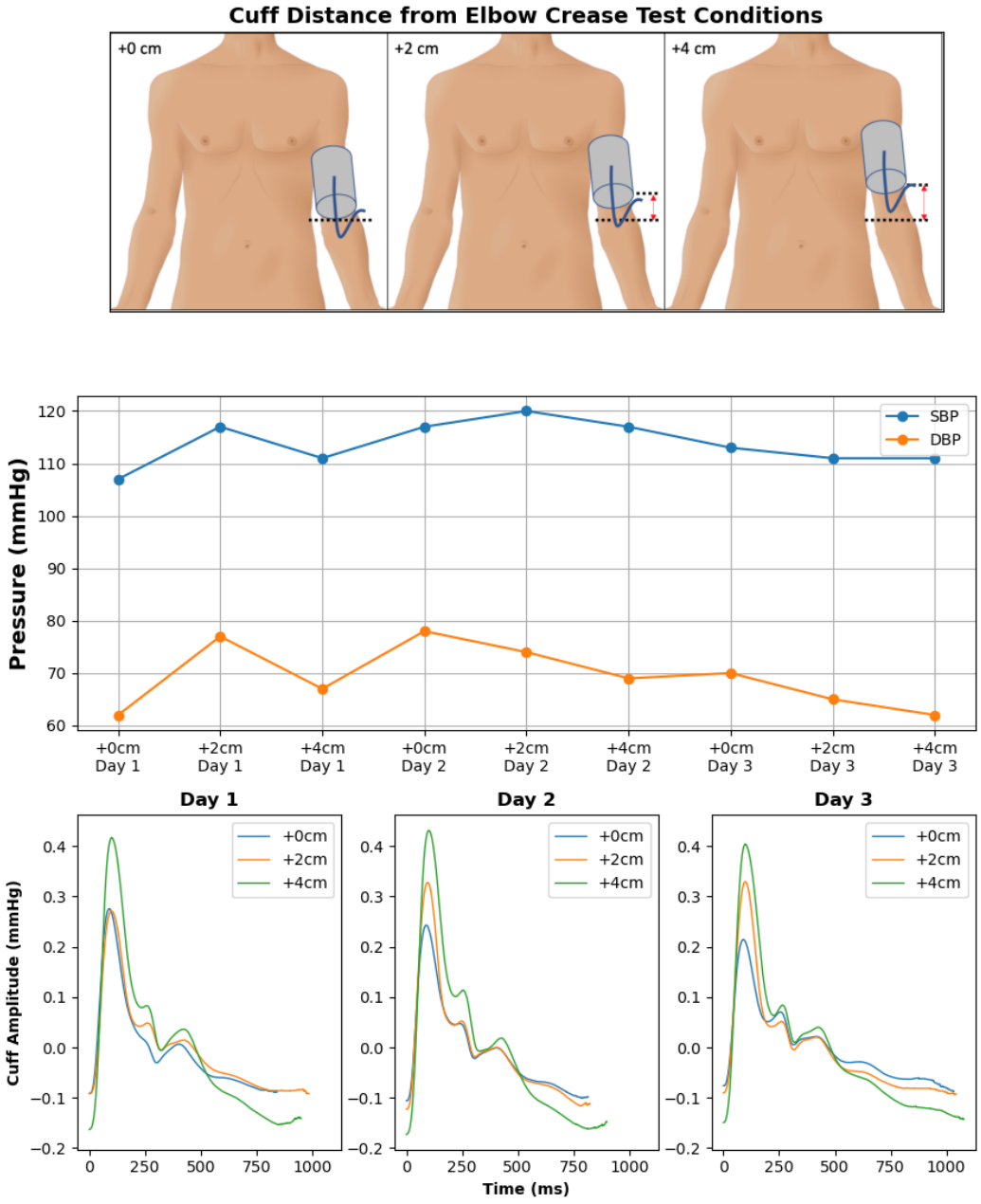

Figure 2.18: Cuff device results from cuff distance from elbow test. (Top) shows the tested vertical displacement of the cuff from the elbow crease. (Middle) shows the SBP and DBP throughout the test. (Bottom) shows the averaged sSBP pulse waveform shape for the different testing days. [Digital image; modified]. (n.d.). Created by Goran tek-en. Retrieved May 2, 2023, from Wikimedia Commons website: https://commons.wikimedia.org/wiki/File:Male_front-back_3d-shaded_human_illustration.svg

In conclusion, this section analyzed the repeatability of the cuff measurement results under a series of test conditions that deviate from the regular cuff placement. From all four testing conditions, the oscillometric BP measurement results are not affects by cuff placement, all observed variability originates from the methodology's uncertainty and the physiological BP fluctuations. Waveform morphology was not affected throughout the testing conditions. Only raw signal amplitude is affected and this behavior comes from the cuff damping factor. Considering the signals will then be calibrated, the variability in raw amplitude is not of much impact to the measurement validity. Although these test conditions are extreme exaggerations of real-world human error, the low variability observed throughout gives confidence in the reliability of the measurement with this device.

References

[1] Michael F. O'Rourke, Alfredo Pauca, and Xiong-Jing Jiang. "Pulse Wave Analysis." In: *British Journal of Clinical Pharmacology* 51.6 (June 2001), pp. 507–522. DOI: 10.1046/j.0306-5251.2001.01400.x. URL: https://doi.org/10.1046/j.0306-5251.2001.01400.x.

[2] Louis-Charles Desbiens et al. "Prediction of Cardiovascular Events by Pulse Waveform Parameters: Analysis of CARTaGENE." In: *Journal of the American Heart Association* 11.17 (Sept. 2022). DOI: 10.1161/jaha.122.026603. URL: https://doi.org/10.1161/jaha.122.026603.

[3] Paolo Salvi, Andrea Grillo, and Gianfranco Parati. "Noninvasive Estimation of Central Blood Pressure and Analysis of Pulse Waves by Applanation Tonometry." In: *Hypertension Research* 38.10 (July 2015), pp. 646–648. DOI: 10.1038/hr.2015.78. URL: https://doi.org/10.1038/hr.2015.78.

[4] Gary M. Drzewiecki, Julius Melbin, and Abraham Noordergraaf. "Arterial Tonometry: Review and Analysis." In: *Journal of Biomechanics* 16.2 (Jan. 1983), pp. 141–152. DOI: 10.1016/0021-9290(83)90037-4. URL: https://doi.org/10.1016/0021-9290(83)90037-4.

[5] Fuyou Liang. "Numerical Validation of a Suprasystolic Brachial Cuff-Based Method for Estimating Aortic Pressure." In: *Bio-Medical Materials and Engineering* 24.1 (2014), pp. 1053–1062. DOI: 10.3233/bme-130903. URL: https://doi.org/10.3233/bme-130903.

[6] B. T. Costello et al. "Evaluation of a Brachial Cuff and Suprasystolic Waveform Algorithm Method to Noninvasively Derive Central Blood Pressure." In: *American Journal of Hypertension* 28.4 (Sept. 2014), pp. 480–486. DOI: 10.1093/ajh/hpu163. URL: https://doi.org/10.1093/ajh/hpu163.

[7] M-H Hwang et al. "Validity and Reliability of Aortic Pulse Wave Velocity and Augmentation Index Determined by the New Cuff-Based Sphygmocor Xcel." In: *Journal of Human Hypertension* 28.8 (Jan. 2014), pp. 475–481. DOI: 10.1038/jhh.2013.144. URL: https://doi.org/10.1038/jhh.2013.144.

[8] Ivan G Horvath et al. "Invasive Validation of a New Oscillometric Device (Arteriograph) For Measuring Augmentation Index, Central Blood Pressure and Aortic Pulse Wave Velocity." In: *Journal of Hypertension* 28.10 (Oct. 2010), pp. 2068–2075. DOI: 10.1097/hjh.0b013e32833c8a1a. URL: https://doi.org/10.1097/hjh.0b013e32833c8a1a.

[9] Giacomo Pucci et al. "Evaluation of the Vicorder, A Novel Cuff-Based Device for the Noninvasive Estimation of Central Blood Pressure." In: *Journal of Hypertension* 31.1 (Jan. 2013), pp. 77–85. DOI: 10.1097/hjh.0b013e32835a8eb1. URL: https://doi.org/10.1097/hjh.0b013e32835a8eb1.

[10] Thomas Weber et al. “Validation of a Brachial Cuff-Based Method for Estimating Central Systolic Blood Pressure.” In: *Hypertension* 58.5 (Nov. 2011), pp. 825–832. DOI: 10.1161/hypertensionaha.111.176313. URL: https://doi.org/10.1161/hypertensionaha.111.176313.

[11] Hiroshi Miyashita. “Clinical Assessment of Central Blood Pressure.” In: *Current Hypertension Reviews* 8.2 (June 2012), pp. 80–90. DOI: 10.2174/157340212800840708. URL: https://doi.org/10.2174/157340212800840708.

[12] Vratislav Fabian et al. “Noninvasive Assessment of Aortic Pulse Wave Velocity by the Brachial Occlusion-Cuff Technique: Comparative Study.” In: *Sensors* 19.16 (Aug. 2019), p. 3467. DOI: 10.3390/s19163467. URL: https://doi.org/10.3390/s19163467.

[13] A. Lowe et al. “Non-invasive Model-Based Estimation of Aortic Pulse Pressure Using Suprasystolic Brachial Pressure Waveforms.” In: *Journal of Biomechanics* 42.13 (Sept. 2009), pp. 2111–2115. DOI: 10.1016/j.jbiomech.2009.05.029. URL: https://doi.org/10.1016/j.jbiomech.2009.05.029.

[14] Keerthana Natarajan et al. “Central Blood Pressure Monitoring via a Standard Automatic Arm Cuff.” In: *Scientific Reports* 7.1 (Oct. 2017). DOI: 10.1038/s41598-017-14844-5. URL: https://doi.org/10.1038/s41598-017-14844-5.

[15] Davide Agnoletti et al. “Pulse Pressure Amplification, Pressure Waveform Calibration and Clinical Applications.” In: *Atherosclerosis* 224.1 (Sept. 2012), pp. 108–112. DOI: 10.1016/j.atherosclerosis.2012.06.055. URL: https://doi.org/10.1016/j.atherosclerosis.2012.06.055.

[16] James A Hodgkinson et al. “Accuracy of Blood-Pressure Monitors Owned by Patients With Hypertension (Accu-Rate Study): A Cross-Sectional, Observational Study in Central England.” In: *British Journal of General Practice* 70.697 (June 2020), e548–e554. DOI: 10.3399/bjgp20x710381. URL: https://doi.org/10.3399/bjgp20x710381.

C h a p t e r 3

MATHEMATICAL CHARACTERIZATION OF THE PNEUMATIC LOW PASS FILTER

“It doesn’t matter how beautiful your theory is, it doesn’t matter how smart you are. If it doesn’t agree with experiment, it’s wrong."

— Richard P. Feynman

CHAPTER 3 INTENTIONALLY REDACTED

Chapter 4

FUNCTIONAL EVALUATION OF THE CUFF DEVICE IN A HEALTHY POPULATION

A CALTECH IRB STUDY

"Science is but a perversion of itself unless it has as its ultimate goal the betterment of humanity"

— Nikola Tesla

4.1 Introduction

The process of clinically translating medical devices requires incremental progress to ensure reliability, accuracy, and correct interpretation of results. Medical data is inherently complex, with high dimensionality, sparsity, and uncertainty. In experiments involving human subjects, controlling input variables can be difficult, leading to output data with large variances. Therefore, it is the responsibility of a diligent medical scientist to design well-planned experiments that reduce the dimensionality of the data.

In Chapter 2, we have introduced a novel cuff-based device for high-resolution pulse waveform acquisition at the brachial artery. A cuff-based design was chosen for its measurement consistency as this is one of the major limitations of the current gold-standard tonometer. The introduction of the pLPF system offers a potential solution to the issue of low-signal resolution in cuff-based measurements. The chapter will discuss the first human study performed at Caltech with the system described previously. The purpose of this study was twofold: (1) evaluate device functionality on a diverse subject population and (2) get a benchmark of the healthy pulse waveform from our cuff-based device. The first objective seeks to understand

how subject features influence result generalizability within the population, whether and how subject characteristic affect measurement quality and if any factors should be used for exclusions. The second objective aims to get a qualitative understanding of what healthy recordings look like with our device. In light of implementing this device for diagnostic purposes in the future, setting the benchmark on result consistency amongst healthy individuals is a necessary condition.

User experience plays a critical role in the clinical translation of medical devices, from the lab to the clinic. In addition to functionality, engineers must also consider the human aspect of clinical measurements, taking into account the comfort of test subjects and the ease of use for physicians. To assess user experience on the device, the Caltech human study will be conducted. The study will evaluate both the device-to-physician interaction and the device-to-user interaction. The purpose of the device and study is to demonstrate the accuracy and reliability of cuff-based pulse waveform analysis, and to promote its widespread use.

4.2 Methods

Study Information

IRB approval was obtained at Caltech for a device functionality and proof-of-concept study (protocol number 21-1114; approval date on September 17th, 2021). The IRB classified this study as minimal risk considering the cuff device is an iteration of the traditional BP monitor used in clinics and at home. Prior to testing, the physician obtained informed consent from all volunteers, ensuring that they were fully aware of the nature and purpose of the study, as well as any risks or benefits associated with their participation. All methods were carried out in accordance with relevant guidelines and regulations. Work adheres to the Declaration of Helsinki. Data were de-identified upon collection to protect subject privacy.

Subject Selection

The target population for this study was healthy individuals of at least 18 years of age with no history of cardiovascular disease. Exclusion criteria included inability to perform a brachial cuff measurement on the left arm and a history of any major cardiovascular event. Individuals for the study were recruited within the Caltech community and included students, postdoc, staff, and faculty. Prior to sign-up, subjects were informed of the risks and benefits of participating in the study. Participants volunteered for the study and no incentive was provided for

participation. At any moment a participant could decide to withdraw from the study and the data must be deleted.

Protecting Privacy and Anonymity

Subject privacy and anonymity throughout the study was a primary concern given the community style environment in which the study was conducted. Below are the steps that have been taken to protect privacy and anonymity during the IRB study:

1. **Informed consent:** The physician obtained informed consent from the volunteers prior to starting the procedure. The objective of the informed consent is to inform volunteers about the purpose of the study, what will be expected of them, and what risks and benefits may be associated with participating. The informed consent was also sent via email prior to the study to allow ample time for reading.

2. **Data deidentification:** All data collected during the study was stored in deidentified format utilizing SUBIDs. All the data was saved and processed using the SUBID nomenclature. The data associating the SUBIDs with the subject personal identifiers was stored within a password-protected file present on a offline hard-disk. The file was deleted upon completion of the study.

3. **Limited data access:** Access to the data was limited to the personnel approved on the IRB protocol ensuring only authorized access and that data is used for its intended purpose.

4. **Private testing environment:** The study was conducted in a private room with restricted access. The room is located in a low traffic area of the building reducing interactions with people external to the protocol.

5. **Secure data storage:** Data collected during the study is stored on a password-protected offline hard-drive stored at Caltech.

6. **Association file destruction:** Upon completion of the study the file associating the SUBIDs with the subject personal identifiers was destroyed to eliminate the risk of identification of tested subjects.

Overall, protecting the privacy and anonymity of study participants was crucial for maintaining ethical research practices throughout our study.

Testing Procedure

The study procedure was performed in the Heart Lab, Karman 305. Testing involved two components: (1) the case report form and (2) the device measurement. The case report form included subject characteristics, medical history, and cardiovascular influencing factors; all parameters were self-reported by the individuals except for height, weight, and left arm circumference which were measured during the procedure. The device measurement was performed on the subject's left arm in supine position. Figure 4.1 shows an image of the testing setup in the Heart Lab. The study involved three individuals: a physician, a chaperone, and an additional female chaperone for female testers. Dr. Francisco Padilla, a general practitioner physician, volunteered to perform the medical procedures for the study. The chaperone was present to supervise and monitor the proper operation of the device during the procedure. They also collected qualitative feedback on the device and observed its interactions with the user. An additional female chaperone was required to ensure the comfort and privacy of female testers during the procedure.

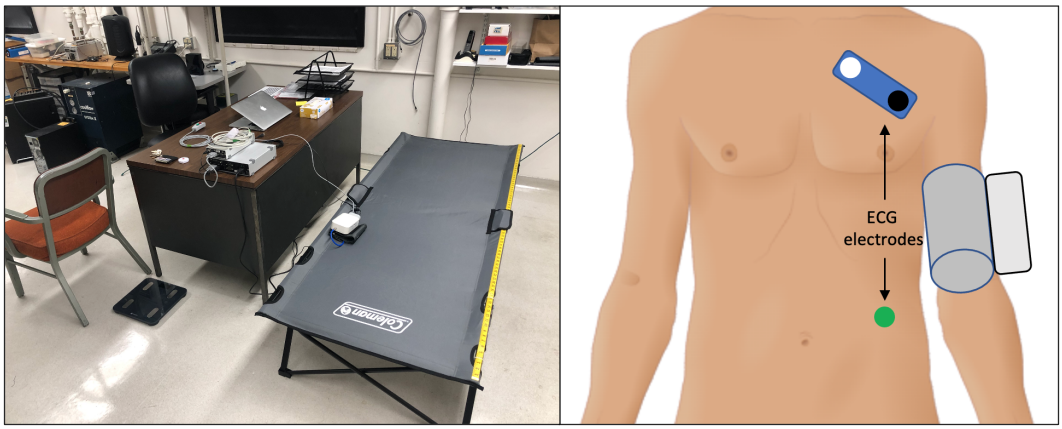

Figure 4.1: Testing configuration for Caltech IRB. (Left) shows the setup used for testing in the Heart Lab. (Right) shows the device and ecg configuration. [Digital image; modified]. (n.d.). Created by Goran tek-en. Retrieved May 2, 2023, from Wikimedia Commons website: https://commons.wikimedia.org/wiki/File:Male_front-back_3d-shaded_human_illustration.svg

The signals captured during testing consisted of the cuff device and a three lead ECG. The brachial artery in the left arm is the left subclavian artery that directly connects to the ascending aorta. The device performs the pre-programmed measurement described in Chapter 2, which has a duration of approximately 120 seconds. For more details on the measurement structure, please refer to section 2.6. The ECG was a three electrode three lead shielded ECG: the white electrode over

the right atrium, the black electrode over the left atrium, and the green electrode on the left lower abdomen. A custom ECG patch for the right atrium and left atrium electrodes was designed to ensure repeatable placement of the electrodes (Figure 4.1). Data acquisition was done using the AD Instrument PowerLab 26 Series, PowerLab 4/26 with the LabChart software. The sampling rate for data acquisition was set at 1kHz.

Subject data was collected with the CRF. The CRF was completed by the physician with the information verbally provided by the subject during the testing preparation. No verification to the accuracy of the data provided by the subjects was available. The CRF included information on both general demographic characteristics and medical characteristics. No identifiable information was stored in the CRF and the document was associated with the SUBID.

The participants were welcomed to the testing room by the physician and supervising personnel, testing was performed in the Heart Lab in Karman building 305. Upon arrival the individuals were given a quick briefing about the procedure and were asked to read and sign the informed consent form. Following the physician measured the left arm circumference, weight, and height of the individual. The subject was asked to move to supine position on the testing bed. A correct testing position consisted of the supine position with legs straight down with uncrossed feet, arms lying along the body, open hands, and no muscular tension. The physician conducted the CRF medical questionnaire. The supervising personnel was excused from the room during the entire medical questionnaire procedure to guarantee privacy. After the medical questionnaire, the physician prepared the subject for testing; this involved removing any clothing obstructing the left arm, placing the brachial cuff on the left arm and the three ECG patches. The placement of the ECG patches was optional: the procedure was first demonstrated by the physician, and subsequently the individual was given the option of self-performing, having the physician place the electrodes or abstaining from the procedure. Once all testing devices correcting placed, a five-minute rest period started. During the rest period, no talking, movement, or external stimuli from phone or email were allowed. At the end of the rest period, the physician informed the subject the procedure would start and asked to maintain a regular breathing pattern, not talk and not tense muscles. The cuff measurement lasted between 120 to 180 second. Upon cuff deflation at the end of the measurement, the physician removes the cuff and asks subject to remove

electrodes. The overall testing protocol is expected to last 20 minutes. Figure 4.2 for a flowchart overview of the major procedural steps.

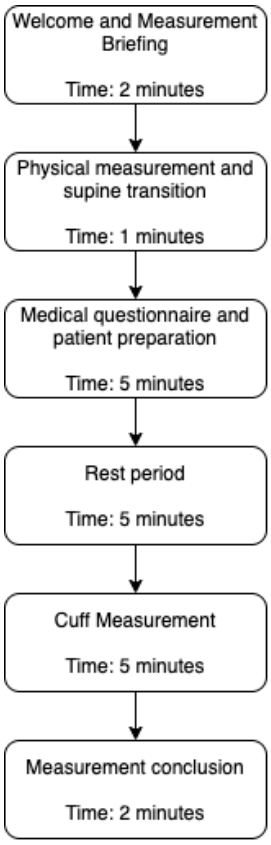

Figure 4.2: Flowchart showing the main steps of the measurement procedure.

Data Analysis

Qualitative analysis of the recording and subject characteristics was manually performed for each individual to ensure high quality data; this step looked for undetected device malfunctions, sensor saturation, and irregular heart activity. The measurement recordings contained time synced signals from cuff-device and ECG. The analysis procedure segmented the cuff device measurement in four segments: (1) BP measurements, (2) DBP hold, (3) MAP hold, and (4) sSBP hold. From the BP measurement, the SBP, DBP, MAP and HR values are extracted as integer values. For segments (2), (3), and (4) the pressure time signals were indexed, and segmented. The algorithm identified the segment of longest sequential pulsations, herein referred to as the sequential segment. Recordings with sequential segments shorter than 8 pulsations were excluded from analysis.

The raw pressure time signal from the sSBP hold is scaled to physiological pressure units using the signal calibration methods discussed in Chapter 2. The BP measurement results from the cuff, in the form of SBP and DBP, are used for calibration. Two calibration methodologies discussed, the static calibration and the dynamic calibration, are separately applied to the waveform. The output signals from the calibration methods are qualitatively compared. Further details on the algorithmic implementation of the static and dynamic signal calibration methods are found in Chapter 2.

Pulse waveform analysis was performed on the waveforms from the sSBP hold. A subset of 9 waveform parameters that characterize cardiovascular health were selected for this analysis, the complete parameter list with respective description is found in Table 4.1. Pulse waveform analysis was performed on a BTB basis for all the high-quality waveforms selected from the algorithm.The pulse waveform analysis parameters were evaluated across the population using two different analysis methods: static analysis and dynamic analysis. The static analysis evaluated the subject-mean pulse waveform feature on the entire study population. The parameters were compared to the ranges reported in the literature for an understanding of the distribution in the context of accuracy and reliability. The dynamic analysis evaluated the pulse waveform magnitude fluctuation in response to physiological breathing. This evaluation was purely qualitative in nature and goes to assess the measurement capability of the device.

4.3 Results

Study Population

The IRB study was performed at Caltech from May 17th, 2022, to June 2nd, 2022. The study enrolled a total of 31 healthy control individuals. Qualitative exclusion criteria from the recording evaluation discarded 0 individuals as no device malfunctions, signal saturation and irregular heart activity were detected. Implementation of the algorithmic filtering excluded an additional 0 individuals from analysis. The total population included in the analysis after filter was of 31 subjects.

The population analyzed in this study (n=31) is composed of 68% men and the average age was 27 years. The mean BMI was 23.7 classifying the average subject as healthy weight. The left arm circumference within the population ranged from 28 cm to 36 cm, all of which fell within the operating range of the brachial cuff. Within the study population, 3% reported hypertension, 13% reported hyperlipidemia, and 26%

Parameter	Description
AIx	The augmentation index is a proxy indicator of left ventricular systolic loading. [1]
AP	The augmentation pressure is a measure of the wave reflection contribution to systolic pressure. [2]
SPTI	The systolic pressure time integral is a surrogate measure for cardiac output and myocardial oxygen demand. [3]
DPTI	The diastolic pressure time integral is an indicator of sub-endocardial blood supply. [3]
SBP	The systolic blood pressure is a measure of the peak pressure exerted on the arterial wall.
DBP	The diastolic blood pressure is a measure of the minimum pressure exerted on the arterial wall.
ST	The systolic time is a measure of the left ventricular ejection time.
DT	The diastolic time is a measure of the left ventricular relaxation time.
HR	The heart rate is a measure of the number of heart contractions per minute.

Table 4.1: Description of the sSBP pulse waveforms parameters used for the Healthy control population study.

reported being current smokers. No prevalence of cardiovascular disease is present within the population. Overall, the general physical and medical characteristics confirm the good health of the selected population and validates their use as a healthy control group for the study's purposes. Table 4.2 shows the medical characteristics of the study population. Note, all the shown numbers are derived from self-reported data from the subject's case report form.

Device Functionality

The device successfully performed the measurement on all 31 subjects during the IRB study. For each subject, the procedure consisted of a complete device measurement: the BP measurement followed by the DBP, MAP, and sSBP pressure holds. Of the 31 BP measurements, 27 (87%) were performed in the default inflation mode, and 4 (13%) automatically resorted to deflation mode. Case-specific reasons for switching to deflation mode are unknown but usually fall within one of the following conditions: low signal amplitude, noisy measurement, or irregular heart rhythm. In all 31 measurements, the pressure holds were performed sequentially following the BP measurement with subject-specific values. The DBP, MAP, and sSBP hold had an inflation time of 30, 20, and 40 seconds, respectively. The pressure

Characteristic	Population (n=31)
General Characteristics	
Male, n (%)	21 (68%)
Age, mean (years)	29 ± 10
Weight, mean (kg)	73 ± 11
Height, mean (m)	1.75 ± 0.09
BMI, mean (kg/m^2)	23.8 ± 3.0
BSA, mean (m^2)	1.89 ± 0.19
Left Arm Circumference, mean (cm)	29 ± 5
White, n (%)	25 (81%)
Comorbidities	
Hypertension, n (%)	1 (3%)
Diabetes, n (%)	1 (3%)
Thyroid, n (%)	1 (3%)
Hyperlipidemia, n (%)	4 (13%)
Smoker, n (%)	8 (26%)
Blood Pressure Medication, n (%)	2 (6%)
Cardiovascular Disease	
Heart Failure, n (%)	0 (0%)
Cardiomyopathy, n (%)	0 (0%)
LV Dysfunction, n (%)	0 (0%)
Stroke, n (%)	0 (0%)
Heart Valve Disease, n	0 (%)

Table 4.2: The medical characteristics of the Caltech IRB study population.

hold waveforms displayed features used in PWA for all 31 volunteers. Examples of segmented and calibrated waveforms from four individuals for all pressure holds are shown in Fig. 4.3. The pulse waveforms from the three pressure holds showed distinct waveform morphologies. Pulse waveform morphologies specific to a pressure hold were consistent throughout the study population. This indicates the device is capable of successfully identifying subject-specific target pressure locations from the oscillometric measurement. The device was successfully operated using the remote controller, and all the operator communications could be directly interpreted from the DAQ without the need to access the device. No device malfunction occurred during the testing protocol.

Evaluation of Calibration Methods

The envelope function is the central component of the dynamic signal calibration method. With the current device design, the envelope function is approximated using the data from the DBP, MAP, and sSBP pressure holds. For each hold, the

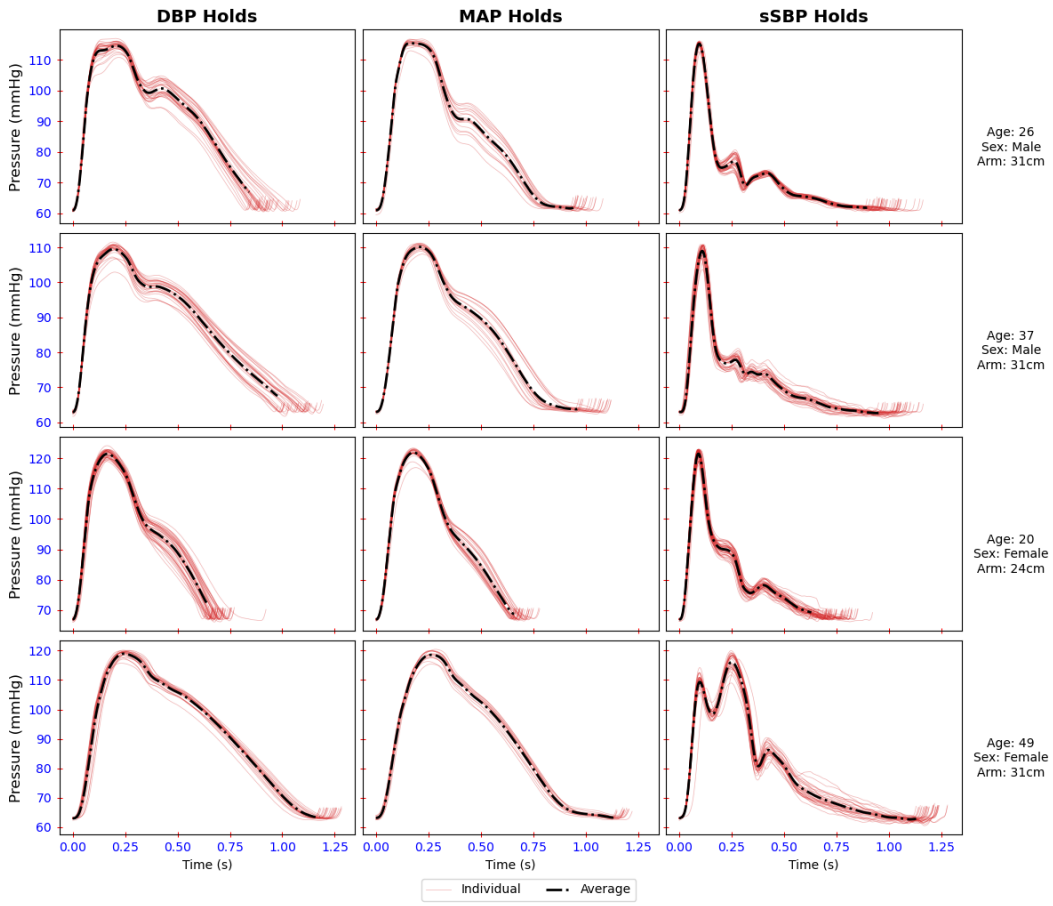

Figure 4.3: Averaged pulse waveform examples from the three hold pressures. The (left) DBP, (middle) MAP, and (right) sSBP hold pulse waveforms from four subjects in the IRB study are shown. The dashed black line is the average of the individual hold pulsations, red lines.

raw signal from the differential pressure sensor and the nominal cuff pressure pressure are averaged to create the three cardinal points of the envelope function. The envelope is recreated by linear interpolation of the points from the DBP to MAP data pair and from the MAP to sSBP data pair. The top panel in Figure 4.4 shows the three point reconstruction of the envelope functions for the study population. The envelope function peaks at the MAP hold pressure indicating this as the point of maximal cuff pulse amplitude. The slopes from the DBP to the MAP had a mean of 0.036 and a standard deviation of 0.022. The slopes from the MAP to the sSBP had a mean of -0.029 and a standard deviation 0.008.

The static and dynamic signal calibration methods were successfully applied to the sSBP hold pressure for the entire study population. Figures 4.5 and 4.6 show

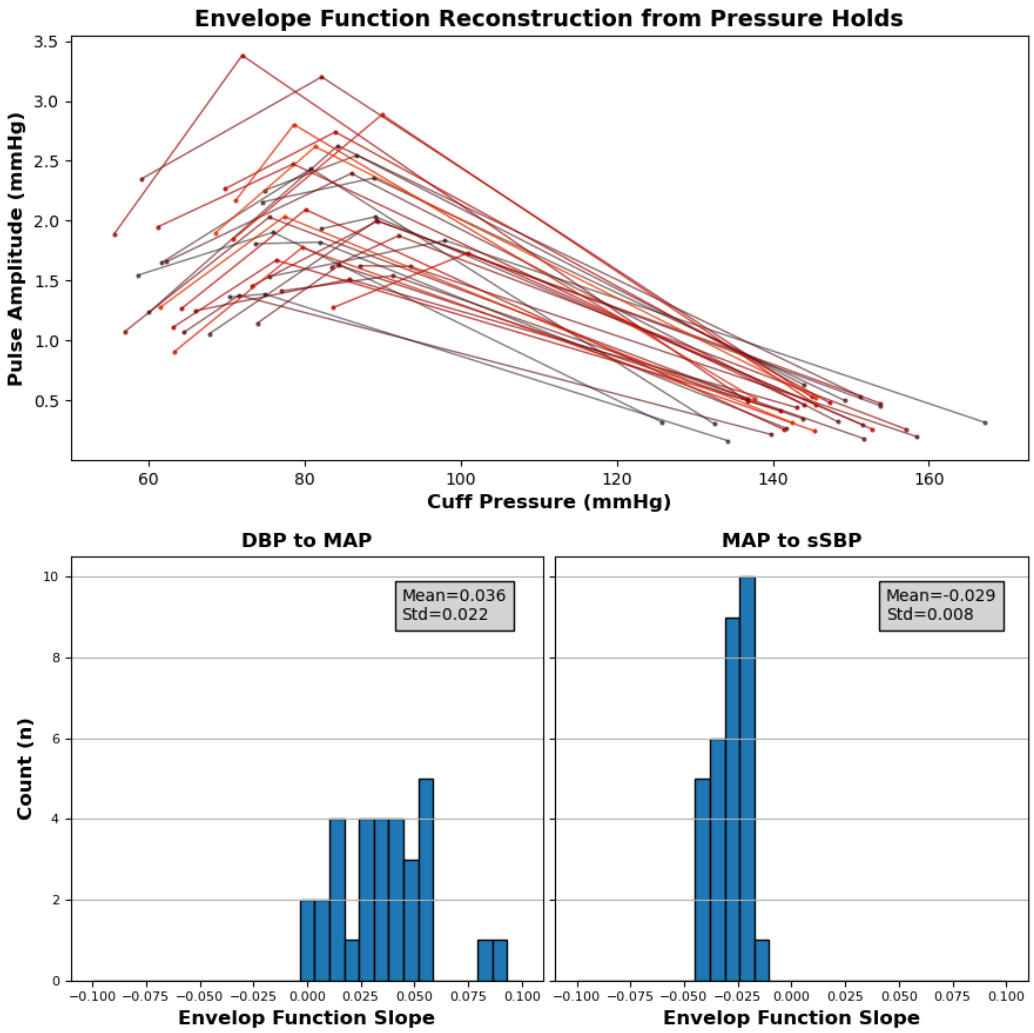

Figure 4.4: The envelope function reconstruction data for the study population. (Top) shows the reconstructed envelope function from the DBP, MAP, and sSBP hold pressure data pairs. Please note that the use of color is solely intended to aid in distinguishing between the lines and does not carry any additional meaning or significance. (Bottom) shows the envelope function slopes from the DBP to MAP point (left) and form the MAP to sSBP point (right).

side by side examples of the static and dynamic signal calibration methods. The static calibration method effectively removed all signal fluctuations in scaling the waveforms to SBP and DBP. The dynamic calibration method maintained breathing related fluctuations of the BP values; in certain cases (Figure 4.5 the BP magnitude fluctuations were significant and in other cases (Figure 4.6 these were a lot more moderate. This behavior was seen throughout the entire population.

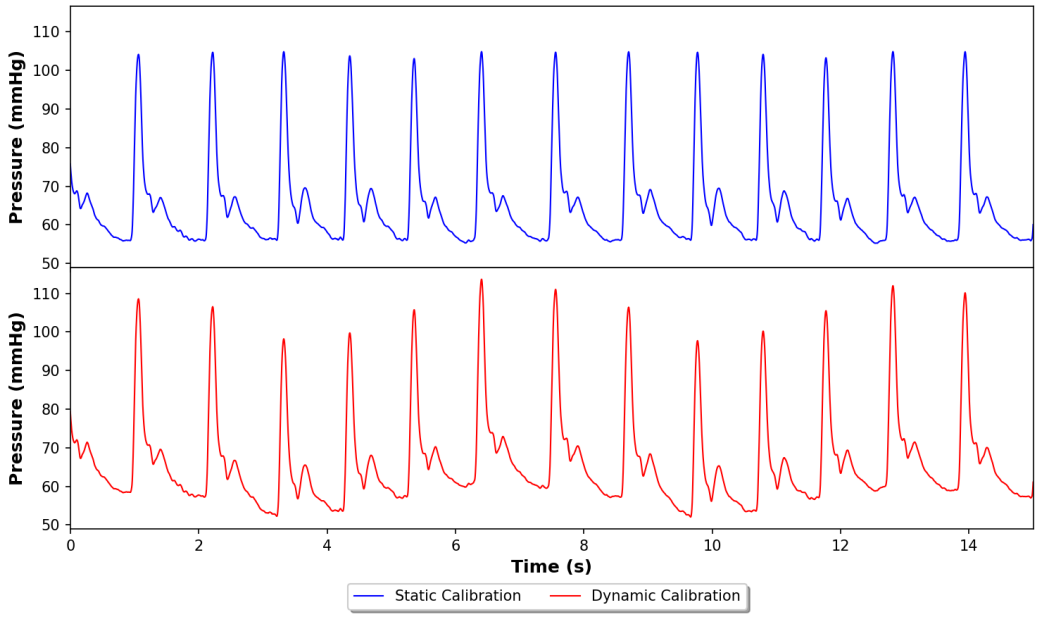

Figure 4.5: The (top) static and (bottom) dynamic signal calibration for a 15 second sSBP hold segment in an individual with large BP breathing fluctuations.

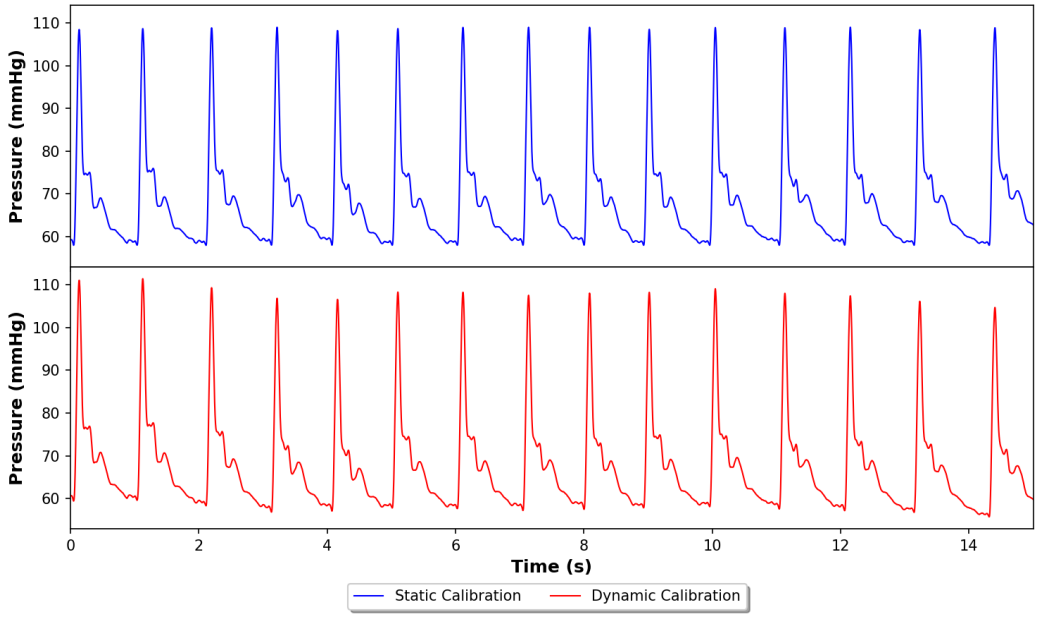

Figure 4.6: The (top) static and (bottom) dynamic signal calibration for a 15 second sSBP hold segment in an individual with small BP breathing fluctuations.

Static Pulse Waveform Analysis

Pulse waveform analysis on the sSBP hold waveforms was successfully performed on all study individuals (n=31) calculating the BTB values for all 9 parame-

ters from Table 4.1. In the static analysis, the pulse waveform features were averaged for each subject. Figure 4.7 shows histogram plots for the 9 pulse waveform features analyzed in this study, the histograms were constructed with subject-averaged features. The distributions were plotted in the range reported in the literature; the narrow distributions show that healthy control individuals are categorically grouped together. The subject averages for the parameters showed the following trend:

- SBP had a mean of 113 mmHg and min-max of 91 and 134 mmHg.
- DBP had a mean of 61 mmHg and min-max of 51 to 74 mmHg.
- SPTI had a mean of 26.8 mmHg and a min-max of 21.1 to 35.0 mmHg.
- DPTI had a mean of 43.2 mmHg and a min-max of 29.0 to 66.2 mmHg.
- AIx had a mean of -61.1 and a min-max of -86.8 to 12.0.
- AP had a mean of 31.4 mmHg and a min-max of -6.5 to 47.5 mmHg.
- ST had a mean of 0.308 s and a min-max of 0.258 to 0.359 s.
- DT had a mean of 0.654 s and a min-max of 0.403 to 1.046 s.
- HR had a mean of 64 bpm and a min-max of 44 to 91 bpm.

Dynamic Signal Fluctuations

The high resolution signal from the brachial cuff device displayed pressure fluctuation characteristics that are consistent with the physiological pressure fluctuations from breathing. Signal amplitude fluctuations are the most obvious breathing induced pressure fluctuations; this phenomenon arises from the fixed cuff pressure and the physiological variation of BP. Figure 4.8 shows that this signal characteristic is present in all three pressure holds. At a qualitative level, one can also notice that the pulse waveform features also experience sinusoidal fluctuations, this is most obvious for features like AIx and the relative height of the dicrotic notch. These observations are consistent with the pressure behaviors that are observed in typical invasive catheter recordings [4].

The dynamic analysis on the pulse waveform features looked at the BTB variation of the parameter magnitude across the sSBP pressure hold. Breathing fluctuations were also measured on the parameter magnitudes; the magnitude of

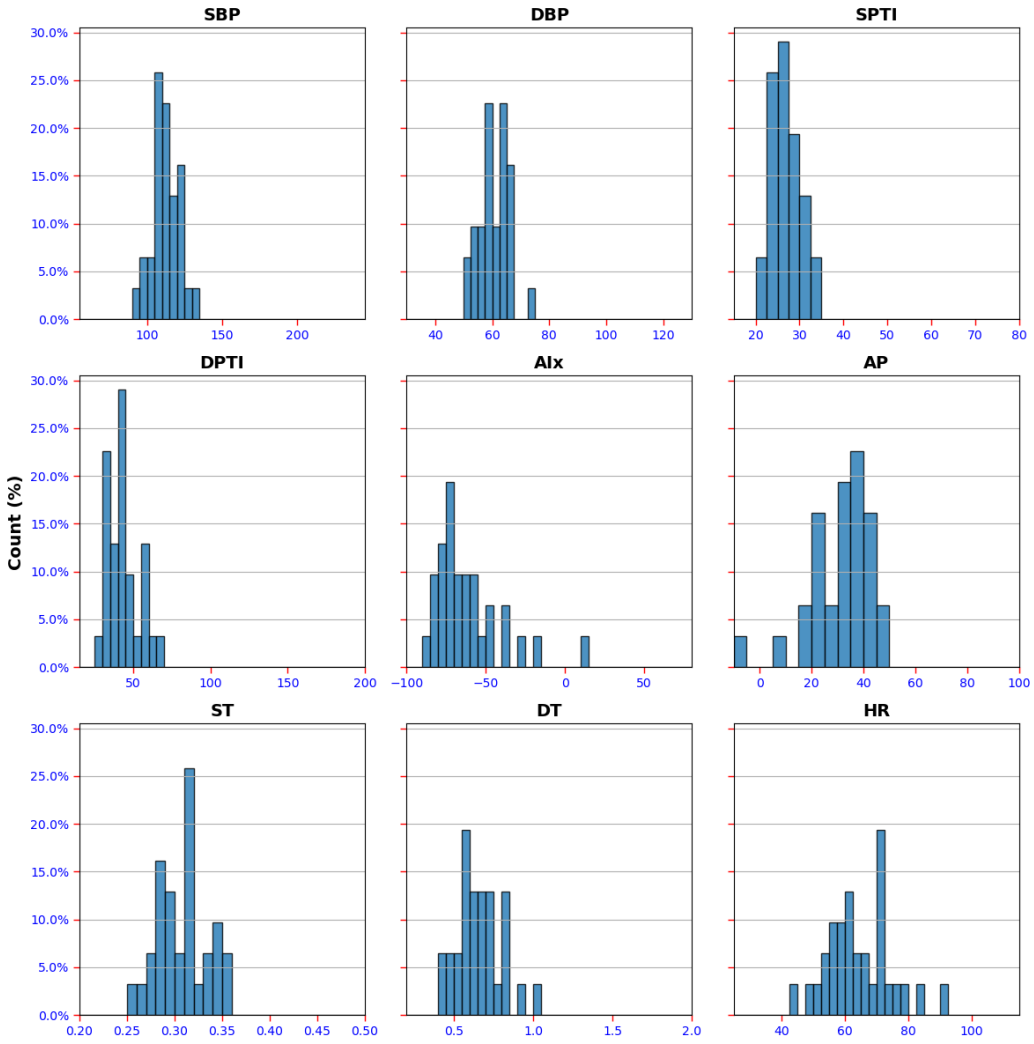

Figure 4.7: The population-wide mean distribution of the analyzed pulse waveform parameters. Histograms ranges are taken from literature as a means of comparison.

these fluctuations varied amongst individuals. Figures 4.9 and 4.10 show examples of the dynamic fluctuations for two test volunteers on the sSBP hold pressure data. The top panels show the pulse waveform from the sSBP hold and the bottom three panels shows the BTB pulse waveform features for SPTI, AIx, and HR. All three pulse waveform features show sinusoidal fluctuations that can be associated with the breathing process. These behaviors are observed across the entire population yet for conciseness only two examples as shown.

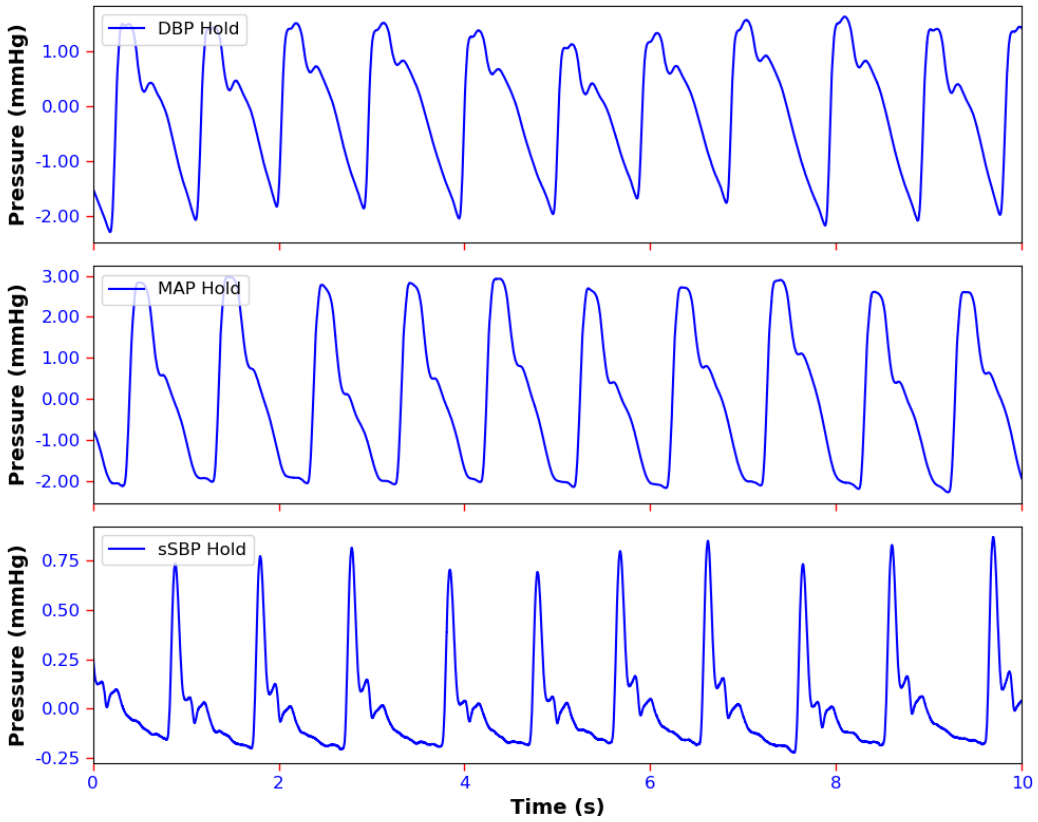

Figure 4.8: Ten second segments of the raw pressure signal captured with the cuff device for the DBP, MAP, and sSBP hold pressures.

Observations on Device to User Interactions

Overall, the cuff-device was well-received by both physicians and test subjects due to its similarity to a traditional BP cuff. Placement of the cuff on the left arm was a smooth process that could be easily repeated with the subject in a standing position. However, the connection of the device casing to the cuff proved to be a challenge due to the short connector tubing (22cm), limited audio feedback from the clipping mechanism, and the arrangement of the test setup which did not provide the operator with sufficient confidence in the successful connection between the cuff and the casing.

During testing, no complaints were reported by the subjects regarding the measurement portion. As expected, the subjects commented on an increasing pressure from the cuff as the measurement progressed due to the increase in cuff pressure. Although the sSBP portion of the measurement was described as tight, no subjects reported pain or the inability to complete the measurement due to pressure.

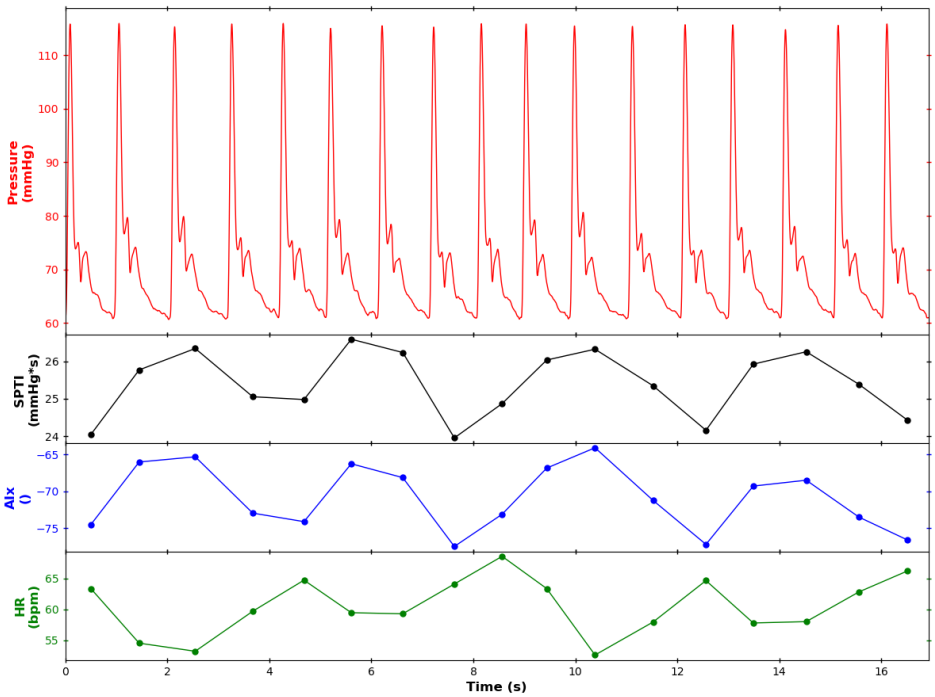

Figure 4.9: The pulse waveform feature fluctuations for Subject 1. Top panel shows the calibrated pressure time signal. The bottom three panels show the calculated feature evaluated for the corresponding pulse waveform. The SPTI, AIx, and HR are sequentially shown from top to bottom.

It was observed that anticipating the progressive cuff tightness helped to reduce unexpected discomfort for the subjects. Moreover, no measurements had to be repeated due to subject movement or failure to comply with instructions, indicating a successful execution of the measurement procedure.

The physician did not encounter any difficulties while operating the device through the remote controller, which was found to be intuitive and user-friendly. However, interpreting the device output required assistance from the device operator. Due to the multi-segment structure of the measurement, there was some uncertainty in the expected output for each segment, although this process became progressively easier over the course of the study. Nevertheless, it would require a longer period to fully master the interpretation of the device output. Device error messages were easily noticeable, but understanding their source was non-trivial, and their rare occurrence during the study added to the complexity of interpretation.

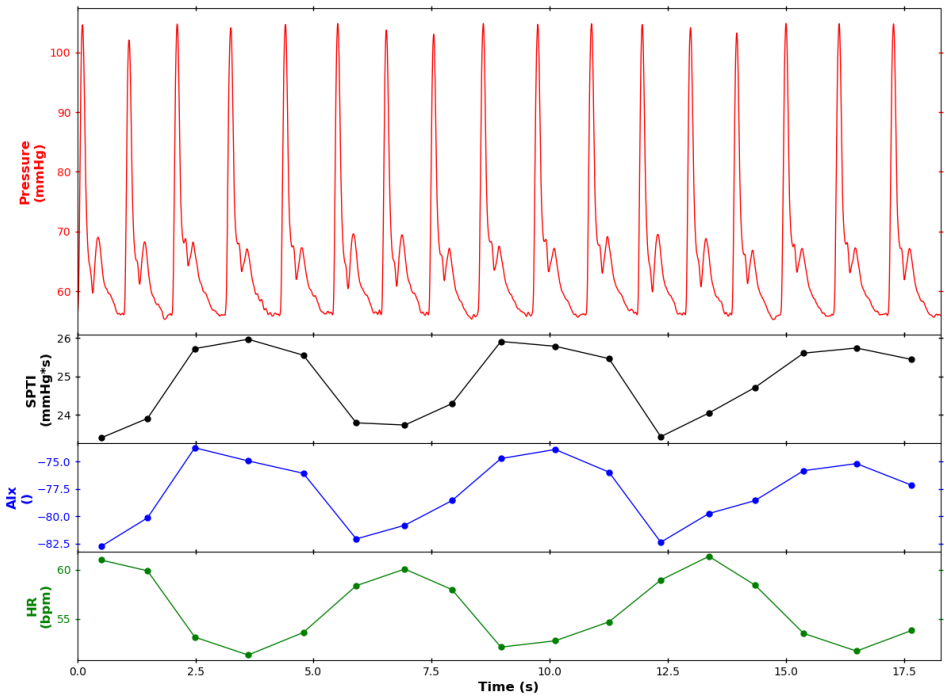

Figure 4.10: The pulse waveform feature fluctuations for Subject 2. Top panel shows the calibrated pressure time signal. The bottom three panels show the calculated feature evaluated for the corresponding pulse waveform. The SPTI, AIx, and HR are sequentially shown from top to bottom.

In summary, the device was successfully operated by the physician during the entire test, and the subjects demonstrated a positive acceptance of the device and its programmed measurement.

4.4 Discussion

The limitations of tonometer-based pulse waveform acquisition systems have motivated the development of cuff-based approaches. However, the low resolution of captured pulse waveforms has hindered the adoption of these systems in cardiovascular applications. This thesis proposes a novel high-fidelity pulse waveform acquisition approach that combines a pLPF and a high-resolution differential pressure sensor. The differential pressure sensor measures the difference between cuff signal in the measurement port and a dynamic mean signal in the reference port. The pLPF acts as a moving average filter, enabling the differential pressure sensor to operate at a net differential pressure of zero. As a result, the signal from the pressure sensor is always centered, irrespective of the pressure behavior in the system. This facilitates the configuration of a pressure sensor optimized for the

pulse waveform amplitude, with a single filter conformation designed to fit all BP physiological operating ranges. The proposed pneumatic filter requires minimal hardware components to configure an NIBP module with tourniquet capabilities for high-resolution signal capture, making it a promising solution for high-resolution cuff-based pulse waveform acquisition.

This chapter reports on a proof-of-concept study conducted at Caltech under IRB protocol number 21-1114, which aimed to validate the concept of a passive pLPF for high-resolution pulse waveform acquisition using a cuff-based device. The study successfully demonstrated the device's ability to capture the pulse waveform in all three pressure holds. The morphology of the pulse pressure waveform displayed consistent behavior in all volunteers, with the MAP waveform showing the largest amplitude and the sSBP waveform containing the highest information content, as indicated by the pressure wave morphology. These results suggest that the device effectively uses the BP measurement from the initial oscillometric measurement to perform pressure holds at subject-specific targets.

Furthermore, the study confirmed the fluid-dynamic relationship between the exerted cuff pressure and the physiological pressure signal. Increasing cuff pressure reduces the inner diameter of the brachial artery, leading to a reduction in brachial artery flow. When the cuff pressure reaches a level greater than the SBP, the artery fully collapses, and flow in the brachial artery ceases. As the cuff pressure increases, greater levels of detail appear in the pressure signal captured with the brachial cuff, with maximal detail observed at sSBP. This observation confirms previous findings from the literature that the sSBP hold pressure is equivalent to a pressure tap in the ascending aorta, providing a purely pressure-dependent signal rich in content [5]. The study also found that physical characteristics such as age, gender, height, weight, and left arm circumference did not affect the recording quality or observed behavior within the limited ranges tested. Overall, the device appeared to be a robust solution for general population measurement of the pulse waveform.

Signal calibration is an algorithmic process to convert the non-invasive pulse waveform signal to physiological BP units. This thesis proposes a new method to dynamically scale the pulse waveforms by using the oscillometric envelope function such that pressure fluctuation data in conserved. The reconstruction of the envelope function with sparse pressure hold data proved successful and displayed the typical characteristic of the amplitude maximum at MAP pressure. The DBP to MAP slope

in the envelope function reported a wide distribution; these results are most likely associated with the proximity between these two magnitudes and could potentially be a source of BP overestimation in the oscillometric measurement. The dynamic scaling method produced a signal with sinusoidal pressure fluctuations that varied in magnitude across subjects, similar to what would be expected in an invasive measurement. This approach holds promise in physiologically scaling the pressure time signal with breathing fluctuations. The next step would be to validate this method with invasive physiological data to further assess its accuracy and applicability.

The static pulse waveform analysis performed on the sSBP hold waveform showed a narrow distribution for the parameter space. The parameter space interrogates a multitude of cardiovascular factors ranging from the heart cardiac output to the cardiovascular stiffness. Considering the young and healthy nature of the study population, these results indicate that the device results are repeatable and accurate.

In many non-invasive pulse waveform acquisition devices, the dynamic behavior of the pressure time signal is often not detected or overlooked. However, in this study, all pressure hold recordings displayed the physiological fluctuations of the cardiovascular system in response to breathing. Qualitatively, all three pressure time signals displayed sinusoidal amplitude and mean fluctuations, as shown in Fig. 4.8. These fluctuations are also known to occur in pulse waveform features, and this fact is confirmed by the results shown in Figures 4.9 and 4.10, which demonstrate the BTB fluctuation of a small subset of pulse waveform features in the sSBP hold. The high-fidelity signal allows for the measurement of these pulse waveform features with elevated accuracy, giving confidence that the observed fluctuations are physiology-based. These results are consistent with behaviors observed in invasive catheter measurements [4]. The importance of these results is twofold: firstly, they show that non-invasive systems can more accurately match their invasive counterparts, and secondly, such devices can meet the demands of the rising interest in cardiovascular dynamics for diagnostic purposes.

With the rise of cardiovascular disease in the U.S. and worldwide, improving non-invasive pulse waveform acquisition methodologies for diagnosis and subject monitoring is essential. This study demonstrated the feasibility of using passive pneumatic filters, the pLPF, to obtain high-resolution pulse waveform data with cuff-based devices across a healthy control population. This is achieved using the pLPF on the reference port of the high-resolution differential pressure sensors

to capture the mean pressure as a measurement base dynamically. The results from the study show that the high-fidelity signal generates consistent waveform morphologies that exhibit characteristic pulse waveform features. Furthermore, the improved sensor resolution also captures dynamic aspects of the cardiovascular waveform that closely resemble the invasive catheter. The improved signal quality from the proposed approach for cuff-based BP devices allows for a more widespread application of non-invasive pulse waveform acquisition both in the clinic and at home.

Limitations

While the study provided valuable insights into the reliability and accuracy of the cuff-device, it is important to acknowledge some limitations of this work. One limitation is that the study population consisted of young, healthy individuals. As people age and develop various health conditions, multiple cardiovascular and physical factors can impact the strength and quality of the pulse waveform throughout the body. This can potentially affect the quality of the non-invasive recording at the brachial artery [6]. Therefore, further testing of the device on a more diverse population will be necessary to fully optimize the system's configuration. Another limitation is that many of the study's observations are based on qualitative comparisons with other literature results, and no direct comparison was tested in this study. Future studies must assess the reliability and reproducibility of this device configuration by comparing it with the invasive counterpart. This would provide more concrete evidence of the device's accuracy in capturing pulse waveforms and enable better validation of the device's diagnostic potential. Overall, while the study provided encouraging results, further research is necessary to address these limitations and fully evaluate the device's potential in clinical settings.

References

[1] James E. Sharman et al. "Augmentation Index, Left Ventricular Contractility, and Wave Reflection." In: *Hypertension* 54.5 (Nov. 2009), pp. 1099–1105. DOI: 10.1161/hypertensionaha.109.133066. URL: https://doi.org/10.1161/hypertensionaha.109.133066.

[2] F. Fantin et al. "Is Augmentation Index a Good Measure of Vascular Stiffness in the Elderly?" In: *Age and Ageing* 36.1 (Nov. 2006), pp. 43–48. DOI: 10.1093/ageing/afl115. URL: https://doi.org/10.1093/ageing/afl115.

[3] T Mannion et al. "The Relationship Between the Buckberg Index and Functional Capacity in Stable Chronic Heart Failure Patients." In: *General poster session 1*. BMJ Publishing Group Ltd and British Cardiovascular Society, Oct. 2017. DOI: 10.1136/heartjnl-2017-ics17.15. URL: https://doi.org/10.1136/heartjnl-2017-ics17.15.

[4] Sheldon Magder. "Clinical Usefulness of Respiratory Variations in Arterial Pressure." In: *American Journal of Respiratory and Critical Care Medicine* 169.2 (Jan. 2004), pp. 151–155. DOI: 10.1164/rccm.200211-1360cc. URL: https://doi.org/10.1164/rccm.200211-1360cc.

[5] A. Lowe et al. "Non-invasive Model-Based Estimation of Aortic Pulse Pressure Using Suprasystolic Brachial Pressure Waveforms." In: *Journal of Biomechanics* 42.13 (Sept. 2009), pp. 2111–2115. DOI: 10.1016/j.jbiomech.2009.05.029. URL: https://doi.org/10.1016/j.jbiomech.2009.05.029.

[6] Gary E. McVeigh et al. "Age-Related Abnormalities in Arterial Compliance Identified by Pressure Pulse Contour Analysis." In: *Hypertension* 33.6 (June 1999), pp. 1392–1398. DOI: 10.1161/01.hyp.33.6.1392. URL: https://doi.org/10.1161/01.hyp.33.6.1392.

Chapter 5

A SUPRA-SYSTOLIC CUFF-BASED METHOD FOR ACCURATE MEASUREMENT OF CENTRAL CARDIOVASCULAR PULSE WAVEFORM FEATURES

"Dimidium facti, qui coepit, habet: sapere aude, incipe."
He who has begun is half done: dare to know, begin.
— Quinto Orazio Flacco, *Epistole*

This chapter is based on the following manuscript:

Alessio Tamborini and Morteza Gharib. "A Supra-Systolic Cuff-Based Method for Accurate Measurement of Central Cardiovascular Pulse Waveform Features." In Preparation. N.D..

CHAPTER 5 INTENTIONALLY REDACTED

Chapter 6

A BRACHIAL CUFF DEVICE METHOD FOR CARDIOVASCULAR AUSCULTATION OF THE LEFT SIDE OF THE HEART

> *"Conta ciò che si può contare, misura ciò che é misurabile e rendi misurabile ciò che non le é."*
> Count what can be counted, measure what is measurable and make measurable what is not so.
>
> — Galileo Galilei

This chapter is based on the following manuscript in preparation:

Alessio Tamborini and Morteza Gharib. "A Brachial Cuff Device Method for Cardiovascular Auscultation of the Left Side of the Heart." In Preparation. N.D..

CHAPTER 6 INTENTIONALLY REDACTED

Chapter 7

AN OBSERVATIONAL STUDY ON THE IMPACT OF BREATHING ON LEFT VENTRICULAR AND BRACHIAL CUFF WAVEFORM PARAMETERS

"The fastest way to succeed is to double your failure rate."

— Thomas J. Watson

CHAPTER 7 INTENTIONALLY REDACTED

Chapter 8

CONCLUSION

"If I have seen further, it is by standing on the shoulders of giants."

— Isaac Newton

This thesis documents the scientific journey of a medical device from a bench top prototype to a multi-site clinical study. Throughout this process we have had a flavor of all intricacies that are involved with ideation, design, development, manufacturing, and testing of a non-invasive diagnostic medical device. This experience taught how to take ideas from a whiteboard and create functional prototypes that can be safely tested, how to translate laboratory prototypes into manufacturable devices, and how to analyze human data to develop algorithmic models that reflect the underlying physiology. In particular this work focused on the development of a brachial cuff technology for high-resolution pulse waveform acquisition. The tests and studies performed have shown its accuracy and reliability in capturing high fidelity information about the heart and cardiovascular system. These efforts aim to narrow the information gap between invasive measurements and their non-invasive counterpart in the field of cardiology.

Chapters 2 and 3 discuss the design and functionality of the components in the cuff-based system for high-resolution pulse waveform acquisition. The device proposed herein aims to improve wide-spread applicability of non-invasive pulse waveform analysis by addressing ease of measurement and result repeatability. The challenge in this part of the project was the acquisition of a small pressure signal in a large operating range. We exploited our knowledge of fluid dynamics to design a pneumatic low pass filter to obtain the running mean pressure from a

pulsatile input signal. This component was combined with a differential pressure sensor to effectively capture a high-pass filtered version of the input signal. We mathematically showed that the pneumatic low pass filter's behavior is governed by a set of equations that closely mimic the well-known electrical low pass filter. From these set of equations we extracted the time constants of the model allowing the reader to redesign the components for an application of their interest. The filter characteristics were specified for a physiological application that would theoretically generalize well to the entire population. The shape friendly design was integrated into the device for high-resolution pulse waveform acquisition. Preliminary testing results showed the system is user friendly and highly mitigates operator errors. The iterative design process culminated with a medical device that captures high-resolution pulse waveforms at distinct subject-specific pressure-flow conditions.

Chapters 4 and 5 discuss the human studies that were used to evaluate the device's accuracy. The first human IRB study was performed at Caltech and recruited healthy volunteers for a quality control on the system. The study evaluated the reliability of the measurement and validated that within a healthy population pulse waveform parameters generate consistent results. The second human study was a multi site clinical study with individuals referred for left heart catheterization. The study consisted of simultaneous recordings with an invasive catheter, the cuff measurement and an electrocardiogram; the study performed a measurement in the left ventricle followed by a measurement in the aorta. The clinical data from the catheter in the ascending aorta and the cuff measurement was analyzed to assess the capability of the brachial cuff to accurately measure central cardiovascular health. The study revealed that our cuff with sSBP hold pressure produces an high-fidelity representation of the central cardiovascular signal parameters. Chapters 3 and 4 also discuss the work done to study and conserve the dynamic modulation of the cardiovascular pressure signal, one of the measurement aspects that is typically neglected in non-invasive systems. I introduce a novel method for signal calibration using the subject-specific oscillometric envelope function to preserve the dynamic breathing fluctuations. Evaluation against the pressure signal from the catheter showed the calculated fluctuations from the cuff are proportional to those measured invasively. These results show that advances in cuff-based systems allow to accurately measure central cardiovascular parameters in a non-invasive and consistent manner.

Chapters 6 and 7 correlate the pulse pressure signal from the brachial cuff to left ventricular functions. Chapter 6 introduces a method to extract the pressure-sound

equivalent of the heart sounds from the brachial cuff measurement. These pressure vibrations are shown to originate from the forceful opening and the closing stretch-and-recoil behavior of the aortic valve. Left ventricular pressure gradients are found to be one of the determining physiological factors in the generation of these sounds. The cuff pressure-sound waveform parameters followed the expected physiological behavior setting a first stepping stone towards the non-invasive characterization of the left ventricular contractile function. Future studies will target developing predictive models for the systolic and diastolic contractile function using cuff derived pressure-sound waveform parameters. In Chapter 7 we perform an observational study on the influence of breathing on the catheter signal in the left ventricular and the cuff parameters. Pressure fluctuations caused by physiological breathing were shown to produce measurable and equivalent effects in the left ventricle and the cuff signal. With the improvement of medical technologies, the dynamic components of the pressure time signal are starting to gain more attention in the cardiovascular space and we hope the steps presented in this analysis can further motivate their advance. In summary, accurately characterizing left ventricular functions is a big step towards creating more informative non-invasive diagnostic tools.

Appendix A

CUFF DEVICE PROGRESSION THROUGH TIME

The device used throughout this thesis is the latest version of our non-invasive pulse waveform acquisition device. Yet, as most engineers would appreciate, the design process required multiple iterations to reach a final version. This section highlights the major device iterations that led to the final version shining light on the iterative nature of the engineering design process and the lessons learned in designing a medical device. The device stages that will be discussed below include proof-of-concept, in-house prototype, medical grade prototype, and upgraded pneumatic prototype.

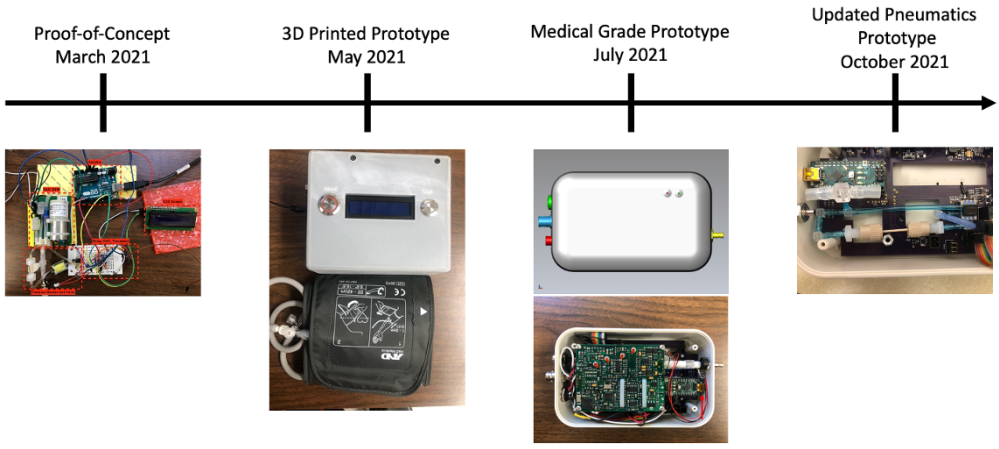

Figure A.1: Timeline showing the major device iterations through time.

A.1 Proof-of-Concept Prototype

The main goal of this project was to design a medical device for non-invasive pulse waveform acquisition that addresses the reliability issues of current tonometers while maintaining the high-fidelity signal. The arm cuff was the preferred candidate as it addresses measurement repeatability, reduces operator result dependence and has a clear reference force, yet as previously discussed these systems suffer from low signal resolution. The proof-of-concept phase had two main milestones: firstly, shows that the reference force applied as the cuff pressure to the arm has an impact

on the waveform shape, and, secondly, build a benchtop prototype to autonomously perform the measurement.

The first milestone served as a motivation for building a system that imposed a controlled forcing condition on the measurement location; the hypothesis was that the forcing function alters the pressure-flow relationship inside the artery causing the wave morphology to change. Without accurate control on this condition, no system can generate repeatable results regardless of the resolution. To show the waveform morphological changes with hold pressure, a pressure sensing pneumatic circuit was attached to a handheld manual blood pressure system. This system allowed to measure BP in the form of SBP and DBP using the Korotkoff sound method with a stethoscope. Using these BP values as reference the entire spectrum from sub DBP to sSBP pressures were tested in ten mmHg incremental intervals. For each pressure, the cuff was inflated with the manual pump and the pressure was maintained to capture at least ten seconds of pulse waveforms. The waveform morphologies from the measured ten second segments are overlayed in Figure A.2. These results clearly show that the nominal cuff pressure, the forcing condition on the brachial artery, has a direct impact on the shape and amplitude of the measured waveform. Signal amplitude is maximal at the MAP pressure, yet the signal is poor in pressure features. As the cuff is inflated to pressures higher than MAP, the signal amplitude decreased, yet the signal become more rich in pressure features. These results motivated the next step in the design of the device.

The first build of the device was a breadboard-based bench top model. The device in its bare form included all the components necessary for its functionality:

- the Arduino Uno was the microcontroller running the device operations,
- the PAR Medizintechnik NIBP module is the OEM board with BP monitor functionality,
- the pressure sensor and air-valve are used to capture the high-resolution signal,
- the relay, DAC, and transistor are for signal output, and
- the LCD screen is used for operator communication.

All electrical connections were made using jumper wires on a breadboard for flexible and fast prototyping. The pneumatic circuit was built with Luer fittings for similar

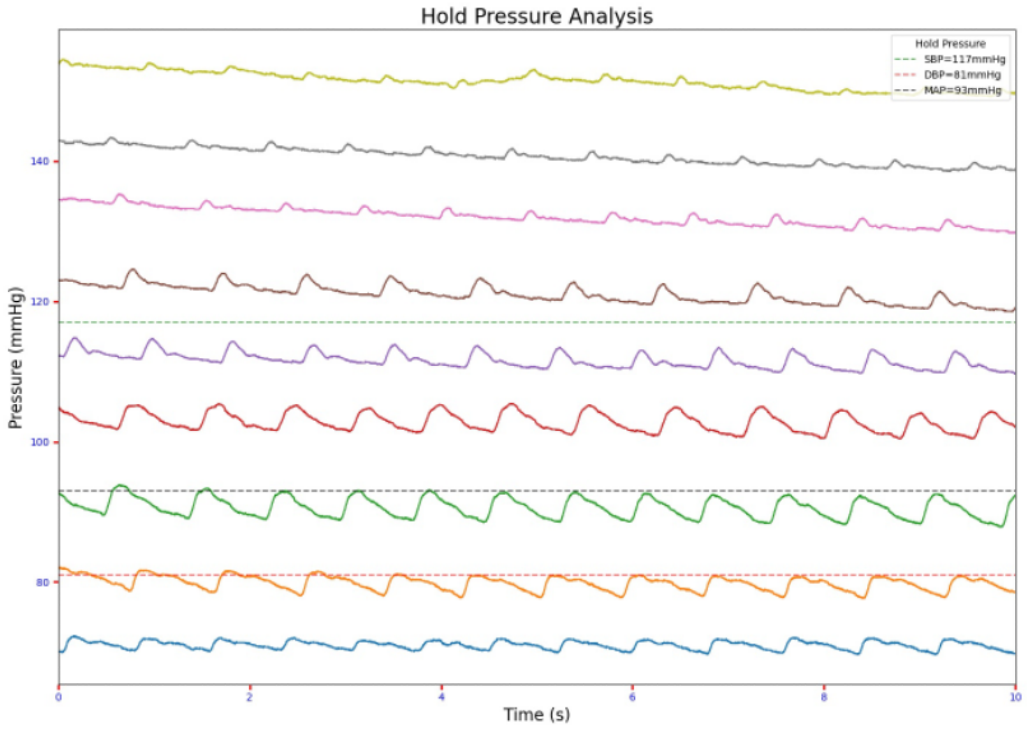

Figure A.2: Figure shows ten second recording segments of pulse waveforms at hold pressures in ten mmHg steps. Observe how the waveform morphology is dependent on the hold pressure.

reasons. Serial communication between the Arduino and the NIBP module was done using jumper wires. Multiple power units were used to accommodate for the different input voltages: Arduino was USB powered from the computer, the NIBP module was powered from an external power source and all other components were powered from the Arduino. The output signal is an analog voltage and was measured using the Arduino board. The measurement is initiated by manually closing a loop trigger on an input pin. The device in its raw form is shown in Figure A.3. The device described above successfully completed a measurement comprising a BP measurement and a hold pressure acquisition. The captured waveform contained all the features of a physiological waveform giving a solid benchmark for the first design.

A.2 In-House Prototype

Following the successful build of the proof-of-concept prototype, the next step must combine the components in a device that can be operated safely. This design stage consisted of placing all components in an enclosure, facilitating measurement

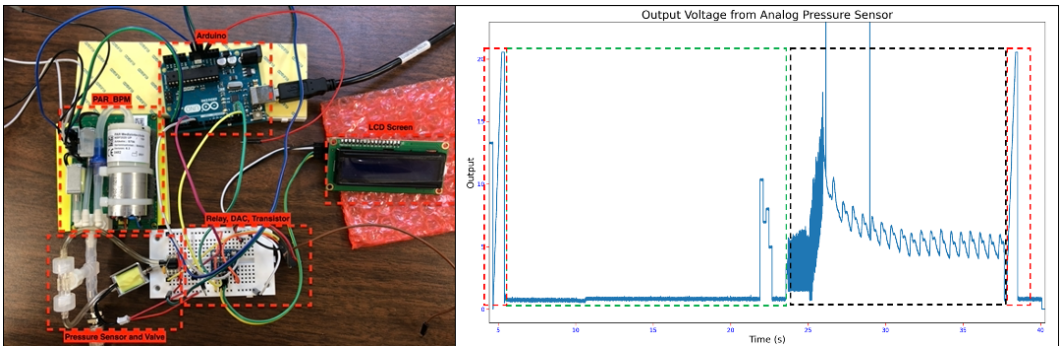

Figure A.3: First device build and measurement. (Left) shows the proof-of-concept prototype built on a breadboard and jumper wires design. (Right) shows a sample measurement from the device. The red dashed line circles the communication signals, the green dashed line circles the BP measurement, and the black dashed line circles the hold pressure signal acquisition section.

procedures, and structuring the measurement. A 3D enclosure was designed using SolidWorks to fit all the device components and inner pneumatics. The device was now operated using push buttons on the device casing, LED feedback was built in. The start button is pressed once to initiate a measurement and the abort button (red) is pressed to cut power to the device, acting as a kill switch. Upon removal of power, the device deflates and stops the measurement. The electronics on this design have been manually soldered to a PCB. As space was a concern in this design, the Arduino Uno was replaced with the Arduino Nano, which maintains all functionality yet has a form advantage. This design also contains voltage stepping on the PCB to allow for a single power input and voltage modification as necessary for each unit. The device has three connections: power and analog out which are electrical and the cuff which is pneumatic. The power is a power jack connection, the analog out is a BNC connection, and the cuff is a push to connect two-piece stainless-steel fitting.

Once powered, the device sits in idle state till the operator interacts using the buttons. In idle state, the Arduino is waiting for a command to initiate the measurement. Upon pressing the start button, the measurement starts with an oscillometric BP measurement and followed by two pressure holds. Upon measurement termination, the device returns to idle state and waits for another user input. Pressing the abort button at any time during the measurement, will immediately cancel the measurement, deflate the cuff, and return to idle state. The 3D printed version of the device successfully enclosed all electronics and pneumatics with a user-friendly interface for operations.

Figure A.4: Second device build and measurement. (Left) shows a 3D rendering of the CAD model from isometric view with transparent top cover. (Middle) shows the device enclosure from a top view with the cuff. (Right) the electronics of the device safely placed within the enclosure.

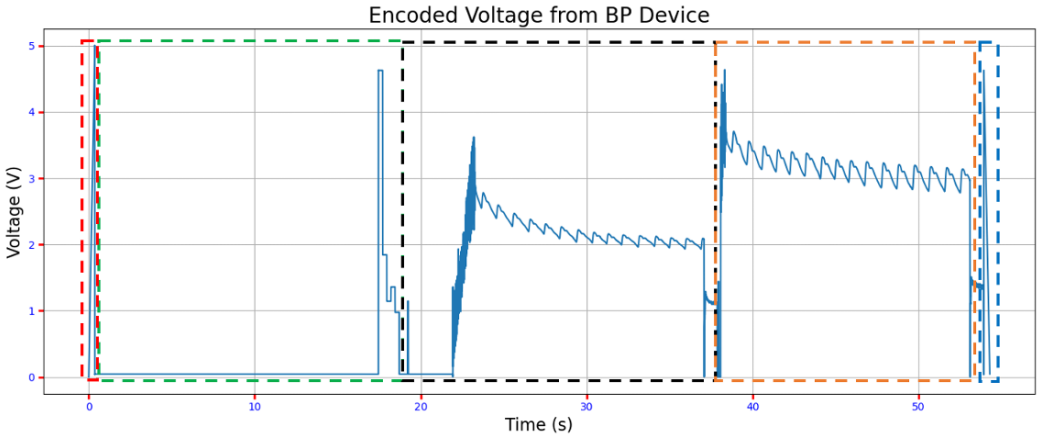

Figure A.5: Figure shows the measurement structured used in this device. This measurement features a unique start (red) and stop (blue) signal, a BP measurement (red) and two pressure holds (black and orange).

A.3 Medical Grade Prototype

Translating a medical device from a laboratory environment to a clinical setting requires meeting the safety standards within the operating procedure. One of the most important aspects to consider in testing a medical device is patient safety. In the context of the arm cuff device, electrical and operational safety apply. Generally, for a sphygmomanometer system, the safety standards describe the allowed maximal pressure and pressurized time for the cuff. For adult applications, the overpressure limit is of 300 mmHg and the maximal continuous inflated time is of 180 seconds. The system must deflate upon reaching any of these conditions. These safety measures were both programmed in the microcontroller and the NIBP module. Further information on the standards for a non-invasive sphygmomanometer can be

found in EN ISO 81060-2. On the other hand, medical electrical equipment safety for the device looks at the hardware composition, these elements are described in EN 60601. While the PAR Medizintechnik NIBP subsystem is certified from the manufacturer to meet these standards, the assembled device must also meet these requirements. For this design task, three main items had to be addressed. Firstly, power input must come from a medical graded source, these solutions are commercially available. Secondly, all system components must be rated for electrical and fire safety. These tests are typically performed by manufacturers and specified within component manuals. Lastly, internal electrical wiring must be at least 10 mm from the device enclosure. While these are minor details in the design, failure to comply with any component will not allow the device to be used in a clinical setting. The device enclosure was purchased from a medical device enclosure manufacturer such that the enclosure can be disinfected and to meet our size and water tightness requirements. Connectors to the device were selected to meet the medical grade rating as described in the documents above. With the reported modifications, the device is shown in the Figure A.7. CAD models were designed to layout the device and ensure all elements would fit inside the model (Figure A.6). Assembly protocols, assembly testing manuals, and standard operating procedure documents were designed for this version of the device.

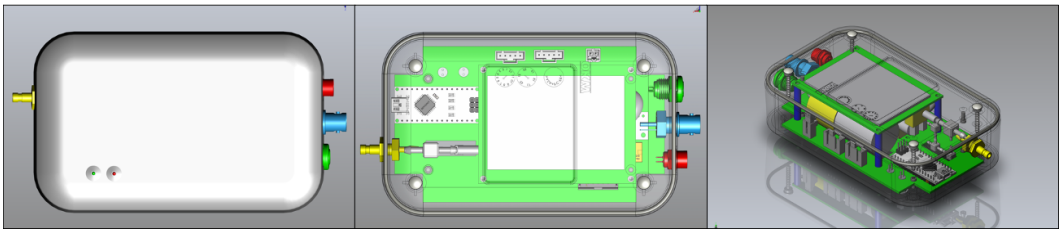

Figure A.6: Figure shows the CAD rendering used to build the device. (Left) shows the device within its enclosure in its bottom view. (Middle) shows the bottom view of the device with transparent casing to show the layout of the inside components. (Right) shows an isometric view of the device with transparent casing.

A.4 Upgraded Pneumatics Prototype

The first device versions shown above use an on-off air-valve to create a pressure differential across the differential pressure sensor. The air-valve technology had significant drawbacks including data losses from pressure decays, significant energy consumption, and increased complexity from active control systems. The new proposed design reduces the energy consumption, minimize the active control necessary and improves data acquisition.

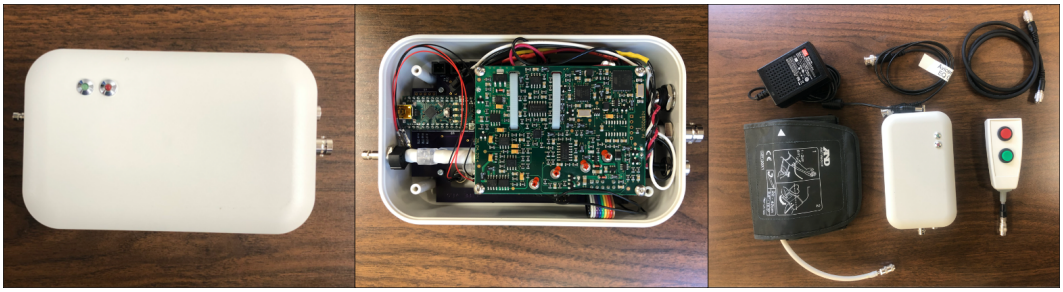

Figure A.7: Device Version 3 Build. (Left) shows the device within its enclosure in top view. (Middle) shows the device in bottom view without the base. Bottom view shows the electronics of the device. (Right) shows all the components necessary to operate the device.

The idea was to create a LPF by introducing a resistance to flow. In a tube with a large radius to length and no blockage, there is negligible resistance to air flow. On the other hand, blocking the tube is equivalent to adding infinite resistance. Thus theoretically, inserting the correct amount of resistance should act as a LPF and only pass mean flow. This hypothesis was first validated by inserting increasing lengths of cotton in a tube to act as a resistance. As the the amount of cotton in the tube increased, the output signal started resembling the pulse waveform. Once the amount of cotton reached a given threshold, this acted as an obstruction and no signal passed through. This effectively showed that it was possible to create a pneumatic LPF using flow resistance.

After a couple iterations, the final filter design consisted of tubing with very small radius to length ratio and a compliant tubing, effectively making up the resistance and capacitance elements. The radius to length ratio and the compliance are the filter characteristics that determine the cutoff frequency, more details about this are described in Chapter 3. The build of the LPF filter is shown in the figure below. This system together removed the air valve and created a passive method to maintain the reference port always at mean pressure effectively removing power consumption of the valve and the active system controls. The design of the resistance element also allowed for a more robust pneumatic connection removing the leakage problem encountered before. As the behavior of the system is now governed by fixed fluid dynamic behaviors, a pressure sensor with a smaller operating range and a higher resolution was substituted. On the overall this new technology gave a substantial technological upgrade to the device. The invention described herein has been patented and is currently under review by the USPTO as US20200323427A1.

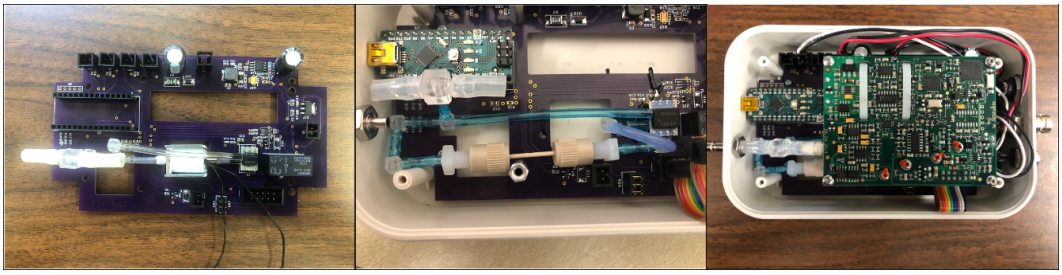

Figure A.8: Illustration shows the pneumatic system upgrades discussed above. (Left) shows the PCB design with the air valve and the pneumatics. (Middle) shows the PCB with the passive RC filter and the pneumatics. (Right) shows the assembled device within its enclosure with the upgraded pneumatics. Note that in all three figures elements have been removed to highlight specific parts of the design.

LIST OF ABBREVIATIONS

A-wave Atrial wave.

AES Aortic Ejection Sound.

AIx Augmentation Index.

AO Aorta.

AP Augmentation Pressure.

BMI Body mass index.

BP Blood pressure.

BPM Beats per minute.

BSA Body surface area.

BTB Beat-to-Beat.

CRF Case Report Form.

CVD Cardiovascular Disease.

DAC Digital to analog converter.

DAQ Data acquisition.

DBP Diastolic blood pressure.

dPdt-Dia Maximal Diastolic Pressure Fall Rate.

dPdt-Fall Maximal Systolic Pressure Fall Rate.

dPdt-Max Maximum Pressure Gradient during Isovolumetric Contraction.

dPdt-Rise Maximal Systolic Pressure Gradient.

DPTI Diastolic Pressure Time Integral.

DT Diastolic Time.

ECG Electrocardiogram.

FF Form Factor.

FSS Full Scale Span.

HR Heart Rate.

IC Informed Consent.

inH20 inches of H2O.

IRB Institutional Review Board.

LPF Low pass filter.

LV Left ventricle.

LVEDP Left ventricule end diastolic pressure.

MAP Mean blood pressure.

mmHg millimeter of mercury.

ms milliseconds.

ndPdt-Max Maximum Negative Pressure Gradient during Isovolumetric Relaxation.

NIBP Non-Invasive Blood Pressure.

PCB Printed Circuit Board.

pLPF Pneumatic Low-Pass Filter.

PP Pulse Pressure.

PT Pulse Time.

PWA Pulse Waveform Analysis.

RC Resistor capacitor.

RMSE Root Mean Squared Error.

RT Systolic Rise Time.

SBP Systolic blood pressure.

SPTI Systolic Pressure Time Integral.

sSBP Supra systolic blood pressure.

ST Systolic Time.

SUBID Subject Identification.

LIST OF ILLUSTRATIONS

LIST OF TABLES